Università degli Studi di Milano

Department of Medical Biotechnology and Translational Medicine

PhD School of Biochemical Sciences

XXXIII Cycle

The novel mitochondrial regulator Zc3h10 controls the white adipocyte differentiation program

BIO/10

Silvia Pedretti

Student ID: R11916

Tutor: Professor Nico Mitro

Coordinator: Professor Alessandro Prinetti

Academic Year 2019/2020

Summary

Abbreviations

acetyl-CoA carboxylase (ACC)

actin-binding proteins (ABPs)

adipocyte triglyceride lipase (ATGL)

brown adipose tissue (BAT)

cAMP-dependent protein kinase A (PKA)

carbohydrate-responsive element-binding protein (ChREBP)

CCAAT/enhancer-binding proteins (C/EBPs)

coding sequence (CDS)

cyclic AMP response element binding (CREB)

cyclin-dependent kinases (cdks)

dexamethasone (DEXA)

diglycerides (DGs)

dynamin-related/-like protein 1 (Drp1)

eIF4E-binding proteins (4EBPs)

electron transport chain (ECT)

embryonic stem (ES)

embryotic fibroblasts (MEFs)

eukaryotic translation initiation factor (eIF)

farnesyltransferase (FTase)

fatty acid synthase (FAS)

geranylgeranyltransferase I (GGTase I)

glycogen synthase kinase 3 β (GSK-3β)

guanine nucleotide exchange factors (GEFs)

guanosine diphosphate (GDP)

guanosine triphosphate (GTP)

hormone sensitive lipase (HSL)

human adipose-derived stromal/stem cells (hADSCs)

inner mitochondrial membrane (IMM)

insulin Receptor (IR)

isobutylmethylxanthine (IBMX)

knockout (KO)

Kruppel-like factor 5 (KLF5)

lipoprotein lipase (LPL)

low-density lipoproteins (VLDL)

lysophosphatidic acid (LPA)

mesenchymal stem cells (MSCs)

mitofusin 1 and 2 (Mfn1 and 2)

mitogen-activated protein kinase (MAPK)

mitotic clonal expansion (MCE)

monoacylglcerol lipase (MGL)

monoglycerides (MGs)

myogenic factor 5 (MYF5)

myosin light chain (MLC)

neural-WASP (N-WASP)

nuclear respiratory factors 1 and 2 (NRF-1, NRF-2)

optic atrophy 1 (OPA1)

outer mitochondrial membrane (OMM)

oxidative phosphorylation (OXPHOS)

oxygen consumption rate (OCR)

p21 activated kinase 1 (PAK1)

peroxisome proliferator-activated receptor gamma (PPARγ)

phosphodiesterase (PDE)

phosphoinositide 3-kinase (PI3K)

protein kinase A (PKA)

retinoic X receptor (RXR)

Rho guanine dissociation inhibitors (RhoGDIs)

Rho-associated kinase (ROCK)

rosiglitazone (ROSI)

single nucleotide polymorphism (SNP)

slingshot1 (SSH1)

sterol regulatory element-binding protein 1 (SREPB1)

stromal Vascular Fraction (SVF)

tricarboxylic acid (TCA)

triglycerides (TGs)

tumor Necrosis Factor alpha (TNF alpha)

uncoupling protein-1 (UCP1)

WASP family verprolin homologous protein 1 or 2 (WAVE 1/2)

white adipose tissue (WAT)

wild type (WT)

Wiskott-Aldrich Syndrome protein (WASP)

Zinc Finger Ccch-Type Containing 10 (Zc3h10)

1. INTRODUCTION

1.1 OBESITY

The World Health Organization (WHO) defines obesity and overweight as abnormal or excessive fat accumulation that may impair health and reduce an individual's quality of life. They are commonly measured and classified using the body mass index (BMI) obtained with the following formula: a person's weight (in kilograms) divided by the square of his or her height (in meters). For adults:

- BMI between 24.9 and 18.5 = healthy weight
- BMI between 25.0 and 30.0 = overweight
- BMI > 30.0 = obesity

BMI index is used for both sexes and disregards the different ages of the adult. It must be considered a rough guide because the same number does not necessarily correspond to the same degree of fatness in different individuals. However, despite these limitations, BMI is widely used as an indicator of pathologies as obesity and overweight.

The main cause of these conditions is an energy imbalance between calorie intake and energy expended. Overweight and obesity are associated with increased intake of energy-dense foods (high in fat and sugar) and decreased physical activity due to people's increasingly sedentary nature. Therefore, body weight is the result of genetics, metabolism, environment, behavior, and culture. Additionally, genetic can play an important role; in fact, variants in different genes may affect hunger and satiety. Furthermore, some illnesses, such as Cushing's disease, polycystic ovary syndrome, and drugs, such as steroids and some antidepressants, may alter metabolism and lead to weight gain (Blüher, 2019).

Obesity is one of the most massive health problems in the world, and WHO shows that, globally, 13% of adults are obese in 2016 (source: https://ourworldindata.org/obesity#citation). As shown on the map (Fig. 1.1), the prevalence of obesity is higher in industrialized (Europe, North America, and Oceania) than in developing countries (South Asia, Africa). The frequency of obesity has increased dramatically worldwide over the last 50 years, affecting teenagers and children and the point of reaching a pandemic level (Blüher, 2019).

Overweight and obesity are major risk factors for several chronic diseases, including cardiovascular disease, hypertension, diabetes, dyslipidemia, metabolic syndrome, sleep apnea, and different cancer types. The risk of these conditions is positively associated with BMI. Furthermore, these conditions are also associated with psychological problems, such as depression, and several studies demonstrate that obesity and overweight harm longevity (Kopelman, 2000; Williams et al., 2015).

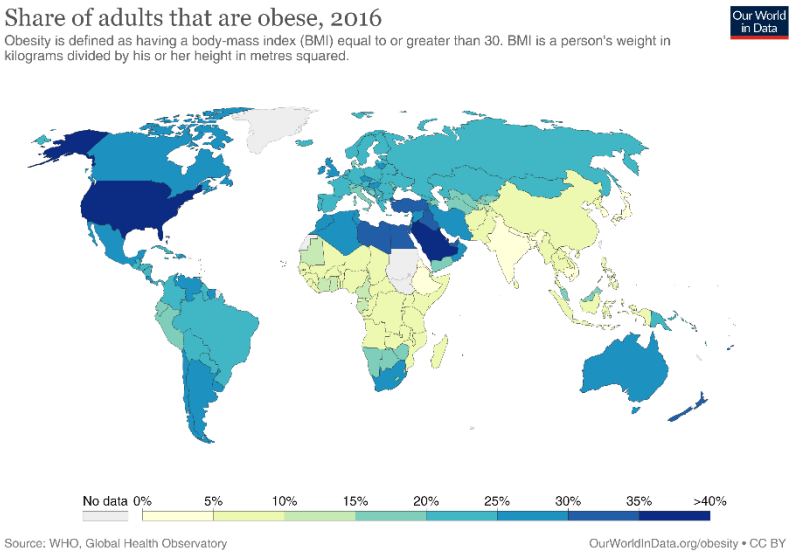

Figure 1.1: Epidemiological distribution of obesity. Figure from http://apps.who.int/gho/data/view.main.REGION2480A?lang=en

Treatment of overweight and obesity usually involves a lifestyle change with the introduction of physical activity and a reduction in fatty foods consumption. If these changes are not sufficient, drugs that act on the sense of hunger and satiety or, in extreme cases, gastric surgery are used.

1.2 THE ADIPOSE TISSUE

1.2.1 ADIPOSE TISSUE BIOLOGY

Adipose tissue is a complex organ with profound effects on physiology and pathophysiology. It has been ignored for years because it was considered only as an energy storage depot. Recently, the rising incidence of obesity and metabolic diseases had attracted considerable attention to the study of this organ. The knowledge about its physiology and endocrine organ function has been deepened.

Adipose tissue is a loose connective tissue and its principally composed by adipocytes and other cell types such as pre-adipocytes, fibroblast, vascular endothelial cells, and immune cells.
In mammals, adipose tissue can be classified into two subtypes: brown adipose tissue (BAT) and white adipose tissue (WAT) that are different for morphology and function (Fig. 1.2).

Brown adipose tissue is composed of brown adipocytes containing numerous and distinct lipid droplets within the cytoplasm. They also have a high number of mitochondria; the cytochromes present in the inner mitochondrial membrane give the brown color to this tissue. The primary function of this tissue is the generation of heat, a process known as non-shivering thermogenesis. BAT is a “heat-producing tissue” that oxidizes deposited fat and releases the stored energy as heat to maintain correct body temperature in a cold environment. In this tissue, mitochondria contain uncoupling protein-1 (UCP1), also called thermogenin. UCP1 can

uncouple oxidative phosphorylation from ATP production, and energy originated from the electron transport chain is dissipated in the form of heat (Rosen and Spiegelman, 2014)(Goto et al., 2016). In mouse model, brown adipocytes are located mainly in the interscapular and peri-renal regions while in adult human BAT is identified in the neck region and supraclavicular areas (Bartness et al., 2010).

On the other hand, white adipose tissue is composed of white adipocytes with a unilocular lipid droplet that takes up much of the space within the cell. Nuclei are peripherally located, and the cytoplasm forms a ring around the central vacuole. WAT's primary function is the high capacity of storing energy in the form of triglycerides (TGs) and protect organs from lipotoxicity. The surplus energy intake from diet is deposited in the form of TGs in adipose tissue through the lipogenic pathway. Imbalance in calory intake and energy expenditure causes adipocytes hypertrophy with an increase in lipid droplet size and adipose expansion. Furthermore, TGs conserved in adipocytes are broken down into glycerol and fatty acids (lipolytic pathway) when energy is required from the body. The released glycerol and fatty acids from adipose tissue can be transported in the blood and reached other organs. Anatomically, in humans WAT is located into two major depots: subcutaneous WAT and visceral WAT around internal organs, including mesenteric, omental, perirenal, and peritoneal depots (Choe et al., 2016).

Recently, it was found another type of WAT called beige or brite (brown-like-in-white) fat. This tissue acquires BAT features (i.e., UCP1 expression) when subjected to certain stimuli such as cold exposure and pharmacological stimuli (such as beta-adrenergic agonist), a process known as browning or beiging of WAT. Beige adipocytes exist mainly in subcutaneous white fat and in a small portion in visceral fat (Luo and Liu, 2016)(Rosen and Spiegelman, 2014).

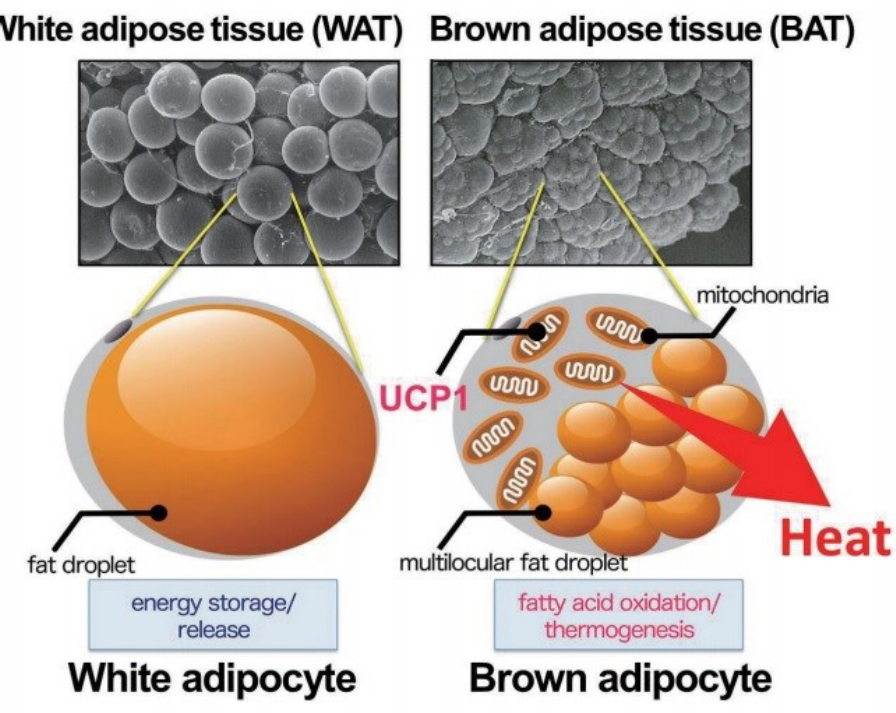

Figure 1.2: Graphical representation of the main characteristics of white and brown adipocytes. White adipocytes present a single lipid droplet within cytoplasm and their function is related to energy storage/release. In contrast, brown adipocytes are compost of multilocular lipid droplets and are indispensable for thermogenic process. Figure from Goto et al., 2016.

Furthermore, adipose tissue is also essential for mechanical properties, serving to protect delicate organs and as cushion body parts exposed to mechanical stress levels.

However, adipose tissue's most crucial function is as a master regulator of energy balance and nutritional homeostasis.

1.2.2 ADIPOSE TISSUE AS AN ENERGY STORAGE ORGAN

One of the main functions of adipose tissue is storing energy in the form of TGs and releasing fatty acids in case of necessity.

In fasting condition (energy depletion), the lipolytic pathway is activated and promotes the release of fatty acids breaking the TGs in adipose depots, while feeding stimulates lipogenesis

and storage of TGs in adipose tissue. Both lipogenic and lipolytic pathways are dependent on nutrition state and hormones such as insulin, norepinephrine, and glucagon (Fig. 1.3).

Lipogenesis is a process by which carbohydrates are converted into fatty acids and promotes TG's biosynthesis and expansion of lipid droplet in adipocytes.

After feeding, glucose stimulates insulin secretion from the pancreatic islet beta-cell to clear the blood's glucose excess and to restore glucose homeostasis. Insulin binds its receptor, Insulin Receptor (IR), and triggers a signaling cascade that results in activation of phosphoinositide 3-kinase (PI3K) and the AKT protein kinase allow GLUT4 translocation, facilitating glucose uptake in adipocytes. Furthermore, insulin stimulates the expression of lipogenic gene sterol regulatory element-binding protein 1 (SREBP1) that controls the synthesis of fatty acids, TG, and cholesterol (Ramalingam et al., 2013). Another transcription factor, carbohydrate-responsive element-binding protein (ChREBP) is also activated and promoted lipogenesis gene expression. After glucose uptake, this molecule is metabolized through glycolysis and tricarboxylic acid cycle and provides acetyl-CoA as the substrate for *de novo* synthesis of fatty acids and the glycerol backbone for esterified fatty acids. The synthesis of fatty acids is made by acetyl-CoA carboxylase (ACC) and fatty acid synthase (FAS) that requires acetyl-CoA, malonyl-CoA, and NADPH. Malonyl-CoA also plays an important role as an inhibitor of carnitine/palmitoyl shuttle used for fatty acid oxidation (Wakil and Abu-Elheiga, 2009).

Moreover, insulin stimulates lipoprotein lipase (LPL) activity that catalyzes the hydrolysis of triglycerides from circulating chylomicrons and very low-density lipoproteins (VLDL) and thereby plays an essential role in lipid clearance from the bloodstream, lipid utilization, and storage in adipose tissue (Frayn, 2002).

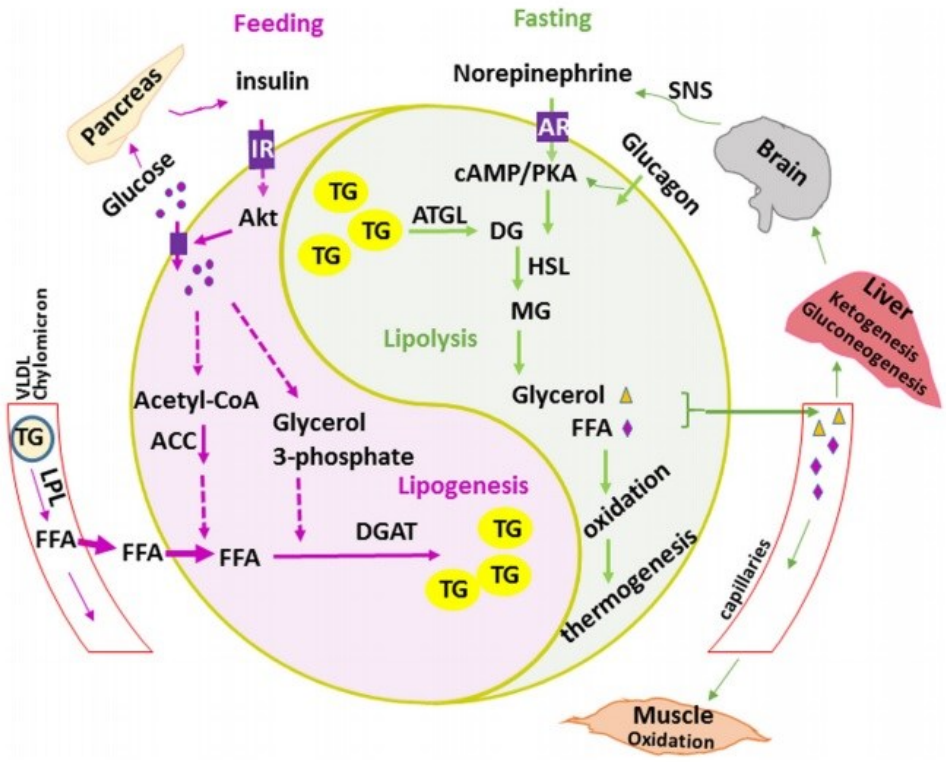

Figure 1.3: Lipogenesis and lipolysis process in adipose tissue. Lipogenesis converts carbohydrate into fatty acids which are stored into cytoplasmatic lipid droplets. This process is stimulated by feeding and insulin. Opposite, lipolysis breaks TG to free fatty acids and glycerol in response to fasting and glucagon stimulation. Figure from Luo and Liu 2016.

During fasting, it is observed a decrease in circulating level of insulin as well as a lipogenesis process while there is an increase in circulating glucagon that is responsible for the activation of cAMP-dependent protein kinase A (PKA) pathway. Meanwhile, catecholamines stimulate the beta-adrenergic receptor, which increases cAMP levels and activates PKA and lipolysis.

In this condition, adipocytes can break down TGs stored into adipocytes and release free fatty acids and glycerol by a multistep process called lipolysis.

This catabolic process involves thee different enzymes: adipocyte triglyceride lipase (ATGL), hormone-sensitive lipase (HSL), and monoacylglycerol lipase (MGL). ATGL and HSL are responsible for the conversion of TGs to diglycerides (DGs) and then to monoglycerides (MGs) while MGL converts MGs into free fatty acids and glycerol (Wakil and Abu-Elheiga, 2009). In

this context, the presence of perilipins, a family of hydrophobic lipid droplet-associated phosphoproteins that are phosphorylated by PKA after lipolytic stimulation, is important. These proteins are specific for adipocytes, and their function is to prevent lipolysis in basal conditions and allow lipid storage. When PKA phosphorylates perilipin, it loses its blocking capability and permits HSL function (Londos et al., 1999).

1.2.3 ADIPOSE TISSUE AS AN ENDOCRINE ORGAN

Recently, it has been found that adipose tissue has an endocrine function and produces a variety of molecules called adipokines, which regulate systemic metabolism and energy homeostasis. Adipokines include cytokines, hormones, and peptide secreted by adipocytes.

Leptin and adiponectin are the most famous and the first that were discovered. Leptin is expressed in adipose tissue and, at lower levels, in gastric epithelium. Leptin is a hormone that acts on the hypothalamus, decreases food intake, and modulates glucose and fatty acids metabolism by inhibiting hunger and inducing satiety effect. High plasma leptin levels are associated with greater body fat content; indeed, obese patients show higher plasma leptin values compared to normal subjects. This data suggests that obesity is associated with insensitivity to leptin (Friedman and Halaas, 1998). Zhang et al. show that mice with a deficiency of leptin expression or receptor function have a higher food intake and lower energy expenditure, which leads to the onset of obesity (Zhang et al., 1994). Leptin also promotes lipid oxidation and mitochondrial biogenesis and increases energy consumption in peripheral tissues (Minokoshi et al., 2002).

Another adipokine secreted from adipose tissue is adiponectin. This hormone can target multiple tissues, possess anti-diabetic properties, increase insulin sensitivity, and stimulate lipid oxidation (Choe et al., 2016). In literature, it is reported that adiponectin-deficient (*Adipo-*

/-) mice showed glucose intolerance and hypertriglyceridemia compared with wild-type mice, and this result indicates that adiponectin has a protective role against insulin resistance (Kubota et al., 2002).

Other secreted adipokines are: restin, FGF21, pro-inflammatory cytokines such as interleukin-6 (IL-6) Tumor Necrosis Factor alpha (TNF alpha) and monocyte chemoattractant protein 1 (MCP1) and these factors can regulate adipose tissue metabolism too.

1.2.4 THE ORIGIN OF ADIPOCYTES

After their early childhood establishment, adipose tissue undergoes active remodeling during adulthood in case of calorie excess or cold stress induction. For this reason, the precursor cells with adipogenic potential must be retained during adulthood.

The stromal vascular fraction (SVF) of adipose tissue comprises different types of cells: adipocytes, mesenchymal stem cells, T cells, M2 macrophages, nerves, and endothelial cells. Mature adipocytes are separated from SVF by collagenase digestion and low-speed centrifugation. SVC can be cultured *ex vivo* (primary culture), and only mesenchymal stem cells can attach themselves to the dish while the rest of the cells (i.e., blood cells, endothelial cells) are lost. What remains can be cultured and completely differentiated *in vitro* using a hormonal cocktail containing insulin, glucocorticoid, a phosphodiesterase inhibitor, and a PPARγ agonist (Cawthorn et al., 2012).

WAT and BAT adipocytes precursors are derived from mesenchymal stem cells (MSCs) (Fig. 1.4). MSCs can be isolated from different type of tissue such as adipose tissue and differentiate into several cell types, i.e., adipocytes, myocytes, chondrocytes, and osteocytes. When receiving correct adipogenic stimuli, these cells undergo a multistep process of commitment in which

progenitors cell became adipocytes after a complex process called adipogenesis (Tang and Daniel Lane, 2012). The myogenic factor 5 (MYF5) is a gene expressed during embryonic myogenesis, and it is involved in muscle development. Genetic-lineage tracing has shown that BAT adipocytes precursor derives from $MYF5^{+}$ lineage and also from stem-cell-like skeletal muscle satellite cells, while WAT adipocytes precursors derive predominantly from $MYF5^{-}$ lineage. However, in a study performed by Sanchez-Gurmaches, they found that a subset of white adipocytes is derived from $MYF5^{+}$ mesenchymal progenitors and the relative contribution of MYF5-lineage cells to WAT seems to vary between the different WAT depots (Sanchez-Gurmaches et al., 2012). Beige adipocytes derive from white adipocytes precursors because they are potentially directed to become white adipocytes, although specific stimuli (i.e., cold exposure) encourage their ability to express UCP1. Furthermore, both white and brown adipocytes may derive from endothelial precursors (Peirce et al., 2014).

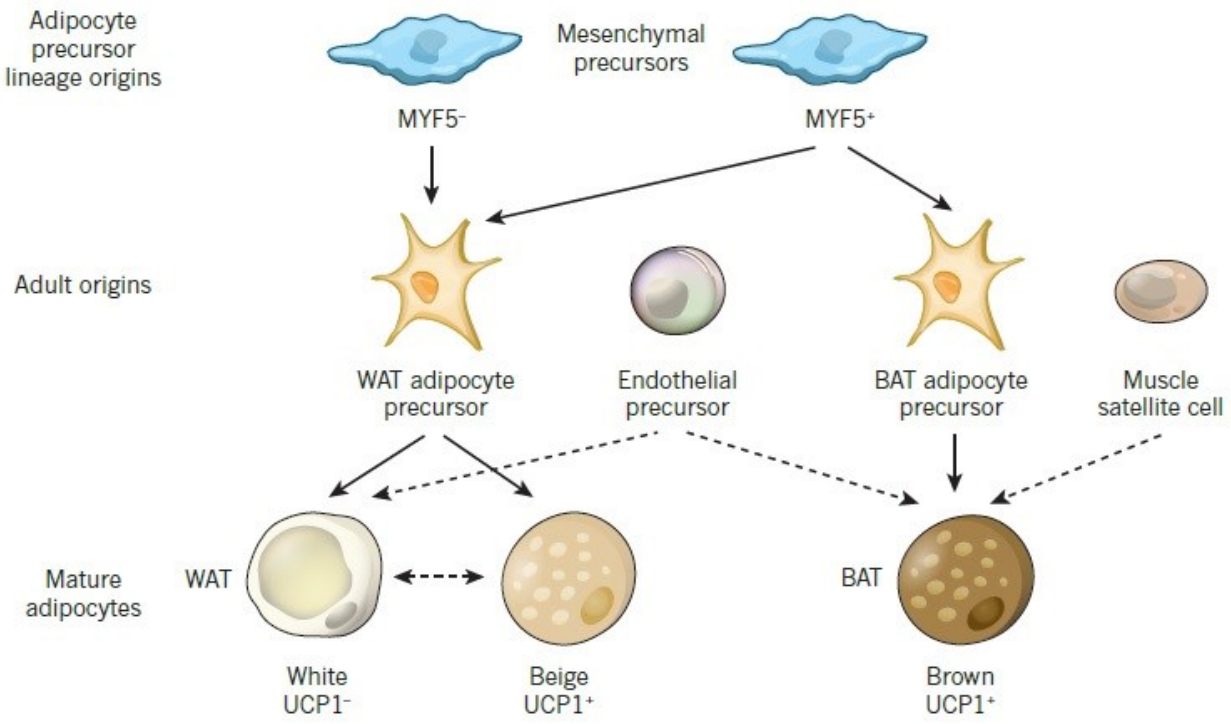

Figure 1.4: Origin of white, beige, and brown adipocytes. WAT adipocyte precursors derive from both MYF5^{-} and MYF5^{+} while BAT adipocytes precursors derive only from MYF5^{+}. Furthermore, brown adipocytes can derive from muscle satellite cell. Figure from Peirce, Carobbio, and Vidal-Puig, 2014.

1.3 THE ADIPOGENESIS

Adipogenesis is a complex process by which undifferentiated mesenchymal stem cells became pre-adipocytes, which then undergoes a secondary differentiation step to be converted into mature lipid-laden and insulin-responsive adipocytes. This process comprises several phases: MSCs change their morphology and their gene expression to allow the successful transformation into mature adipocytes (Ali et al., 2013). Current knowledge indicates that mature adipocytes are incapable of mitotic divisions; therefore, adipocytes hyperplasia is the result of precursor cells' differentiation in response to metabolic needs. For this reason, initial availability of mesenchymal stem cells and pre-adipocytes predisposition to differentiation represent the key regulators of the number of mature adipocytes in adipose tissue (Kras et al., 1999).

This process involves a cascade of transcription factors that coordinate the expression of hundreds of proteins responsible for mature adipocytes phenotype, among which peroxisome proliferator-activated receptor gamma (PPARγ) and CCAAT/enhancer-binding proteins (C/EBPs) are considered the two main adipogenic factors which trigger the terminal differentiation process. Adipocytes differentiation is composed of two different waves of events: when MSCs reach confluence, they enter in a temporary state, arresting at the G0/G1 phase. Specific adipogenic stimuli induce the synchronous re-enter in the cell cycle of growth-arrested pre-adipocytes to accomplish several cell division rounds, a process known as mitotic clonal expansion (MCE). In this context, the upregulation of C/EBPδ and C/EBPβ is important

and induces the expression of C/EBPα and PPARγ that are essential to driving terminal adipogenic program (Fig 1.5) (Lefterova and Lazar, 2009).

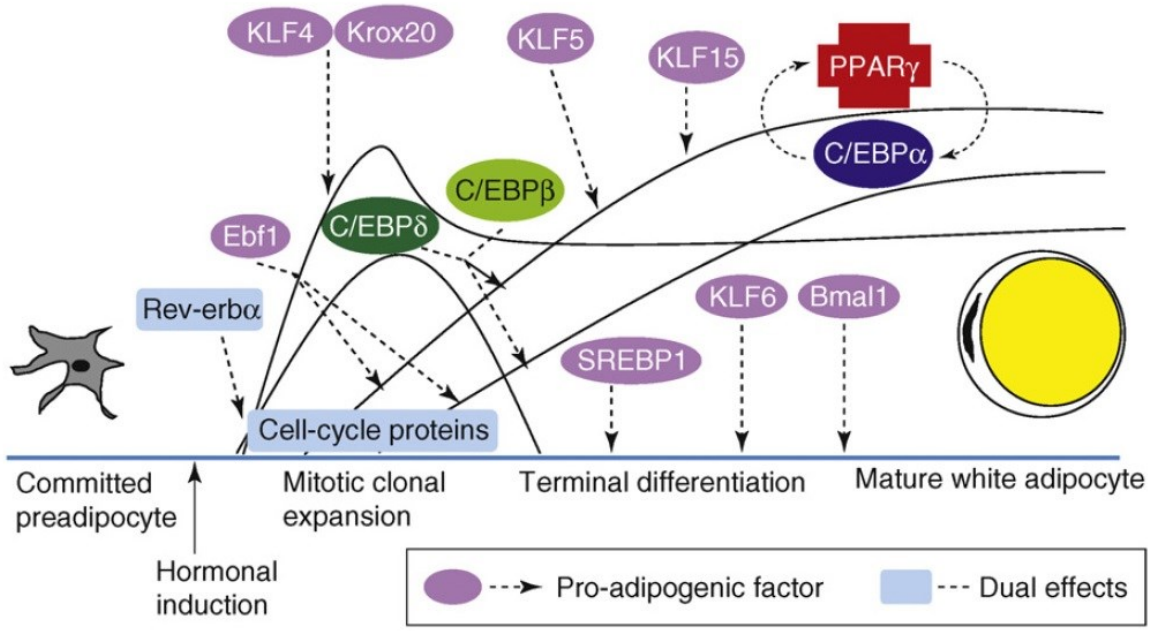

Figure 1.5: Different steps of adipogenesis and multiple pro-adipogenic factors that regulated this process. Figure from Lefterova and Lazar, 2009.

PPARγ is a member of the PPAR subfamily of nuclear hormone receptors, and it is defined as the master regulator of adipocytes differentiation, fatty acid uptake, and lipogenesis. PPARγ is a transcription factor, and its activity is regulated by direct binding of hormones, vitamins, lipid metabolites, and xenobiotics (Chawta et al., 2001). Agonist ligands trigger a conformational change of PPARγ, which can bind specific DNA sequences after its heterodimerization with retinoid X receptor (RXR)(Tontonoz and Spiegelman, 2008). In 1994, Spiegelman and colleagues discovered that expression of PPARγ in fibroblasts induces adipogenic genes expression; this specific event leads to lipid droplets formation, thus ensuring the onset of the adipogenic program (Tontonoz et al., 1994). Many other research groups are focused on PPARγ

expression to unravel its role in adipogenesis. One common and well-known strategy is the generation of knockout (KO) mouse model. Since this latter option has shown numerous adversities because homozygous null mice do not survive, alternative strategies were developed. Rosen and colleagues have generated chimeric mice derived from homozygous target embryonic stem (ES) cells. In these animals, the KO cells could not develop into mature adipocytes, confirming that PPARγ plays a crucial role in adipogenesis (Rosen et al., 1999).

In adipocytes there are two different isoforms of PPARγ derived from two alternative splicing (γ1 and γ2): PPARγ2 has 30 more additional amino acids in N-terminal position, and it is expressed specifically in adipocytes while PPARγ1 is also found in macrophages, colon epithelial and endothelium (Marx et al., 1999; Ricote et al., 1998; Sarraf et al., 1998). Furthermore, PPARγ1 can be functionally relevant also in muscle and liver tissues. Zhang at al. have generated PPARγ2-specific KO mice (PPARγ2$^{-/-}$), and they show that these animals are protected against high-fat diet-induced obesity. In addition, PPARγ2$^{-/-}$ mice exhibit a reduction in the WAT weight even though the food intake is similar compared to wild type (WT) mice. They analyze the histological section of WAT, and they find that in control littermates, white-fat adipocytes are uniform in size while in PPARγ2$^{-/-}$ mice adipocytes are smaller and heterogeneous in size, thus indicating that white fat adipocytes depleted of PPARγ can accumulate less triglyceride compare to control group. Furthermore, they also find a decrease in adipogenic gene expression and impaired insulin sensitivity. The results of this study show that PPARγ1 and PPARγ2 *in vivo* can drive adipose tissue development but that PPARγ2 is fundamental for correct adipogenesis (Zhang et al., 2004).

C/EBPα is the other key factor involved in adipocytes differentiation. It belongs to a family of basic-leucine zipper proteins, and its role in adipogenesis has been confirmed through mouse models. Whole-body C/EBPα KO mice die shortly after birth because of liver defects and fail to accumulate lipid (Wang et al.) while inducible whole-body ablation of C/EBPα leads to a

reduction in WAT weight in adult mice (Yang et al., 2005). As mentioned before, C/EBPα is induced in the second wave of adipogenesis and is crucial for insulin-dependent glucose uptake (Wu et al., 1999). However, a study performed by Spiegelman shows that in C/EBPα-deficient mouse embryonic fibroblasts (MEFs), the ectopic expression of PPARγ can completely rescue adipogenesis (Rosen et al., 2002). However, it is possible that other C/EBP members can compensate for C/EBPα deficiency.

Many other transcription factors are potentially involved in the adipocytes' differentiation program. Krox20 is one of them; it acts in the early stage of adipogenesis and induces the expression of C/EBPβ and cooperates with it in terminal differentiation (Chen et al. 2005). Another important transcription factor known to play a role in adipogenesis is Kruppel-like factor 5 (KLF5). Oishi et al. demonstrate that KLF5 mediates both the early and the late stages of differentiation program: its transcription is activated by C/EBPβ and C/EBPδ, and KLF5 controls PPARγ2 expression. Their results show that even a 50% reduction in the level of KLF5 is enough to impair adipocyte differentiation. Even when C/EBPβ and C/EBPδ are expressed correctly, reduced expression of KLF5 negatively affects the adipogenic program. Indeed, in WAT from $KLF5^{+/-}$ mice, the expression of PPARγ2 is reduced while there are no changes in C/EBPβ and C/EBPδ (Oishi et al., 2005). A cascade of KLFs functions during adipocyte differentiation, and it can be divided into activators (i.e., KLF4, KLF5, KLF6) or inhibitors (i.e., KLF2, KLF 7) of adipogenesis (Birsoy et al. 2008; Li et al. 2005). Moreover, SREBPs are a family of transcription factors that regulate lipid homeostasis, controlling the expression of genes involved in the synthesis of cholesterol, fatty acids, TGs, and phospholipids. SREBP1c is an essential factor involved in adipogenesis: its expression increases during 3T3-L1 adipocytes differentiation, but SREBP1c alone can only induce adipogenesis to a modest level. Additional studies suggest that SREBP1c contributes to PPARγ ligands production, facilitating PPARγ action (Kim et al., 1998).

MSC commitment and differentiation to adipocytes are due to a combination of specific factors. For adipogenic differentiation, MSCs are induced using a specific adipogenic cocktail that is composed of insulin, isobutylmethylxanthine (IBMX), dexamethasone (DEXA), and PPARγ agonist such as rosiglitazone (ROSI). IBMX and DEXA are important for the initiation of adipogenic differentiation: IBMX is a non-selective phosphodiesterase (PDE) inhibitor, which causes an elevation of cAMP levels. cAMP activates protein kinase A (PKA) that stimulate the expression of C/EBPβ, and it is involved in the inhibition of Rho-kinase pathway (Petersen et al. 2008). DEXA activates C/EBPδ expression by binding to the intracellular glucocorticoid receptor. Insulin promotes glucose uptake and its metabolization for the synthesis of TGs. Furthermore, insulin stimulates the phosphorylation and activation of farnesyltransferase (FTase) and geranylgeranyltransferase I (GGTase I), activates cyclic AMP response element-binding (CREB) (Klemm et al., 2001) and enhances the expression of SREBP1 while ROSI is a potent and selective agonist of PPARγ. All these steps are critical for adipogenesis. Proliferation, morphological changes, expression of lineage-specific markers, and lipid accumulation are biological processes that drive MSCs differentiation to adipocytes (Chen et al., 2016).

1.3.1 MITOTIC CLONAL EXPANSION (MCE)

Pre-adipocytes cultured to confluence *in vitro* become growth-arrested at the G0-to-G1 cell cycle transition because of contact inhibition. After induction of differentiation, growth-arrested pre-adipocytes synchronously reenter the cell cycle and undergo several rounds of cell division, a process known as MCE. This process precedes the expression of terminal adipogenic genes that give rise to mature adipocytes phenotype.

After hormonal induction, C/EBPβ is expressed immediately, but it is unable to bind DNA and cannot act as a transcriptional activator. When C/EBPβ is phosphorylated at multiple sites, it

acquires DNA-binding activity, and by gaining this ability, cells can enter the S phase and start the MCE process. After acquiring DNA-binding activity, C/EBPβ induces the expression of C/EBPα and PPARγ genes (Tang and Lane 1999) that are antimitotic factors. For this reason, the timing of this process is critical for the correct MCE route (Tang, Otto, and Lane 2003). MEFs isolated from C/EBPβ-deficient mouse embryos cannot form mitotic foci and acquire adipocyte characteristics such as TGs accumulation. To verify that C/EBPβ is fundamental for MCE, C/EBPβ-deficient MEFs were infected with adenoviral expression vectors for active C/EBPβ (LAP). Expression of C/EBPβ (LAP) restores both MCE and adipogenesis (Tang, Otto, and Lane 2003).

C/EBPβ is phosphorylated first by mitogen-activated protein kinase (MAPK) on Thr-188, but this phosphorylation is insufficient to affect DNA-binding activity but is required for subsequent hyperphosphorylation on Thr-179 and Ser-184 by glycogen synthase kinase 3 β (GSK-3β). Therefore, dual phosphorylation of C/EBPβ on two of these sites (Thr-188 and Thr-179 or Thr-188 and Ser-184) is required to gain the DNA-binding activity (Tang et al. 2005). Tang and colleagues used a potent MEK inhibitor (U0126) that prevent MAPK phosphorylation and block the expression of cell cycle markers (i.e., cyclin A and cdk2). MCE is completely blocked as well as the acquisition of adipocytes phenotype. Moreover, the addition of U0126 after MCE does not affect the adipogenic program and the expression of C/EBPα and PPARγ (Tang, Otto, and Daniel Lane 2003).

Entering the cells cycle is a process regulated by cyclin-dependent kinases (cdks). The coordinated activation of cdk2 and cdk4/cdk6 and the downregulation of p27 are required for the progression of growth-arrested cells through G1 and into S phase. The study conducted by Patel and Lane shows that calpain catalyzes the degradation of cdk inhibitor, p27, and allows G1/S transition, re-entry into the cell cycle and the correct MCE and adipogenesis (Patel and Lane, 2000). Taken together, these data show that MCE is a prerequisite for adipogenesis.

1.3.2 CYTOSKELETON REMODELING

The cytoskeleton is an interconnected network of filamentous polymers and regulatory proteins and is involved in three main functions: i) orchestration of coordinated forces that allow cell movement and cell shape, ii) spatial organization of cell content, and iii) connection between cell and external environment. Despite the connotations of the word "skeleton", the cytoskeleton is not a fixed structure, but it is a dynamic organelle that regulate different cellular processes (i.e., proliferation, differentiation, motility) (Fletcher and Mullins, 2010). The cytoskeleton is composed of three components: microfilaments, composed of actin, microtubules, made up of tubulin, and intermediate fibers. Actin is a very dynamic structure due to its ability to polymerize and depolymerize. It exists as a globular monomer (G-actin) and a filamentous polymer (F-actin) composed by a linear chain of G-actin subunits. The dynamics of actin are essential for actin remodeling (Kim et al. 2019), and it is regulated by a large number of signaling and actin-binding proteins (ABPs)(Lee and Dominguez, 2010).

During adipogenesis, cells must reorganize their cytoskeleton and change their shape from elongated and irregular appearance (fibroblast-like) to round shape that allows the cells to maximize lipid accumulation (Spiegelman and Farmer, 1982). This latter process is strongly influenced by actin polymerization/depolymerization state. Current knowledge shows that adipocytes differentiation is associated with a shift in F-actin structures: from prolonged stress fibers organized across the cell body, typically observed in precursor cells and pre-adipocytes, to cortical fibers presented in fully differentiated adipocytes (Kanzaki and Pessin, 2001). Indeed, throughout the differentiation program, F-actin stress fibers appear disrupted from the central region of the cell body, where lipid droplets are forming, and are organized only as peripheral cortical structures (Fig. 1.6) (W. Yang et al. 2014a).

Actin remodeling can be divided into five steps: I) actin stress fibers (day 0), II) initiation of actin assemblies (day 2), III) disruption of F-actin stress fibers (day 3), IV) replacement of F-

actin blocks with dotted actin structures in the cell cortex (4-5), V) cortical actin structure (mature adipocytes) (W. Yang et al. 2014b).

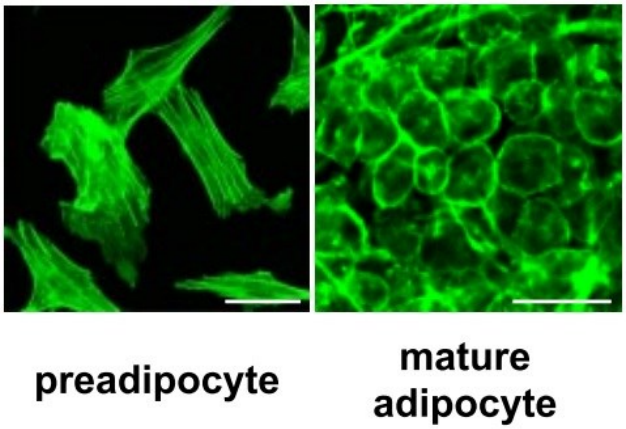

Figure 1.6: F actin remodeling during adipocytes differentiation: from stress fibers organized around the cell to cortical stress fibers with the filaments organized in the periphery of the cell. This allows the morphological change from fibroblasts to mature adipocytes. Figure from Noguchi et al. 2007.

Besides, stem cells' commitment to different lineages is also regulated by shape: changes in cell shape themselves can alter the differentiation of recommitted mesenchymal lineages. Cytochalasin D disrupts stress fibers and inhibits focal adhesion formation. Feng and colleagues incubated embryonic stem cells with cytochalasin D, and they observed an increase in the expression levels of adipogenic markers such as PPARγ and C/EBPα compared to untreated cells. Thus, this result shows that cytoskeleton remodeling and F-actin depolymerization are necessary to accommodate lipid droplets' expansion of and for correct adipogenesis (Feng et al., 2010).

The organization of the cytoskeleton is controlled by members of Rho family of small GTPases. This family includes Rho, Rac1, and Cdc42 GTPases that play an important role in controlling the organization of actin structures, microtubules, and in regulating cell shape, polarity,

movement, differentiation, and many other fundamental cell processes (Fig. 1.7) (Hall, 1998). All of these proteins are also essential for cell cycle progression through the G1 phase, specifically Rho and Cdc42 are required during cytokinesis (Olson et al., 1995). Rho GTPases exist within two different states: an inactive guanosine diphosphate (GDP)-bound and an active guanosine triphosphate (GTP)-bound state. Al least three regulatory proteins control the state of Rho GTPases family. Guanine nucleotide exchange factors (GEFs) activate these proteins by switching from GDP- to GTP-bound while, GTPase-activating proteins (GAPs) inactivate these proteins catalyzing GTP hydrolysis to GDP. Furthermore, Rho guanine dissociation inhibitors (RhoGDIs) bind GDP and maintain these proteins in an inactive state (Møller et al., 2019). Each Rho GTPase controls the activity of numerous downstream effectors and actin-binding proteins with a specific role in the local assembly or disassembly of F-actin and in many cellular processes, including adipogenesis.

Rho regulates the actin skeleton's depolymerization by controlling the Rho kinase, ROCK, and its downstream proteins (such as myosin light chain, MLC), and this process is involved in adipogenesis. Ji and colleagues investigate the role of Rho and RhoA/ROCK signaling during adipogenesis. They show that overexpression of RhoA (RhoA14V) in C3H10T1/2 cell line induced to differentiation into adipocytes, leads to a diminished expression of the key adipogenic gene, PPARγ, and also impairs lipid accumulation (Ji et al., 2017). Another study demonstrates that the activation of ROCK during MSC differentiation reduces the expression of PPARγ and inhibits adipogenic differentiation (Kusuyama et al., 2014). Conversely, inhibition of RhoA or ROCK (using the selective inhibitor, Y-27632) promotes the commitment of MSCs to adipocytes and increases lipid accumulation, whereas osteoblasts differentiation is induced by activation of RhoA and ROCK (Xu et al., 2012). ROCK mediates Rho signaling through phosphorylation of downstream substrates that contribute to actin cytoskeleton reorganization. ROCK exists in two different isoforms: ROCK-I AND ROCK-II. In a work by

Noguchi and colleagues, gene expression and lipid accumulation were evaluated in MEFs derived from ROCK-II (-/-), and ROCK-I (-/-) and induced to differentiation into adipocytes. The Authors found out that ROCK-II (-/-) MEFs present an increase in lipid accumulation and in the expression of PPARγ and C/EBPα, while no changes in adipogenic process are observed in ROCK-I (-/-) mice. Furthermore, they report that lysophosphatidic acid (LPA) activates small GTP Rho and induces stress fiber formation in 3T3-L1 pre-adipocytes while Y-27632 inhibits this effect. So, this result shows that inhibition of ROCK-II enhances adipogenesis (Noguchi et al., 2007). Moreover, ROCK phosphorylates LIM-kinase (LIMK), leading to the phosphorylation and inactivation of cofilin. Cofilin is a family of actin-binding proteins that regulated assembly and disassembly of actin filaments. The inactivation of cofilin promotes F-actin stability and elongation. In adipogenic context, cofilin-1 expression increases during adipocyte differentiation and cofilin-1 knock-down cells show significantly decreased lipid accumulation at day 5 after differentiation induction showing relatively intact F-actin fibers in the cell body (W. Yang, et al. 2014a).

Another effector of Rho is mDIA, and the cooperation between mDIA and ROCK is required for stress fibers formation and actin polymerization. These two proteins antagonize in Rho-dependent Rac activation, and the balance between these two pathways determines the cell shape and pattern of stress fibers (Narumiya et al., 2009).

In this context, cAMP dependent protein kinase A (PKA) plays a key role in adipocyte differentiation. Indeed, molecules or factors such as IBMX or forskolin that stimulate cAMP synthesis promote the suppression of Rho/ROCK pathway, the decrease of active Rho GTPase and, consequently, the diminished rate of MLC phosphorylation by ROCK.

In literature, are presented different mechanisms for PKA-mediated inhibition of Rho: inactivation by phosphorylation of RhoA by PKA (Dong et al., 1998; Lang et al., 1996), phosphorylation of AKAP-Lbc followed by a decrease in GEF activity (Diviani et al., 2004) or the

PKA-catalyzed phosphorylation of Gα13 which inhibits the activation of Rho (Baisamy et al., 2005).

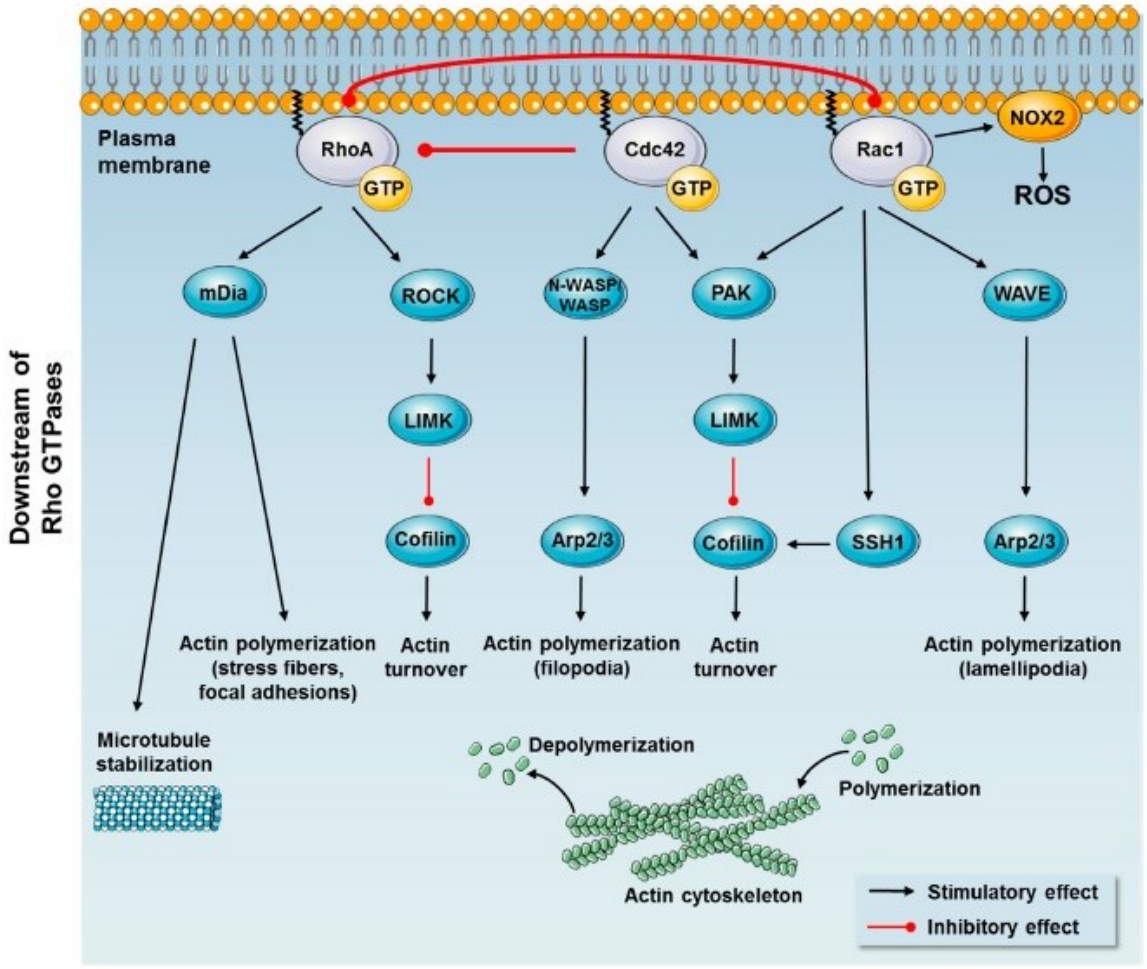

Figure 1.7: Rho GTPases: Rac1, Cdc42, and RhoA and their downstream effector proteins. Mechanism of action by which the Rho GTPases control the remodeling of the cytoskeleton. Figure from Møller, Klip, and Sylow, 2019.

The other two main components of Rho GTPase family are Cdc42 and Rac1. They trigger p21 activated kinase 1 (PAK1), which induces phosphorylation of LIMK that, as mentioned above, inactivate cofilin (Edwards et al., 1999). To counteract LIMK-dependent inactivation of cofilin, Rac1 can activate slingshot1 (SSH1), which acts by dephosphorylating and subsequently activating cofilin (Kligys et al., 2007). Moreover, Cdc42 activates the Wiskott-Aldrich Syndrome family of proteins, including Wiskott-Aldrich Syndrome protein (WASP), neural-

WASP (N-WASP) that mediate filopodia formation through activation of the actin polymerization factor Arp2/3. At the same time, Rac1 stimulates WASP family verprolin homologous protein 1 or 2 (WAVE 1/2) that promote activation of the Arp2/3 complex and lamellipodia polymerization (Spiering and Hodgson, 2011).

In literature, some studies demonstrate the relevance of these factors in adipogenesis. Jung and colleagues show that downregulation of Cdc42 in human adipose-derived stromal/stem cells (hADSCs) causes adipogenic differentiation inhibition, compromising lipid accumulation and the expression of the main adipogenic gene (Jung et al., 2014). Another study demonstrates that RhoGDIβ, a negative regulator of Rho family GTPases, is downregulated by BMP4 in C3H101/2 cells during adipocytes differentiation. Overexpression of this proteins prevents BMP4-induced adipocytes' commitment and induces muscle-like differentiation. Furthermore, Authors show that Rac1 is activated in response to BMP4 and, forcing its expression, Rac1 disrupts stress fibers and recovers the adipogenic phenotype in cells overexpressing RhoGDIβ (Huang et al., 2015).

Additionally, another factor involved in the assembly of the cortical actin cytoskeleton during adipogenesis is actin-related protein 2/3 (Arp2/3). Arp2/3 plays a crucial role in the generation of branched actin networks and changes its localization during adipocytes differentiation progress. At day 0, this complex is distributed on total cell body while at day 2 and 3 starts to accumulate at the cells' periphery, located near the F-actin patches. To verify this relation between Arp2/3 and cortical actin formation, Yang and colleagues generate knockdown of Arp3 in 3T3-L1. There are no significant changes in Arp3-KD cells in the initial steps of adipogenesis, indicating that Arp3 depletion does not modulate the adipogenic transcriptional factors. However, in Arp3-KD cells is observed a cortical actin remodeling inhibition on days 4 and 7 resulting in a decrease in lipid accumulation and in the expression of adipogenic marker (W. Yang et al. 2014b).

In conclusion, taken together, all these results show that actin cytoskeleton remodeling is fundamental to adipogenesis.

1.3.3 THE PROTEIN SYNTHESIS MACHINERY

Translation is a process that allows the synthesis of protein from mRNA and proceeds in three main phases: i) initiation, ii) elongation, and iii) termination. This process takes place inside the ribosome that translates the code of mRNA into specific amino acid sequences. Regulation of translation plays an important role in controlling cell growth, proliferation, and differentiation and is also involved in the commitment of MSCs. The first step of translation is recruiting of the small ribosomal subunit (40s) to mRNA and the identification of the start codon (Met-tRNA). Eukaryotic translation initiation factor (eIF) 4E (eIF4E) binds the 5' cap of mRNA and is a component of eIF4F complex, composed of two other subunits, eIF4G and eIF4A. The biological activity of eIF4E can be regulated by eIF4E-binding proteins (4E-BPs) that bind eIF4E, thus preventing its interaction with eIF4G. 4E-BPs are a family of three small proteins that are competitive ligands of eIF4G on a common binding site, located on eIF4E. 4E-BPs binding to eIF4E is reversible, and it depends on the phosphorylation status of 4E-BP. Hyperphosphorylation of 4E-BP1 provokes the release eIF4E leading to increased translation activity, instead 4E-BP1 hypophosphorylation support the binding to eIF4E resulting in cap-dependent mRNA translation inhibition (Gingras et al., 1999). Exposing cells to extracellular stimuli affects hyper or hypophosphorylation of 4E-BP1. Gingras and colleagues propose a two-step model for 4E-BP1 phosphorylation: firstly, FRAP and mTOR phosphorylates Thr-37 and Thr-46 on 4E-BP1 complexed with eIF4E, subsequentially, extracellular stimuli induce Ser-65 and Thr-70 phosphorylation. This latter step is required for the release of eIF4E and the beginning of translation (Gingras et al., 1999). Importantly, mutation of Thr37 and Thr46 to

alanines completely prevents the dissociation of eIF4E/4E-BP1 complex, mutation of Thr70 alone largely prevents dissociation while mutation of Ser65 to alanine does not affect the release of eIF4E (Gingras et al., 2001).

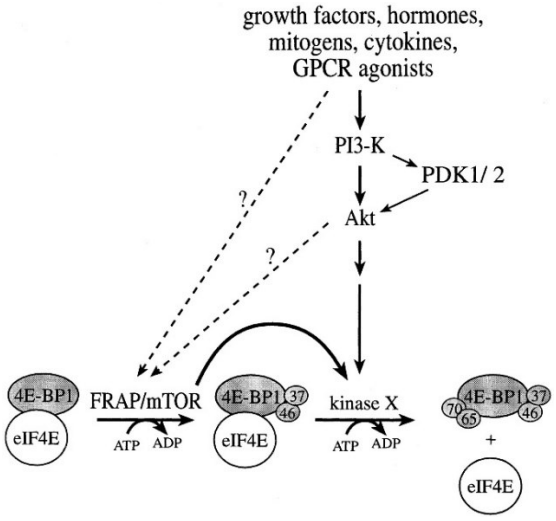

Figure 1.8: 4E-BP1 phosphorylation enhance translation process, releasing eIF4E and allowing the translation process to begin. Figure from Gingras et al. 1999.

Marcon and colleagues show that this process is also essential in the adipogenic process. During the early phase of adipogenesis, they observed an increase in the amount of hypophosphorylated 4E-BP1, which correlates with the downregulation of protein synthesis in hADSCs induced to adipocytes differentiation (Marcon et al., 2017). In addition, Eif4ebp1$^{-/-}$ (4E-BP1 KO mice) show a decrease in body weight compare to the control group, but this difference is not due to hypophagia because food intake does not change. Researchers have discovered a considerable reduction in WAT weight and the level of circulating leptin in Eif4ebp1$^{-/-}$ mice (Tsukiyama-Kohara et al., 2001).

In conclusion, 4E-BP1 and the inhibition of translational program are mediators of adipogenesis and adipose tissue development.

1.3.4 *IN VITRO* MODELS TO STUDY ADIPOGENESIS

There are many cellular models of pre-adipocytes that have allowed us to understand the adipogenic process's molecular mechanism. All these cell models have a fibroblast-like morphology during proliferation. After exposure to adipogenic stimuli, pre-adipocytes change their phenotype, become spherical, accumulate lipids, and acquire many typical characteristics of differentiated adipocytes in vivo. Two different types of cell lines are available: pre-adipocytes cell lines, already committed to adipocytes lineage, and multipotent stem cell lines, that can differentiate into different lineages, including adipose, bone, or muscle cells (Armani et al., 2010).

The most frequently used pre-adipocytes lines are 3T3-L1 and 3T3-F442A cells, isolated from the Swiss 3T3 mouse embryos (Green and Meuth, 1974). These cells are homogeneous and are all at the same differentiation stage and can be passaged indefinitely. 3T3-L1 spontaneously differentiate over several weeks into fat-cell when maintained in culture medium with fetal calf serum, and this process can be accelerated by inducing agents (differentiation cocktail) such as dexamethasone, IBMX and high insulin concentration (Gregoire et al., 1998). 3T3-F442A cells are generally used as a model with a more advanced commitment than 3T3-L1, and for this reason, they do not require glucocorticoids into the differentiation cocktail (Gregoire et al., 1998).

Also, multipotent stem cell lines can differentiate to adipocytes *in vitro*. C3H10T1/2 cells derive from 14 to 17-day-old C3H mouse embryos and do not differentiate spontaneously into adipocytes. These cells can differentiate into mature adipocytes using bone morphogenic protein 4 (BMP4) or adipogenic cocktail containing glucocorticoids, IBMX, insulin, and PPARγ agonist (Tang et al., 2004). Furthermore, adipocyte precursors can also be isolated from adult WAT of various species (i.e., human, mouse) and can be differentiated *in vitro* into mature

adipocytes. The use of primary adipocytes cultures presents several advantages, such as the possibility to support data obtained from immortalized cell lines with a more physiological model. On the other hand, their collection from mouse tissue (fat pads) is challenging, since a large amount of fat tissue is required to achieve a good yield of pre-adipocytes, which are presented in a small percentage. Furthermore, primary cultures have a limited life span, do not undergo continuous passage, and aging of animals can negatively impact terminal differentiation (Armani et al., 2010).

1.4 THE MITOCHONDRIA

Mitochondria are cytoplasmatic organelles involved in many cellular processes. They are also called the *powerhouse* of the cell because of their ability to generate chemical energy inside the cells. Mitochondria are commonly between 0.75 and 3 μm^2 in area, and their number and morphology can vary in different cell types and tissues. This organelle is characterized by two different membranes composed of phospholipid bilayer and proteins: the outer mitochondrial membrane (OMM) and the inner mitochondrial membrane (IMM).

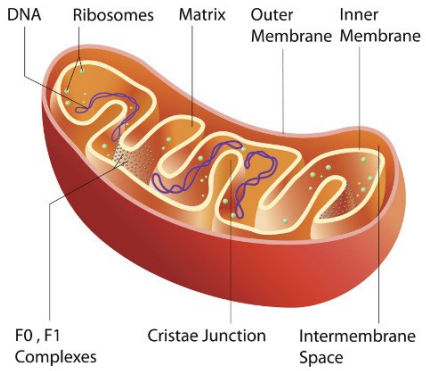

Figure 1.9: Mitochondrial structures. Mitochondria are composed by two membrane: inner and outer membranes, causing the formation of intermembrane space, the crista space, and the matrix. Figure from https://biologywise.com/mitochondrial-function

These two membranes create different compartments inside the mitochondrion: I) the intramembrane space located between the outer and the inner membranes, II) the cristae formed by infoldings of the IMM and III) the matrix which is the space within the IMM (Fig. 1.9). The endosymbiotic hypothesis suggests that mitochondria were prokaryotic cells, α-proteobacteria, that became endosymbionts living inside the eukaryote cells and maintaining some characteristics as their genome and limited translation machinery. Mitochondrial DNA (mtDNA) is presented in multiple copies in the matrix, organized into nucleoids, and reduced during evolution, transferring mitochondrial gene to the nuclear DNA (nDNA). mtDNA is circular and double-strand DNA molecule of about 16.5 kb in vertebrates and encodes 37 genes: 13 for the synthesis of proteins which serve as subunits of the respiratory chain (complex I, III, IV, and V; complex II is composed of proteins encoded by nuclear DNA), 22 for tRNAs and 2 for rRNAs that are essential for translation of mtDNA (Chan, 2006). In this context, the presence of Transcription Factor A (TFAM), the nuclear-DNA encoded gene that enhances both transcription and replication of mtDNA, is important. It is required to maintain the normal levels of mtDNA and play a role in the organizing and repairing of mitochondrial DNA. However, mitochondria depend on the cell to function correctly, and nuclear DNA encodes many mitochondrial proteins. For example, enzymes of different catabolic pathways localized in mitochondria and mtDNA replication and transcription machinery are encoded by nDNA. The mitochondrial nuclear-encoded proteins are synthesized in cytosolic ribosomes and successively imported into mitochondria (Taanman, 1999).

The main functions of mitochondria are energy (ATP) production and the control of energy metabolism. Furthermore, these organelles are involved in heme synthesis, iron-sulfur clusters biosynthetic pathway, apoptosis, calcium homeostasis, and many other cellular processes.

1.4.1 ENERGY METABOLISM AND ATP PRODUCTION

Energy metabolism can be defined as the combination of reactions involved in the generation of adenosine triphosphate (ATP) from nutrients. ATP is a source of energy, utilized from cells and tissue to perform their functions. It is obtained by the oxidation of the energetic substrate (i.e., glucose, fatty acids) through different metabolic pathways (i.e., glycolysis, β-oxidation, tricarboxylic acid (TCA) cycle, oxidative phosphorylation (OXPHOS)). Glycolysis is a cytoplasmatic pathway that is necessary for the conversion of glucose into pyruvate. The yield for each glucose molecule is two molecules of pyruvate, two ATP, two NADH, and two H^+. At this point, pyruvate can be transported across the inner mitochondrial membrane and into the mitochondrial matrix. Here, it can be metabolized and combined with coenzyme A to form acetyl-CoA, that is the starting point for the TCA cycle. TCA cycle is composed of ten different reactions, and the products of one turn are one GTP, three NADH, one QH_2, one $FADH_2$ and two CO_2. Also, fatty acids are transported into the mitochondria to be metabolized through β-oxidation and generate acetyl-CoA that can be used in the TCA cycle. Then, NADH and $FADH_2$, are used as electron carriers that donate electrons to the OXPHOS. This pathway occurs in mitochondria and is composed of five complexes (complex I to V): the first four complexes represent the electron transport chain (ECT) while the complex V is the ATP synthase. ATP synthesis is not an energetically favorable reaction, and the energy derives from the oxidation of NADH and $FADH_2$ by ETC. Electrons are transferred from electron donors to electron acceptors: electrons are passed from NADH to ETC complex I and from $FADH_2$ to ETC complex II. Electrons from complex I and II flow through complex III and arrive at complex IV, where they are transferred to a molecule of oxygen to form water. Electrons' movement through the complexes is used to pump the protons out into intramembrane space, creating a proton electrochemical gradient. The gradient created drives protons back in the mitochondrial matrix through the ATP synthase, which utilizes protons' flow to synthesize ATP.

Except for glycolysis and fatty acids synthesis, the other main metabolic pathways take place in mitochondria, and, for this reason, mitochondria activity affects metabolic function.

1.4.2 MITOCHONDRIA DYNAMICS

Mitochondria are dynamic organelles that can change their morphology, number, and intracellular distribution in response to external cues. Mitochondria rearrange their structure through two different processes, fusion and fission, and the balance between these two events controls not only mitochondrial morphology but also mitochondrial activity and function. Critical regulators of mitochondrial dynamics consist of three GTPases that fuse and divide the mitochondrial membranes. Mitochondrial fusion is a complex biological process consisting of the union of two mitochondria resulting in one mitochondrion and requires the action of mitofusin 1 and 2 (Mfn1 and 2) and optic atrophy 1 (OPA1), which control OMM and IMM fusion, respectively. On the contrary, mitochondrial fission leads to the division of one mitochondrion into two daughter mitochondria, and this process is carried out by the dynamin-related/-like protein 1 (Drp1) (Tilokani et al., 2018). Recent data show that mitochondrial dynamics are involved in the regulation of cellular metabolism. Mitochondrial fusion increases in energy demand state, whereas mitochondrial fragmentation is induced by nutrient excess, cellular dysfunction, and favors mitophagy, the autophagic clearance of mitochondria (Wai and Langer, 2016).

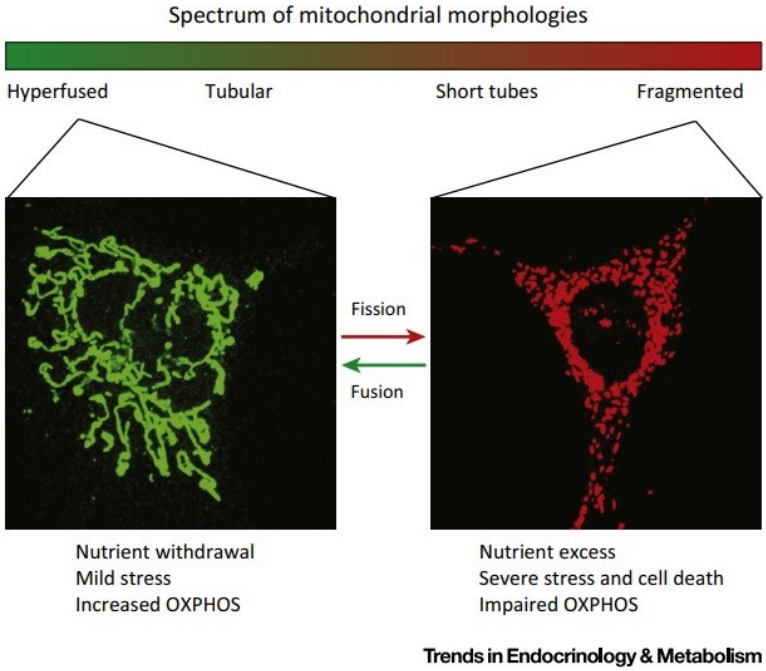

Figure 1.10: Mitochondrial morphology is also controlled by metabolic stimuli. Nutrient excess is linked to fragmented mitochondrial while nutrient withdrawal is connected with hyperfused morphology. Figure from Wai and Langer 2016.

In vivo and *in vitro* studies show that fasting causes elongation of mitochondria while obesity causes mitochondrial fission in skeletal muscle of mice and high levels of saturated FAs provokes the same result in cultured muscle cells (C2C12). The inhibition of mitochondrial fission protects these cells against mitochondrial dysfunction and insulin resistance (Jheng et al., 2012).

During fusion and fission processes, there is not only the merge or division of OMM and IMM, but also mitochondria matrix components are redistributed among the different organelles, protecting mitochondria for example from mtDNA mutation. In the absence of fusion events, these deficiencies persist and cause mitochondria dysfunction. For this reason, a block in the fusion event gives rise to small and fragmentated mitochondria that completely lack mtDNA or are enriched with mutant mtDNA. These mitochondria lose their functional electron transport chain and have a compromised oxygen consumption rate (Chen et al., 2005a; McBride et al.,

2006). The inability to perform fusion events leads to reduce metabolism, and Bach and Colleagues show that Mfn2 is crucial to maintain mitochondrial network and metabolism. Downregulation of Mfn2 reduces mitochondrial network and decreases mitochondrial membrane potential, glucose oxidation, and cellular oxygen consumption in skeletal muscle cells (Bach et al., 2003) and represses nuclear-encoded subunits of OXPHOS complexes (Pich et al., 2005). Conversely, overexpression of Mfn2 enhances mitochondrial membrane potential, increase the rate of glucose oxidation, and the expression of subunits of the OXPHOS system (Pich et al., 2005). Furthermore, other studies show that the cells in which both Opa1 and both Mfn (1 and 2) are downregulated, present fragmented mitochondria with reduced oxygen consumption rate (Chen, Chomyn, and Chan 2005).

In the maintenance of the mitochondrial network and structure, dynamic interactions between mitochondria and cytoskeleton play an important role. The three main components of cytoskeleton (microtubules (MT), actin fibers, intermediate filaments) are also involved in mitochondrial movement and distribution (Anesti and Scorrano, 2006). Actin polymerization and depolymerization act to regulate steady-state mitochondrial morphology: polymerization promotes fission events and inhibits mitochondrial fusion. On the other hand, actin depolymerization regulates mitochondrial network formation and allows mitochondrial fusion. Shorter, smaller, and less tubular mitochondria are usually associated with actin filaments whereas, more elongate, tubular, and interconnected mitochondria are not related with actin cytoskeleton. Moreover, morphological analysis shows that Phalloidin-positive mitochondria (actin-bind mitochondria) are more fragmented than mitochondria not associated with actin (Moore et al., 2016). Mitochondria can also interact with microtubules through microtubule-associated proteins (MAPs) that control MT polymerization and function, bind the OMM, and are responsible for movement along MT of mitochondria (Leterrier et al., 1994; Nogales, 2000).

1.4.3 MITOCHONDRIA IN ADIPOGENESIS

Mitochondria are fundamental organelles for adipocytes' correct functioning: they control differentiation, lipid accumulation, insulin sensitivity, and thermogenesis in brown adipose tissue. During adipocytes differentiation, there is an increase in mitochondrial biogenesis to get the energy needed to complete this process correctly. There is also an increase in mitochondrial proteins and a qualitative change in the composition of mitochondria themselves that lead to greater lipid accumulation and, therefore, allows these cells' function to be carried out.

Forni and colleagues show that during adipogenesis, there is an increase in the expression of PGC1a, mitochondrial biogenesis marker, and an increase in mtDNA, mitochondrial mass marker. They also analyzed the mitochondrial dynamics during the commitment toward differentiation. As previously explained, mitochondria morphology is mediated by fusion (Mfn1, Mfn2, Opa1) and fission (Drp1) regulators. During the adipogenic process, the expression of Mfn1 and Mfn2 increases while Opa1 and Drp1, mitochondrial fission marker, does not change (Forni et al., 2016). It has been established that morphological changes in mitochondria are correlated to functional alterations. For instance, during adipocyte differentiation, mitochondria undergo morphological changes that reflect on oxygen consumption rate, which is increased in differentiated adipocytes compared to pre-adipocytes. Surprisingly, ATP levels in mature adipocytes are lower than in pre-adipocytes; however, it could be argued that mature adipocytes consume a big amount of ATP during lipogenesis.

During pre-adipocytes differentiation, TCA cycle generates the reducing cofactors used within the respiratory chain and allows the complete oxidation of mitochondrial acetyl-CoA.

Zhang and colleagues treated hMSCs with rotenone during adipocytes differentiation. Rotenone inhibits the transfer of an electron from the iron-sulfur center in complex 1 to ubiquinone. Treatment with rotenone causes decreased OCR (oxygen consumption rate) and negatively

impact lipid accumulation(Zhang et al., 2013). These results show that proper mitochondrial functioning is necessary to have completely differentiated adipocytes.

1.4.4 RNA-BINDING PROTEIN AS MITOCHONDRIAL REGULATORS

Physiological and pathological stimuli such as stress, aging, and energy demand, can influence mitochondrial morphological, function, and even mitochondrial mass. Mitochondria respond dynamically to these changes, and to do this, it is essential gene expression regulation that allows them to maintain the correct mitochondrial function. This mitochondrial plasticity depends on transcription or post-transcription mechanisms. Over the years, several transcription factors have been identified as mediators of the nuclear and mitochondrial gene expression. Among them, Tfam is a well-known mitochondrial transcription factor that binds the mitochondrial DNA and regulates its stability and replication. Other examples are nuclear respiratory factors 1 and 2 (NRF-1, NRF-2), which can be defined as "indirect regulators" because they regulate the transcription of nuclear-encoded genes important for mitochondrial function and biogenesis (Leigh-Brown et al., 2010).

Post-transcriptional mechanisms can coordinate faster and more flexible responses than transcriptional responses. In this context are included the RNA-binding proteins (RBP) that regulate mRNA metabolism and function by modulation splicing, stability, localization, and the maturation of the mRNA. RBPs act as mitochondrial regulators by modulating a mitochondrial specific RNA to adjust mitochondrial function under environmental conditions. Schatton and colleagues reported the list of RBPs regulating mRNAs encoding mitochondrial proteins (Table 1) and described their function and localization (Schatton and Rugarli, 2018). For example, Clu1/CluA homolog (CLUH) is a cytoplasmatic protein that acts as RBP. It has been demonstrated that bind a subset of mRNAs encoding mitochondrial proteins, and its depletion

decreased the levels of proteins translated by target mRNAs (Gao et al., 2014). Furthermore, it is reported that RBPs misregulation or mutation may cause mitochondrial damage and dysfunction (Ravanidis and Doxakis, 2020).

1.5 ZINC FINGER CCCH-TYPE CONTAINING 10 (Zc3h10)

Zc3h10 is a poorly characterized protein belonging to the CCCH (Cys-Cys-Cys-His) zinc finger family. Zc3h10 is localized in chromosome 12 and consists of 3 exons and 2 introns. The coding sequence (CDS) is present only in exon 3 and is highly conserved among different species. This protein consists of 434 amino acid residues (molecular weight of 46KDa), and it contains a glycine-rich domain and three different zinc finger (CCCH) motifs in N-terminal portion, and a proline-rich domain in C-terminal portion. A proline-rich domain usually mediates protein-protein interactions, suggesting that this protein may form a complex with other proteins. Zinc finger proteins can interact with nucleic acids and are known as DNA-binding proteins, but different studies showed that zinc finger domain could also mediate interaction to RNA, proteins, and lipids (Liang et al., 2008). During proteomic screen, Treiber and colleagues identified a specific interaction between Zc310 and pri-miR-143. They defined that the first two zinc fingers are essential for the interaction and reported the binding motif of Zc3h10: 5'-GCAGCGC-3'. Any mutation in the binding motif disrupted the interaction (Treiber et al., 2017). Additionally, it has been described as an RNA-binding protein that can bind mRNA in Hela cells (Castello et al., 2012).

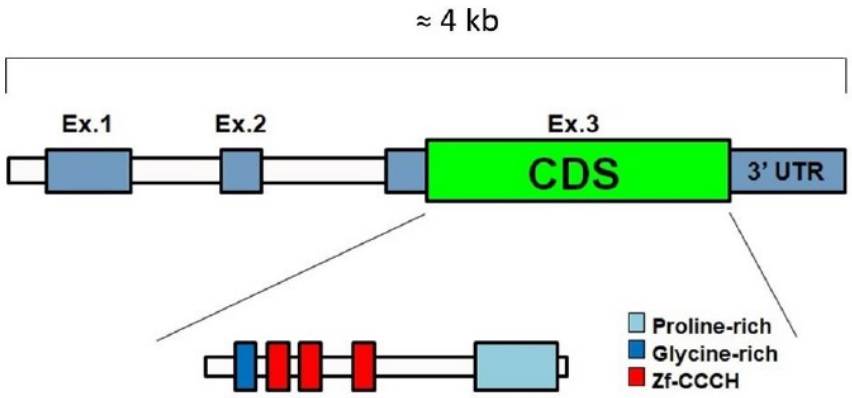

Figure 1.11: Schematic representation of the structure of Zc3h10. The protein is encoded by exon 3 and has a region rich in proline, a site rich in wisteria and 3 domains zinc finger type CCCH.

Using a genome-wide functional screen followed by assay of mitochondrial activity, this protein has been identified as a new mitochondrial regulator. Briefly, 16000 genes were individually transfected into HEK293 cells with a luciferase reporter to evaluate their ability to control Tfam promoter activity. From primary screen, 440 cDNAs (384 positives and 92 negatives) have been selected because they can modulate Tfam promoter activity and are expressed in metabolic tissues. These selected hits have been evaluated in secondary screen, assessing mitochondrial density and function. This analysis generated 126 positive and 32 negative hits, which have been limited by selecting only those expressed in the skeletal muscle and C2C12 cells, and those hits are still not associated with mitochondrial biology. These 21 positive hits were overexpressed into C2C12 cells, and the increase in mtDNA and basal respiration were assessed. After this screen, the best hit which controls mitochondrial function turned out to be Zc3h10 (Audano et al. 2018).

Recent studies have highlighted the involvement of Zc3h10 in the regulation of mitochondrial function and its impact on the differentiation processes in myoblasts (Audano et al., 2018) and brown adipocytes (Yi et al., 2019). It has been shown that the expression of Zc3h10 increases during myoblast differentiation into myotubes, parallel to mtDNA content, Tfam, and Oxphos

expression. Overexpression of this protein boosted mitochondrial activity and stimulated myotubes formation while Zc3h10 knockdown resulted in decreased expression of some Oxphos subunits, in mitochondrial activity, and delayed myotubes formation. Furthermore, a single nucleotide polymorphism (SNP) has been found in the coding sequence of Zc3h10. This mutation converts tyrosine (Tyr; Y) 105 into cysteine (Cys; C) and is classified as a loss-of-function mutation. Human homozygotes for this mutation have increased BMI, fat mass, changed fat distribution, and altered mitochondrial function in PBMCs (Audano et al. 2018).

Recently, a link between Zc3h10 and adipose tissue has also been demonstrated. Yi and colleagues have identified Zc3h10 as a DNA-binding transcription factor that causes transcriptional activation of UCP1 in mouse brown adipose tissue. Overexpression of this protein causes the increased expression of some genes involved in thermogenesis, while its silencing has the opposite effect and leads to weight gain. Besides, they have shown that Zc3h10 can bind the regions of the Tfam promoter and Nrf1 always through the binding with DNA. Phosphorylation of Zc3h10 at S126 by P38 MAPK is required to increase Zc3h10 binding to the UCP1 promoter and its activation. They show that sympathetic stimulation determines the phosphorylation of Zc3h10 at the Ser126 level by MAPK, and this post-translational modification induces the link to the distal regulatory region upstream of UCP-1. This protein-DNA interaction appears to be independent of the zinc finger domains but seems to involve a leucine zipper domain (bZIP) present at the end C-terminal (Yi et al., 2019).

2. AIM OF STUDY

In the last 50 years, the frequency of obesity has increased worldwide to pandemic proportions, and for this reason, the study of adipose tissue has attracted a lot of interest (Abarca-GÃ et al., 2017; Blüher, 2019; Yanovski, 2018). Initially, the adipose tissue was considered a form of connective tissue containing lipid droplets without connecting it to the body's metabolism in any significant way. It has recently been studied as a tissue that plays a crucial role in nutrient homeostasis as a site of energy storage. Furthermore, its function as an endocrine organ at the center of energetic homeostasis has also been discovered (Rosen and Spiegelman, 2014).

Adipocytes are the main constituent of adipose tissue, and their primary function is to control the energy balance by storing triacylglycerol in periods of excess energy and mobilizing it during the energy deprivation. Adipogenesis is a multistep process that requires the sequential activation of numerous transcription factors to allow the generation of mature adipocytes from mesenchymal precursor (Ali et al., 2013). Although several factors involved in this process have been identified, many of the molecular mechanisms underlying adipogenesis are still unknown.

Mitochondria are cytoplasmic organelles responsible for energy production and play a key role in the adipocyte differentiation process. During adipogenesis, an increase in the cell's energy needs is observed, which is why an increase in mitochondrial biogenesis is reported. In addition, mature adipocytes need active mitochondria to produce large ATP amounts to regulate the intracellular balance of TG (i.e., fatty acid synthesis and oxidation processes) (De Pauw et al., 2009a).

A new mitochondrial regulator has been identified in our laboratory: the protein Zc3h10. In literature, it is reported that Zc3h10 plays a key role in the differentiation of myocytes to myotubes by going to regulate cellular metabolism (Audano et al., 2018). Recently, a study has

also been conducted in brown adipose tissue, and the Authors have shown that Zc3h10 can activate the transcription of ucp1 activating the thermogenic process (Yi et al., 2019).

On these bases, this project aims to characterize the role of Zc3h10 in MSC differentiation to white adipocyte. Specifically, this study has been conducted to understand the molecular mechanism by which this protein exerts its effect on adipogenesis.

3. MATERIALS AND METHODS

3.1 Cell lines and animal models

C3H10T1/2 murine mesenchymal stem cells (MSCs, ATCC CCL-226) were maintained in growth medium high-glucose DMEM supplemented with 10% fetal bovine serum (FBS) (v/v) (Euroclone), 1% glutamine (v/v) (Thermo Fisher Scientific), 1% pen/strep (v/v) (Thermo Fisher Scientific) and in 37°C, 5% CO2 and 90% humidified atmosphere. C3H10T1/2 cells were differentiated to adipocyte 24 hours after reaching complete confluence. Growth medium was then switched to differentiation medium composed by 10% FBS (v/v), 1% glutamine (v/v), 1% pen/strep (v/v), insulin 5µg/ml (Sigma-Aldrich), dexamethasone 2µg/ml (Sigma-Aldrich), 3-isobutyl-1-methylxanthine (IBMX) 0.5mM (Sigma-Aldrich) and rosiglitazone 5µM (Cayman Chemicals). After three days, pre-adipocytes were maintained in complete media supplemented with insulin 5µg/ml for 6 days till complete differentiation. Below is the experimental protocol used for the differentiation of MSCs into mature adipocytes.

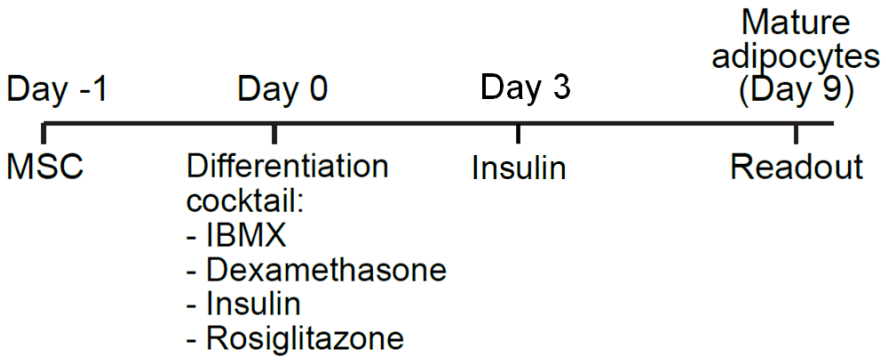

Figure 3.1: Experimental protocol used to differentiate murine mesenchymal stem cells to mature white adipocytes.

Primary Stromal Vascular Cells (SVC) were isolated from inguinal and epididymal white adipose tissue of C57BL6/J male mice. Tissues were minced to a very fine consistency and then incubated in HEPES solution (NaCl 150mM, KCl 62.5mM, D-Glucose 6.2mM, Bovine Serum

Albumin (BSA) 2% (w/v), $CaCl_2$ 1.2mM, pH 7.6) containing 1mg/ml of Type II Collagenase (Sigma Life Science, C6885) for 1 hour at 37°C in shaking (115rpm). Digested fat solution was then poured through 100µm cell strainer and centrifugated 200g for 10 minutes at RT to remove collagenase solution and mature adipocytes. Then cells were incubated with erythrocyte lysis buffer (NH_4Cl 155mM, K_2HPO_4 5.7mM, EDTA 0.1mM) for 5 minutes, and the suspension was then filtered through 100µm cell strainer and centrifugated as above. The supernatant was discarded and pellet containing stromal vascular cells was resuspended in 10ml of plating medium (DMEM/F12 (Thermo Fisher Scientific) supplemented with 10% FBS (v/v) (Euroclone), 1% glutamine (v/v) (Thermo Fisher Scientific), 1% pen/strep (v/v) (Thermo Fisher Scientific), 1% Na-pyruvate (v/v) (Thermo Fisher Scientific). To remove endothelial cell clumps, cell suspension was filtered through 40µm cell strainer. 24 hours after confluency, growth medium was then switched to differentiation medium composed by 10% FBS (v/v), 1% glutamine (v/v), 1% pen/strep (v/v), 1% Na-pyruvate (v/v), insulin 10µg/ml (Sigma-Aldrich), dexamethasone 1µM (Sigma-Aldrich), IBMX 0.5mM (Sigma-Aldrich) and rosiglitazone 0.5µM (Cayman Chemicals). After 48 hours, pre-adipocytes were maintained in complete media supplemented with insulin 1µg/ml for 6 days till complete differentiation. All experiments were conducted following the ARRIVE guidelines and regulations of the European Community (EU Directive 2010/663/EU, Official Journal of the European Union L 276/33, 20/10/2010) and local regulations (Italian Legislative Decree n. 26—04/03/2014) for the care and use of laboratory animals. The Italian Ministry of Health approved the animal protocols of this study (ministerial decree n. 579/2015-PR).

3.2 Adenoviral transduction for gene overexpression and downregulation

Zc3h10 overexpression in C3H10T1/2 MSCs was performed in confluent cells (Day 0) by adding adenoviral vectors (Human Adenovirus Type 5 dE1/dE3) in differentiation medium and exposing cells to vector for 3 days or 36h where indicated. Validated adenoviral vector carried mouse Zc3h10 cDNA fused together with a Flag-tag at the C-terminal (Zc3h10-Flag) controlled by a CMV promoter (Vector Biolabs, ADV-276549). As a control, we used the same construct expressing the GFP under the control of CMV promoter (Control Vector) (Vector Biolabs, 1768). Zc3h10-Flag and GFP were overexpressed at a multiplicity of infection (MOI) of 25. Zc3h10 targeted silencing in C3H10T1/2 MSCs was carried out as above. Validated adenoviral construct contained specific short hairpin RNA sequence under a U6 promoter (shADV-276549), while the control vector contained a scrambled sequence (Vector Biolabs, 1122). To silencing Zc3h10, cells were infected with 50 MOI scramble or shZc3h10 adenovectors.

3.3 Cytoplasm-Nucleoplasm-Chromatin separation

36 hours after differentiation induction, C3H10T1/2 MSCs were collected for cytoplasm, nucleoplasm, and chromatin protein extraction. All centrifugations were performed at 4°C and samples were kept on ice throughout all the procedures. Cells were rinsed with ice-cold PBS and suspended in 300µL of cytoplasmatic lysis buffer (Tris-HCl pH 7.5 10mM, NaCl 150mM, NP-40 0,15% (v/v)) and incubated for 5 minutes on ice. Lysates were layered on the top of 750µL of a chilled sucrose cushion (24% (w/v) of sucrose in Cytoplasmatic lysis buffer without NP-40) and centrifugated at 18000g for 10 minutes. The supernatant contained cytoplasmatic protein fraction. Then nuclei pellet were resuspended in 300µL of cold glycerol buffer (Tris-HCl pH 7.9 20mM, NaCl 75mM, EDTA 0.5mM, DTT 0,85mM, glycerol 50% (v/v)) and then has been added 300µL of nuclei lysis buffer (Hepes pH 7.6 20mM, $MgCl_2$ 7.5mM, EDTA 0.2mM, NaCl

300mM, urea 1M, NP-40 1% (v/v), DTT 0.1mM). Samples were incubated on ice for 1 minute and then were centrifugated at 18000g for 2 minutes. The supernatant contained nucleoplasmic protein fraction. Chromatin pellet was resuspended in 50µL of PBS and was used for chromatin-associated proteins analysis. Proteins were then equally loaded on SDS-PAGE.

3.4 Total DNA and mitochondrial DNA quantification

Total genomic and mtDNA were isolated using genomic DNA from tissues kit (Macherey-Nagel, 740952/250). Briefly, cells were lysed in 200µL of Buffer T1, and then DNA was isolated following the manufacturer's instructions. Samples were eluted in 100µl of DNase and RNase free water and quantified by UV spectrophotometry (NanoDrop 1000 Spectrophotometer, Thermo Fisher Scientific). Mitochondrial DNA content was evaluated by assessing mt-Co2 and 36B4 content as mitochondrial and nuclear-encoded genes, respectively. Primers and probes were obtained from Eurofins Genomics MWG-Operon and are available upon request.

3.5 Gene expression analysis

Total RNA was obtained from C3H10T1/2 cells by a commercial kit (NucleoSpin® RNA extraction kit, Macherey-Nagel, 740955.250). Briefly, cells were washed in ice-cold PBS and lysed in 350µL of lysis buffer (RA1) supplemented with 1% (v/v) β-mercaptoethanol. Total RNA was then isolated by following manufacturer's instructions and eluted from columns with 60µl of RNase free water. Total RNA amount was then quantified by UV spectrophotometry (NanoDrop 1000 Spectrophotometer, Thermo Fisher Scientific). Samples were then diluted to 10ng/µl and used for mRNA quantification. RNA was quantitated by qRT-PCR using iScriptTM One Step for Probes (Bio-rad, 1725141) and iTaq Universal SYBR Green One-Step Kit for qPCR

(Bio-rad, 1725151), following the manufacturer's instructions. The qRT-PCR protocol is made up of 40 cycles of amplification, each consisting of a denaturation step at 95° C for 15 seconds and an annealing/extension step at 60° C for 60 seconds. The oligonucleotides used for qRT-PCR were obtained from Eurofins MWG Operon (Ebersberg, Germany). qRT-PCR primers sequences are available upon request.

3.6 Microarray analysis

Microarray analysis for whole transcriptome analysis was performed using a MoGene 2.0 chip. Briefly, differentiated adipocytes (day 9) were rinsed in 1 ml of ice-cold PBS. Total RNA was isolated as described above, and 3µg of RNA were used for the following analyses. Total RNA concentration and purity were assessed by UV spectrophotometry (NanoDrop 1000 Spectrophotometer, Thermo Fisher Scientific). Total RNA integrity was assessed by Agilent Bioanalyzer, and the RNA Integrity Number (RIN) was calculated before differential gene expression evaluation. C3H10T1/2 RNA was analyzed by the Genopolis Consortium (Italy) using an Affimetrix platform.

3.7 RNA synthesis assay

4-thiouridine (4sU, Sigma Aldrich, T4509) labeled RNA isolation was performed as previously described (Rabani et al., 2011). Briefly, 300µM 4-thiouridine was used for 10 minutes labeling in confluent 36h differentiated scramble and shZc3h10 pre-adipocytes. Total RNA extraction was described above, and 1/50 of total RNA was saved as input. The labeled RNA was isolated and processed as described (Austenaa et al., 2015). Briefly, the nascent 4sU-labelled RNA was extracted from 50µg of total TRIZOL-isolated RNA, conjugated to biotin-HPDP (Abcam) and

precipitated with 50µl of streptavidin (MyOne Steptavidin T1, Invitrogen). 4sU RNA samples were eluted in 20µl of RNase-free water and analyzed by next-generation sequencing. 20-30ng of the isolated nascent 4sU-labelled RNA was used for cDNA-library synthesis using the QIAseq Stranded Total RNA Lib Kit (Qiagen, 180745) with no ribosomal depletion or polyA-selection.

3.8 Western blot

Protein relative quantification analyses were carried out by separating cell lysates on SDS-PAGE. Cells were rinsed in ice-cold PBS and lysed in RIPA buffer. Protein concentration was measured using BCA methods (Euroclone). The proper protein amount was then loaded on 12.5% SDS-PAGE. After gel run, proteins were transferred to a nitrocellulose membrane and blocked in 0,1% TBS-Tween20 and 5% (w/v) BSA for 1 hour at RT. Membranes were then incubated O/N at 4°C with primary antibodies, previously suspended in 0,1% TBS-Tween20 and 3% BSA. After extensive washes, membranes were incubated with HRP-conjugated secondary antibodies for 1 hour at RT. After washing, membranes were finally incubated with ECL substrate for bands detection. Primary and secondary antibodies were diluted as follows: Zc3h10 1:1000 (Aviva systems biology, ARP60671_P050), Tfam 1:500 (Aviva systems biology, ARP31400_P050), OXPHOS cocktail 1:2000 (Abcam, ab110413), Hsp90 1:1000 (Santa Cruz Biotech., sc-13119), β-actin 1:5000 (Sigma Aldrich, A5441), Histone H3 1:1000 (Millipore, 06-755), α-tubulin 1:1000 (Sigma Aldrich, T9026), Flag-M2 1:5000 (Sigma Aldrich, F3165), Pparγ 1:1000 (Cell Signaling, 2443S), Nup98 1:1000 (Cell Signaling, 2597s), 4E-BP1 1:1000 (Cell Signaling, 9644), Phospho-4E-BP1 (Thr37/46) 1:1000 (Cell Signaling, 2855), Phospho-4E-BP1 (Thr70) 1:1000 (Cell Signaling, 9455), DRP1 1:1000 (Cell Signaling, 14647), Phospho-DRP1 (Ser637) 1:1000 (Cell Signaling, 6319), Phospho-DRP1 (Ser616) 1:1000 (Cell Signaling, 4494), OPA1 1:1000 (Cell Signaling, 80471), Mitofusin-2 1:1000 (Cell Signaling, 9482), Anti-mouse

IgG, HRP-linked (Cell Signaling, 7076) and Anti-rabbit IgG, HRP-linked (Cell Signaling, 7074). Blots were quantified by ImageJ software.

3.9 Metabolite extraction and LC-MS/MS analysis

Cells were grown in 6-well plates, harvested in 250µl of ice-cold methanol/acetonitrile 1:1 containing [U-$^{13}C_6$]-Glucose 1ng/µl (internal standard, Sigma Aldrich, 389374) and [U-$^{13}C_5$]-Glutamine 1ng/µl (internal standard, Sigma Aldrich, 605166) and spun at 20,000g for 5 min at 4°C. The supernatant was then passed through a regenerated cellulose filter, dried, and resuspended in 100µl of MeOH for subsequent analysis. Amino acids quantification was performed through previous derivatization. Briefly, 50µl of 5% phenyl isothiocyanate (PITC) in 31.5% EtOH and 31.5% pyridine in water were added to 10µl of each sample. Mixtures were then incubated with PITC solution for 20 min at RT, dried under N_2 flow, and suspended in 100µl of 5mM ammonium acetate in MeOH/H2O 1:1.

The identity of all metabolites was confirmed using pure standards. Quantification of different metabolites was performed with a liquid chromatography/tandem mass spectrometry (LC-MS/MS) method using a C18 column (Biocrates) for amino acids, Pursuit XRs Ultra 2.8 Diphenyl (Varian, Palo Alto, CA, USA) for acyl-carnitine and cyano-phase LUNA column (50mm x 4.6mm, 5µm; Phenomenex) for metabolites, respectively. Methanolic samples were analyzed by a 10 and 3 min run in positive (amino acids and acyl-carnitine) and 5 min run in negative (all other metabolites) ion mode with a 35 multiple reaction monitoring (MRM) transitions in positive ion mode and 30 MRM transitions in negative ion mode, respectively. The mobile phases for amino acids analysis were: phase A: 0.2% formic acid in water and phase B: 0.2% formic acid in acetonitrile. The gradient was T0 100%A, T5.5min. 5%A, T7min 100%A with a flow rate of 500µl/min. The mobile phase for acyl-carnitine analysis was 0.1% formic acid in MeOH in

isocratic condition with a flow rate of 300µl/min. The mobile phases for negative ion mode analysis (all other metabolites) were: phase A: Water and B: 2mM ammonium acetate in MeOH. The gradient was 90%B for all the analysis with a flow rate of 500µl/min.

Metabolomic data were performed on an API-4000 triple quadrupole mass spectrometer (AB Sciex) coupled with an HPLC system (Agilent) and CTC PAL HTS autosampler (PAL System) and on SCIEX Triple QuadTM 3500 (AB Sciex). MultiQuant™ software (version 3.0.2) was used for data analysis and peak review of chromatograms.

Metabolomic data were normalized by defining x_n^N (relative metabolite area) as:

$$x_n^N = \frac{Xn}{\sum_{n=a}^{z} n}$$

where x_n represents the peak areas of metabolite *n* for samples *a, b, …, z* and $\sum_{n=a}^{z} n$ represents the sum of peak areas of metabolite *n* for samples *a, b, …, z.*

Relative metabolite area (x_n^N) was then divided by the sum of relative metabolite areas analyzed in each sample to obtain relative metabolite abundance (*m*), as:

$$m_a^N = \frac{x_n^N}{\sum_{a=1}^{n} a}$$

where $\sum_{a=1}^{n} a$ represents the sum of relative metabolite areas *1, 2, …, n* for sample *a.* Internal standards were used to control instrument sensitivity. ATP energy charge was calculated as $\frac{\text{ATP}+1/2\text{ADP}}{\text{ATP}+\text{ADP}+\text{AMP}}$.

For metabolic tracing analyses, two and eight days differentiated cells were exposed for 24 hours to [U-$^{13}C_6$]-Glucose 1mM (Sigma Aldrich, 389374) or [U-$^{13}C_5$]-Glutamine 2mM (Sigma Aldrich, 605166) or [U-$^{13}C_{16}$]-Palmitate 100µM (Sigma Aldrich, 605573). Metabolites quantification was performed as described above by increasing the MRM transitions in negative ion mode to 139 to analyze the different isotopomers

3.10 Glycerol release

A glycerol assay kit (#MAK117, Sigma-Aldrich) was used to quantify glycerol release by analyzing C3H101/2 cell culture supernatant samples from days 3 and 9. The assay was used according to the manufacturer's instructions. Briefly, 100 µl of Master Reaction Mix was added to 10 µl of cell supernatant and incubated for 20 minutes at room temperature. Then, the absorbance was measured at 570 nm. The concentration of glycerol has been determined using a standard curve.

3.11 Oxygen consumption measurements: Clark type oxygen electrode

Oxygen consumption rate (OCR) analysis on whole cells was performed using a Clark type oxygen electrode (Hansatech, DW1 electrode chamber). C3H10T1/2 cells were rinsed in pre-warmed PBS (37°C) and suspended in coupled respiration (CR) buffer (free fatty acids-BSA 2% (w/v), Na-pyruvate 1mM, D-glucose 25 mM, digitonin 40 ng/ml in PBS) or electron flow (EF) buffer (free fatty acids-BSA 2% (w/v), Na-pyruvate 10mM, malate 2mM, carbonyl cyanide m-chlorophenyl hydrazine (CCCP) 4µM, digitonin 40ng/ml in PBS). Samples were then transferred to the electrode chamber for the oxygen consumption rate measurement. After measuring basal respiration, uncoupled and maximal respiration were evaluated by adding 12.5µM oligomycin and 5µM CCCP, respectively. Complex I, II, and IV activities were evaluated through the electron flow protocol. Once transferred into the chamber, CI activity was evaluated. After 20µM rotenone and 1mM succinate addition, we assessed complex II activity. We then added 150µM antimycin A and 40mM/1.6mM Ascorbate/N, N, N', N'-tetramethyl-p-phenylenediamine (TMPD) to measure complex IV activity. All sample values were normalized on total protein content.

3.12 Cytofluorimetric analyses

3.12.1 Lipid accumulation analysis

Cells were grown in 12-well plates and exposed to AdipoRed™ assay Reagent (1:200, Lonza, PT-7009) for 15 minutes in the dark at 37° C. Successively, cells were washed and then harvested in 300µl of ice-cold PBS. Cells were analyzed with cytofluorimeter (Novocyte 3000, Acea, Agilent) at a wavelength of 572nm. The cytofluorometer settings for both side scatters (SSC) and forward scatters (FSC) were dependent on the analytic sensitivity of the machine. The voltages and compensation between scatters were set to the degree so that the majority control cells at day 0 were located below the scale of 10^5 for fluorochrome intensity.

3.12.2 Cell cycle analysis and cells count

Cells were grown in 6-well plates and exposed to Hoechst 33258 (1:500, Life Technologies) in DMEM for 45 minutes at 37° C in the dark. Successively, cells were wash and then harvested in 1200µl of ice-cold PBS. Cell suspension was analyzed with cytofluorimeter (Novocyte 3000, Acea, Agilent) at a wavelength of 445nm. The voltages and compensation between scatters were set to the degree so that the majority of control cells at day 0 were located above the scale of $10^{6.5}$ for fluorochrome intensity.

3.13 Confocal microscopy

Cells were cultured on Nunc glass-based dishes (27mm, Thermo Scientific, 150682) and analyzed at different differentiation stages. The medium was replaced, and cells were incubated with staining medium (High glucose DMEM without phenol red, without FBS and supplemented by 1% glutamine and 1% pen/strep) containing different probes used for staining F-actin,

mitochondria, lipid droplets, and nuclei. For F-Actin staining, we incubated live cells with SiR-actin probe (λ Ex/Em: 652/674nm) and verapamil (1:2000 and 1:1000, respectively) for 1 hour at 37°C, 5% CO_2 in the dark (Tebu-Bio, SC001). Mitochondria were stained in live cells with Mitotracker Red CM-H_2XROS (100nM, λ Ex/Em: 579/599nm) or with Mitotracker Deep Red FM (500nM, λ Ex/Em: 644/665nm) for 30 minutes at 37°C, 5% CO_2 in the dark (Thermo-Fisher Scientific, M7513 and Cell Signaling, 8778). For lipid droplets and nuclei staining, live cells were incubated with AdipoRed™ assay Reagent (1:200, λ Ex/Em: 550/600nm, Lonza, PT-7009) and Hoechst 33258 (1:1000, λ Ex/Em: 350/461nm, Invitrogen, H3569) for 30 min at 37 °C in the dark.

3.13.1 Confocal microscopy image processing and analysis

After smoothing images, F-actin and mitochondrial networks were analyzed as previously described (Valente et al., 2017). The images were binarized and analyzed to evaluate mitochondria morphology. After analyzing particles, the images were skeletonized, and it was analyzed skeleton organization and mitochondrial network.

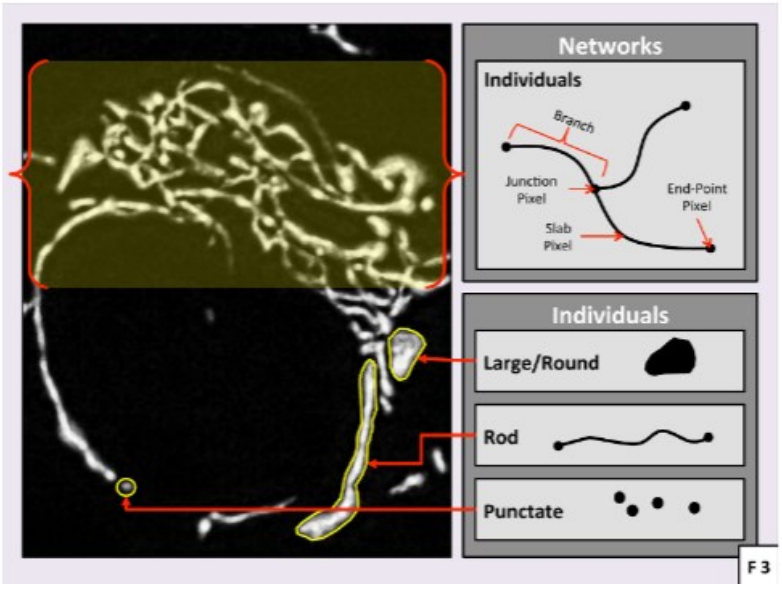

Fig. 3.2 Schematic representation of the terms used for the evaluation of mitochondrial morphology and F actin organization (Valente et al., 2017).

For lipid droplet size, images were first binarized, and particles were then quantified.

3.14 Statistical analysis

Statistical analyses were performed with Student's t test, One-way ANOVA followed by Dunnett's or Tukey's Post-test or Two-way ANOVA followed by Sidak post-test as necessary using GraphPad Prism (version 6.0).

3.15 Data and software availability

Data discussed in this manuscript (have been deposited in NCBI's Gene Expression Omnibus and are accessible through GEO Series accession numbers:

- GSE115913 for C3H10T1/2 microarray dataset

  https://www.ncbi.nlm.nih.gov/geo/query/acc.cgi?acc=GSE115913

  Secure Token for Reviewers: sbihcugmrbujhiv

- GSE147941 for C3H10T1/2 4sU seq dataset

  https://www.ncbi.nlm.nih.gov/geo/query/acc.cgi?acc=GSE147941

  Secure Token for Reviewers: idgjiooubxcpvwl

Generally Applicable Gene-set Enrichment (GAGE) was performed to evaluate significantly enriched gene clusters in C3H10T1/2 pre-adipocytes and mature adipocytes (http://bioinformatics.sdstate.edu/idep/). Images quantifications were performed by ImageJ (https://imagej.nih.gov/ij/). Metabolomic mass spectrometric raw data were analyzed with

the MultiQuant™ software (version 3.0.2) (https://sciex.com/products/software/multiquant-software). Seahorse results were analyzed using Wave Software (Agilent Technologies, Wave for Desktop, Version 2.6.1.53).

4. RESULTS

4.1 Zc3h10 regulates the white adipogenic program.

To assess whether Zc3h10 plays a role in white adipogenic program, we investigated its expression during CH310T1/2 mesenchymal stem cells (MSCs) differentiation into white adipocytes (Fig. 4.1D). Zc3h10 protein level increased during differentiation and preceded the expression of the master regulator of adipogenesis, Pparγ-2, and the mitochondrial transcription factor, Tfam (Fig. 4.1A). Simultaneously with the increase in Zc3h10 protein levels, we observed an increase in the expression of different subunits belonging to the oxidative phosphorylation (Oxphos), mitochondrial DNA content, and basal oxygen consumption rate (Fig. 4.1A,B,C).

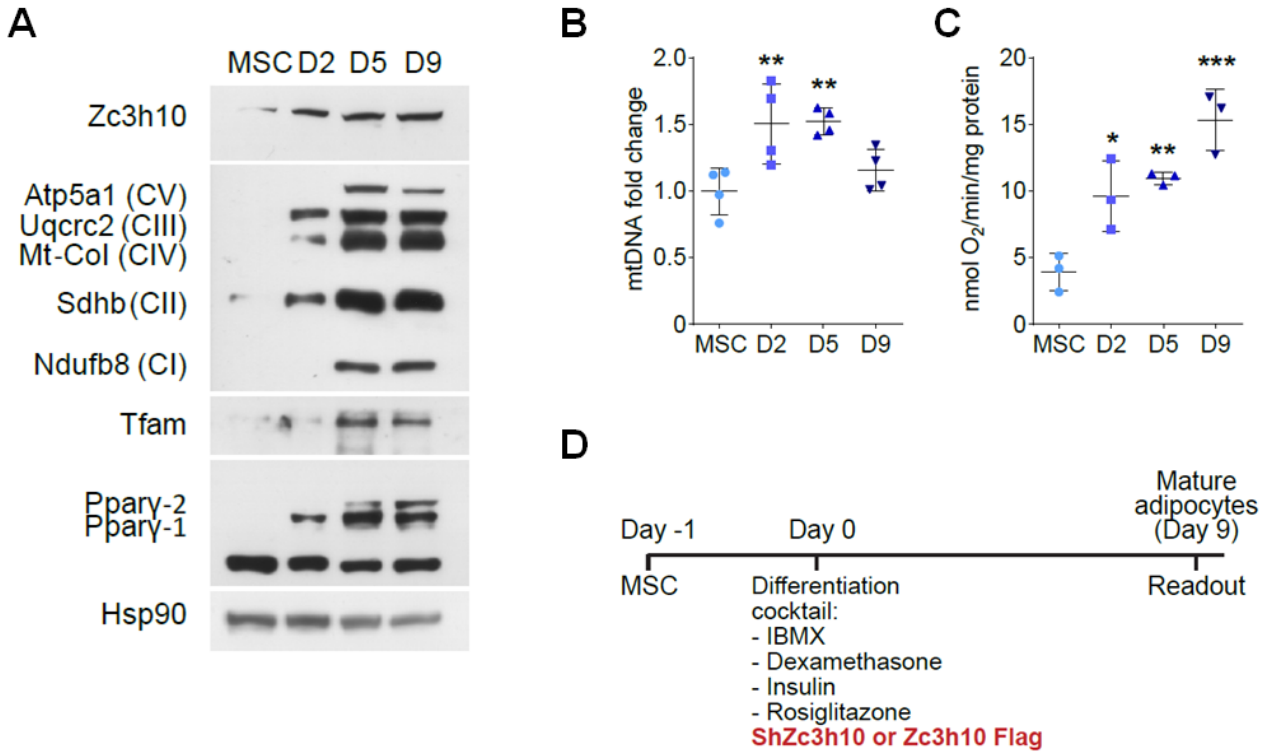

Figure 4.1: C3H10T1/2 cells were induced to white adipocytes differentiation. A: Western blot of Zc3h10, Oxphos subunits (Atp5a1, Uqcrc2, Mt-CoI, Sdhb, Ndufb8), Tfam and Pparγ at different time-points of adipogenesis. B: Mitochondrial DNA and C: oxygen consumption levels in proliferating MSCs,

2, 5 and 9 day after differentiation induction; statistical analysis was performed by One-Way ANOVA followed by Dunnett's post-hoc test; *p<0.05, **p<0.01, ***p<0.001 vs MSCs. D: Representation of the experimental protocol followed for the infection and the differentiation of C3H10T1/2.

At this point, we decided to downregulate and overexpress the expression of this protein at the beginning of adipocytes differentiation (Day 0), and we observed the readout at the end of differentiation program (Day 9)(Fig. 4.1D). Adenovirus-mediated knock-down caused a 50% reduction in protein levels of Zc3h10 (Fig. 4.2A).

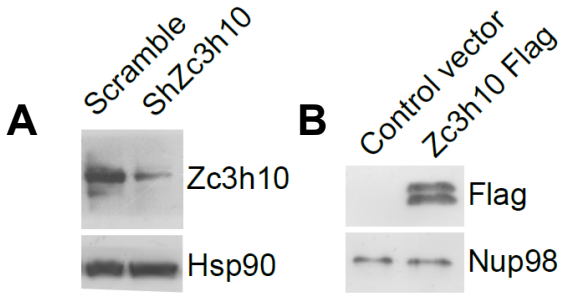

Figure 4.2: Validation of Zc3h10 expression by western blot after silencing (A) or overexpression (B) of Zc3h10, 36h after induction of differentiation.

Zc3h10-silenced mature adipocytes (ShZc3h10) showed a significantly blunted lipid accumulation and decreased expression of classical markers of adipogenesis combined with a reduction in the number of mature adipocytes (Adipored^{+} cell) (Fig. 4.3A, B and 4.4A). We also assessed lipid droplet size, but our results did not show any changes between our two experimental conditions (Fig. 4.3C). In contrast, overexpression of Zc3h10 led to a fewer number of lipid-containing cells, characterized by upregulated expression of adipogenic genes and to a dramatical increased lipid droplet size (Fig. 4.3D, E, F and 4.4B).

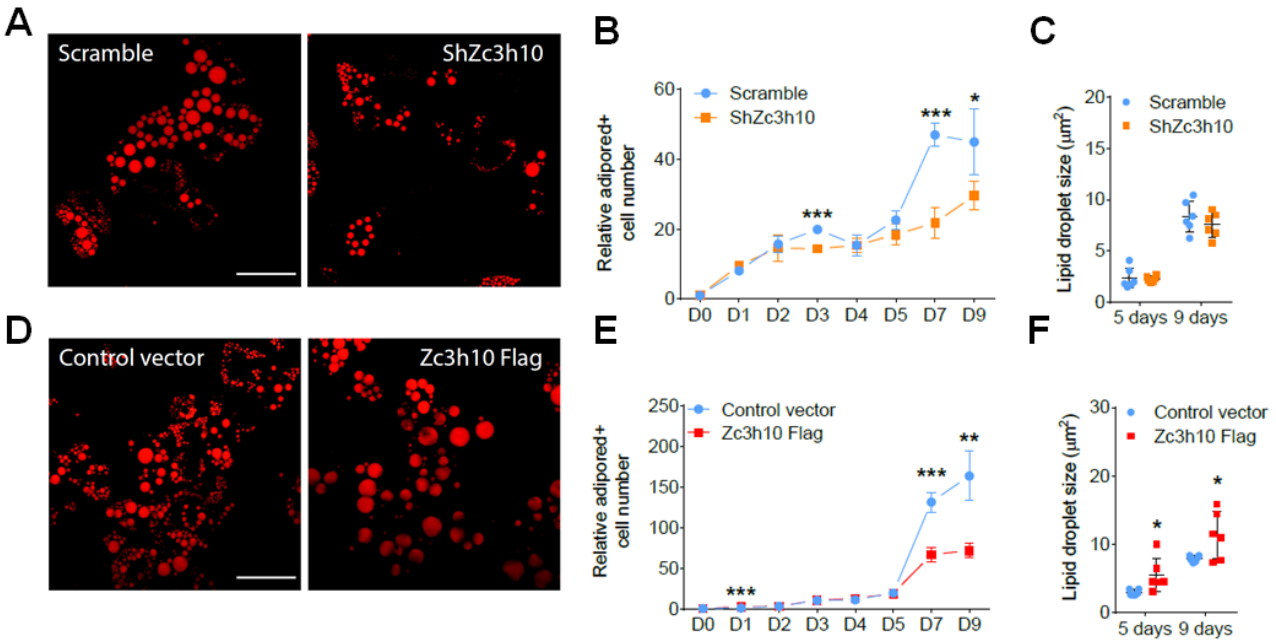

Figure 4.3: Zc3h10 controls white adipogenesis. A and D: Lipid droplets (red) were labelled using AdipoRed dye to evaluate lipid accumulation in Scramble and ShZc3h10 cells, and in Control Vector and Zc3h10-Flag mature adipocytes (day 9), respectively. Scale bar: 50µm. B and E: Relative quantification of Adipored positive (Adipored+) cells during the differentiation of Scramble and ShZc3h10 cells and in Control Vector and Zc3h10-Flag cells; statistical analysis was performed by multiple Student's t-test; *p<0.05, ***p<0.001 vs Scramble, and **p<0.01, ***p<0.001 vs Control Vector. C and F: Lipid droplet size in Scramble and ShZc3h10 adipocytes and in Control Vector and Zc3h10-Flag cells differentiated for 5 and 9 days; statistical analysis was performed by Student's t-test; *p<0.05 vs Control Vector.

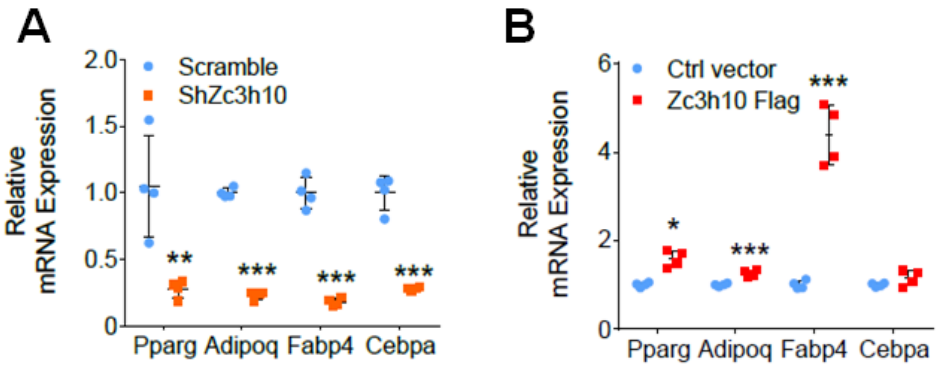

Figure 4.4: Gene expression analysis of main adipogenic markers in ShZc3h10 (A) and Zc3h10 Flag (B) mature adipocytes (day 9); statistical analysis was performed by Student's t-test; *p<0.05, **p<0.01, ***p<0.001 vs Scramble or Ctrl vector, respectively.

We then recapitulated most of these findings in primary mouse stromal vascular cells differentiated to mature white adipocytes. Also in this case, ShZc3h10 cells (Fig. 4.5A, left panel)

showed a decrease in the number of mature adipocytes (Adipored positive cells) while lipid droplets size remained unchanged (Fig. 4.5 B, C). Zc3h10 overexpressing cells (Fig. 4.5A, right panel) exhibited an increased size of adipocytes lipid droplet whereas did not change in the number of cells positive for lipid staining (Fig. 4.5D, E).

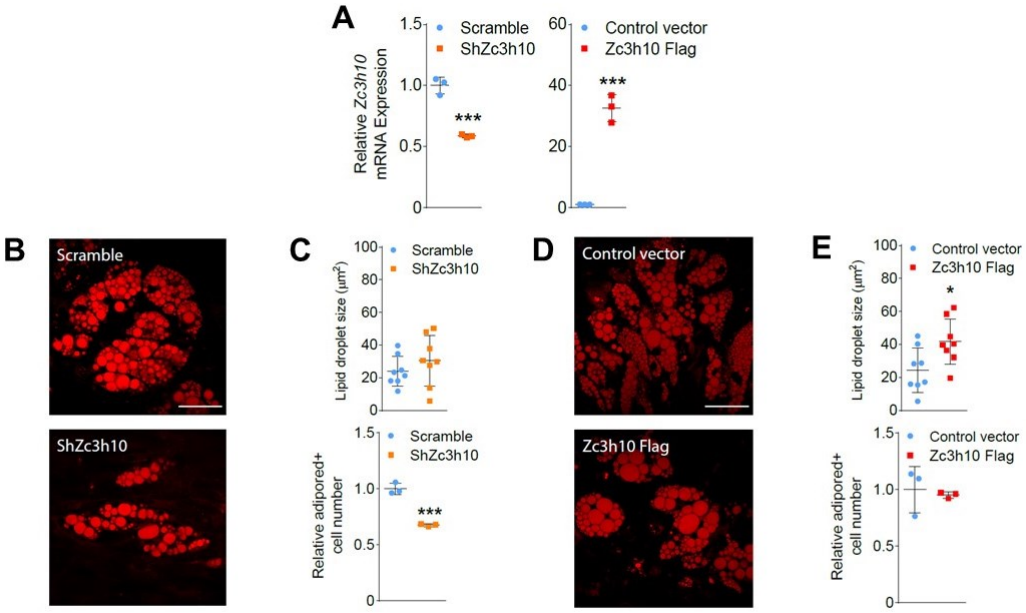

Figure 4.5: Zc3h10 effect on primary stromal vascular cells induced to white adipocytes differentiation (day 8). A: Relative mRNA expression of Zc3h10 in primary mature adipocytes exposed to ShRNA against Zc3h10 and Zc3h10 Flag; statistical analysis was performed by Student's t-test; ***p<0.001 vs Scramble or Ctrl vector, respectively. B: Primary SVCs differentiation was evaluated in Scramble and ShZc3h10 mature adipocytes (Day 8) by AdipoRed dye. Scale bar: 50µm. C: Lipid droplet size and AdipoRed$^+$ cell count in Scramble and ShZc3h10 primary mature adipocytes (day 8); statistical analysis was performed by Student's t-test, ***p<0.001 vs Scramble. D: Primary SVCs differentiation was evaluated in Ctrl vector and Zc3h10 Flag mature adipocytes (day 8) using the fluorescent dye AdipoRed (red). Scale bar: 50µm. E: Lipid droplet size and relative quantification of Adipored$^+$ cells in Ctrl vector and Zc3h10 Flag in 8 days differentiated SVCs; statistical analysis was performed by Student's t-test; *p<0.05 vs Control Vector.

At this point, to understand in which period of differentiation process the presence of Zc3h10 was important, we decided to silence Zc3h10 at the later stage (day 7 instead of day 0, Fig. 4.6A). We found that Zc3h10-depleted (Fig. 4.6B) cells showed no difference in lipid accumulation, basal oxygen consumption, or mtDNA content relative to control cells (Fig. 4.6 C, D, E, F).

These results suggest that Zc3h10 plays a role in the early phase of adipogenesis.

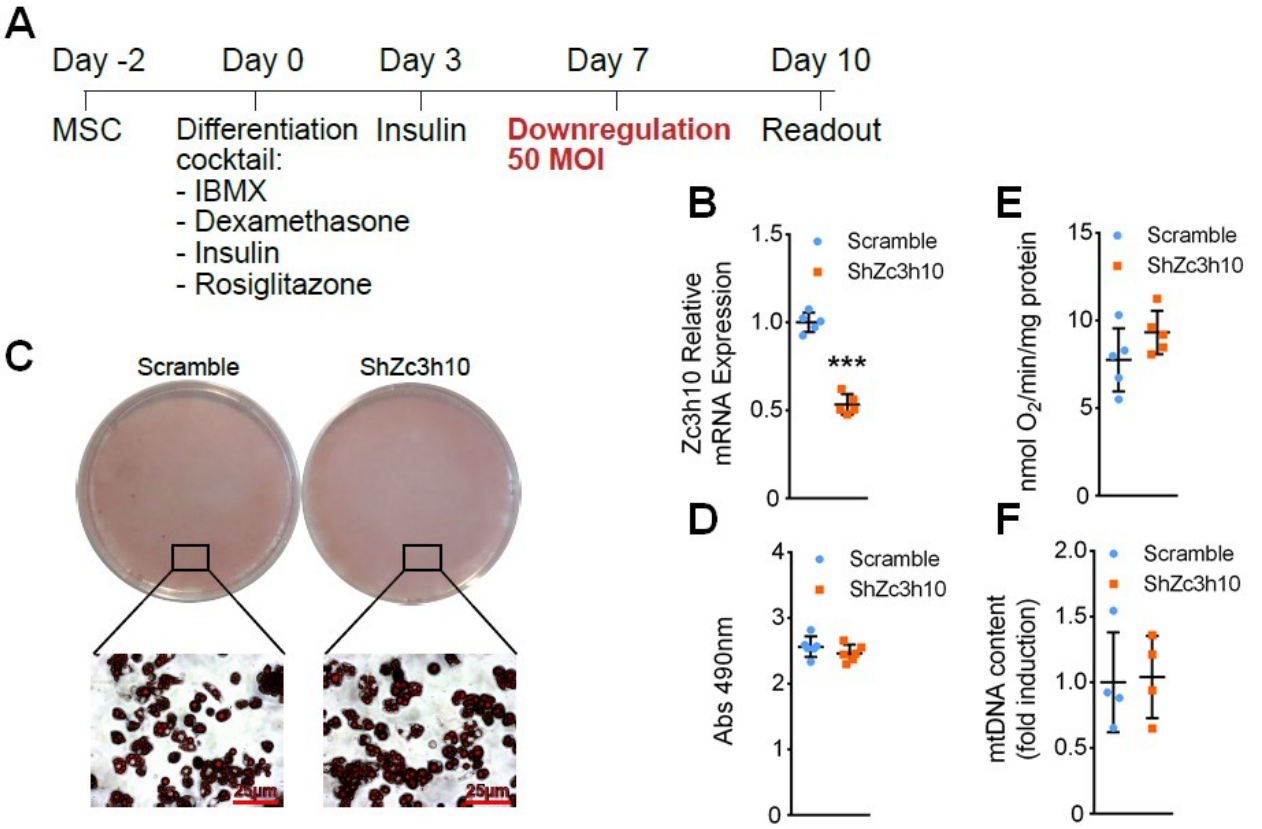

Figure 4.6: A: Experimental plan followed to downregulate Zc3h10 in C3H10T1/2 adipocytes at day 7 of differentiation. B: Relative Zc3h10 mRNA expression levels in Scramble and ShZc3h10 infected at day 7; statistical analysis was performed by Student's t-test; ***p<0.001 vs Scramble. C: Oil-red-O staining, D: relative quantification of lipid content at day 10 of differentiation in Scramble and ShZc3h10 infected at day 7; statistical analysis was performed by Student's t-test. E: Basal oxygen consumption rate and F: mtDNA content at day 10 of differentiation in Scramble and ShZc3h10 infected at the end of differentiation program (day 7).

4.2 Zc3h10 controls nascent mRNA levels of actin filament-based process and translation pathways in pre-adipocytes.

A more detailed analysis showed that Zc3h10 protein levels started to increase 36 hours after exposure to the adipogenic cocktail (Fig. 4.7A). Moreover, we studied the cellular localization of this protein, and we observed that Zc3h10 was enriched in the chromatin fraction, consistently with its transcription factor activity (Yi et al., 2019) (Fig. 4.7B).

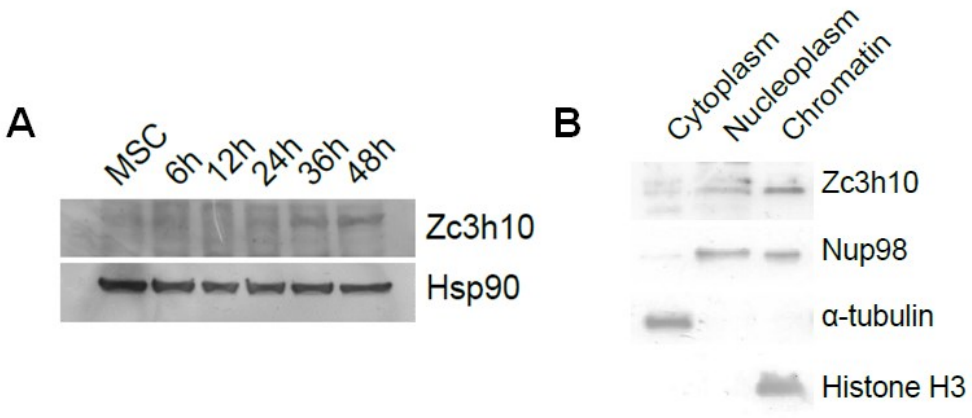

Figure 4.7: Zc3h10 is a chromatin associated protein and its expression increase 36h after differentiation induction. A: Western blot of Zc3h10 in whole cell lysates during the first 48h of differentiation. B: Western blot of Zc3h10, Nup98 (nuclei marker), α-tubulin (cytoplasmic marker) and histone H3 (chromatin marker) in the indicated cell fractions 36h from differentiation induction.

To investigate the target pathways of this protein, we studied the effect of Zc3h10 depletion on nascent/pre-mRNAs synthesis 36 hours after hormonal induction (Fig. 4.8A).

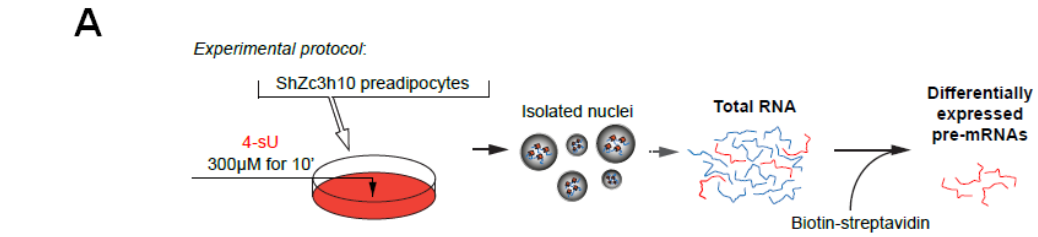

B

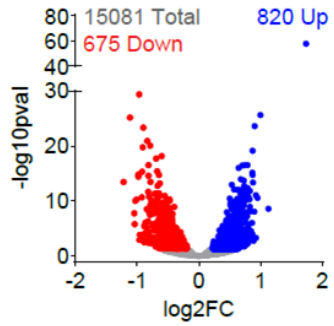

C

Pathway	Direction	NES	DEG (%)	adj.Pval
Actin filament-based process	Down	-5.691	75/418 (18)	3.90E-05
Actin cytoskeleton organization	Down	-5.087	66/381 (17)	5.10E-04
Translation	Up	7.381	132/490 (27)	7.50E-10
Peptide biosynthetic process	Up	7.207	133/500 (26)	1.30E-09
Ribosome biogenesis	Up	6.079	47/223 (21)	1.60E-06
Ribonucleoprotein complex biogenesis	Up	6.012	66/358 (18)	1.60E-06
Ribosomal small subunit assembly	Up	5.568	11/16 (69)	2.00E-03
Ribosome assembly	Up	4.985	22/53 (41)	7.90E-04
RRNA processing	Up	4.967	30/154 (19)	5.10E-04
Cytoplasmic translation	Up	4.956	37/74 (50)	7.30E-04

Figure 4.8: A: Schematic representation of experimental protocol for pre-mRNA labeling, isolation and analysis in Scramble and ShZc3h10 pre-adipocytes. Before nuclei isolation, cells were exposed to 4-thiouridine (4-sU) 300µM for 10 minutes. Total RNA was isolated and quantified. Then, 50µg of total RNA were used to isolate 4sU-labelled pre-mRNA. B: Volcano plot of downregulated (red), upregulated (blue) and unchanged (gray) pre-mRNAs in ShZc3h10 compared to Scramble pre-adipocytes (36h); False Discovery Rate (FDR) <0.05. C: GAGE analysis results of significant down and upregulated pre-mRNAs clusters from Scramble and ShZc3h10 36h differentiated pre-adipocytes. Table indicates

pathway name, trend, normalized enrichment score (NES), number of differentially expressed genes with percentage compared to total genes in the cluster (DEG (%)) and adjusted *p*-value (adj pval).

4-thiouridine (4-sU) labeling of nascent RNAs coupled to next-generation sequencing (4-sU-seq) revealed a significant transcriptomic difference in Zc3h10 silenced pre-adipocytes with 820 upregulated and 675 downregulated pre-mRNAs (adjusted *p*value<=0.05) compared to Scramble cells (Fig. 4.8B). Generically applicable gene-set enrichment (GAGE) pathway analysis showed that Zc3h10 depletion upregulated translation and ribosome biogenesis and downregulated actin filament-based cytoskeleton organization pre-mRNA clusters (Fig. 4.8C). These data indicate that Zc3h10 promotes the expression of actin filament-based cytoskeleton organization genes and represses those involved in protein translation.

Next, we queried published data from chromatin immunoprecipitation coupled to sequencing (ChIP-seq) of Zc3h10 in brown adipocytes (Yi et al., 2019) and found that most of the statistically upregulated or downregulated genes from 4-sU-seq were actually bound by Zc3h10 within 1kb from the gene transcription start sites (TSS) (Fig. 4.9A, B).

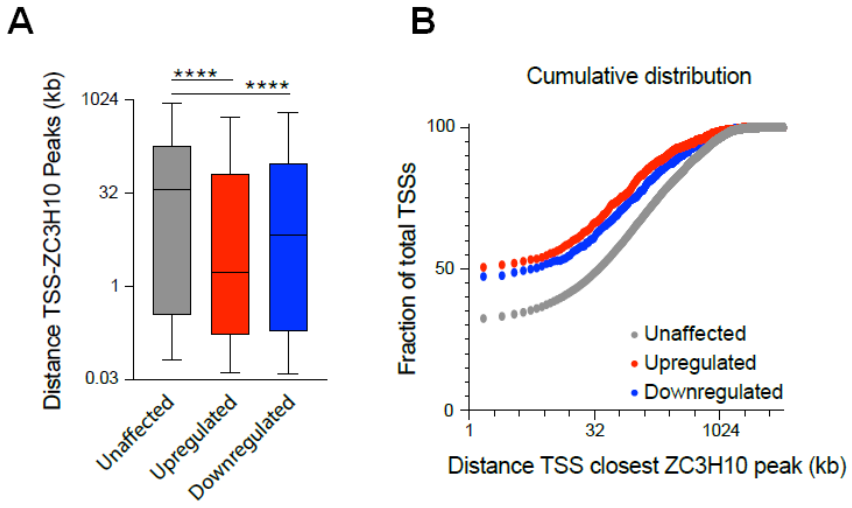

Figure 4.9: A: Box plot representing the distance (kb) of Zc3h10 binding sites on chromatin in unaffected, upregulated (red) and downregulated (blue) pre-mRNAs of ShZc3h10 pre-adipocytes (36h) compared to Scramble control. statistical analysis was performed by Mann-Whitney (non-parametric) two-tailed test (****p<0.0001). B: Cumulative distribution of Zc3h10 binding sites on chromatin in

unaffected, upregulated (red) and downregulated (blue) pre-mRNAs of ShZc3h10 compared to Scramble control pre-adipocytes (36h after differentiation).

4.3 Zc3h10 affects protein translation activity.

4-sU-seq analysis showed that 136 pre-mRNAs of the translation pathway were upregulated in Zc3h10 silenced pre-adipocytes (Fig. 4.10).

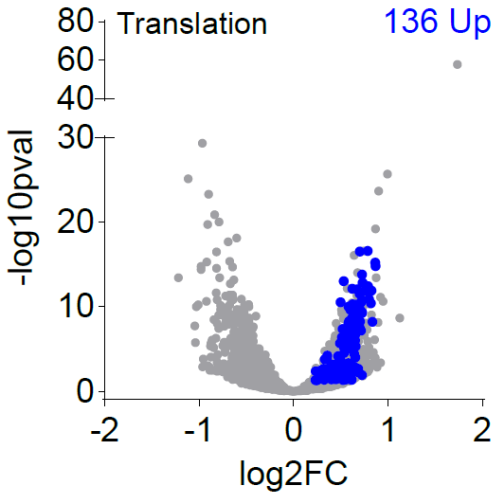

Figure 4.10: Volcano plot of the translation gene cluster upregulated in ShZc3h10 compared to control pre-adipocytes (36h). Blue dots represent differentially expressed genes (DEG) in the clusters (FDR< 0.05).

For this reason, we investigated if these transcriptional changes were associated with increased protein translation activity. To do this, we analyzed the phosphorylation status of 4E-BP1 as a functional marker of translation process at 36h after differentiation induction: hyperphosphorylation provokes an increase in the activity, whereas hypophosphorylation prevents the beginning of this process. Zc3h10 depleted cells showed no differences in the total amount of 4E-BP1 compared to scramble control (Fig. 4.11A). However, Thr37-46 and Thr70 were significantly hyperphosphorylated (Fig. 4.11B, C). Conversely, Zc3h10 overexpressing cells showed a significant increase in 4E-BP1 total levels (Fig. 4.11A) while we observed a

hypophosphorylation of the same amino acid residues (Fig. 4.11B, C). These results indicate that Zc3h10 affects protein translation.

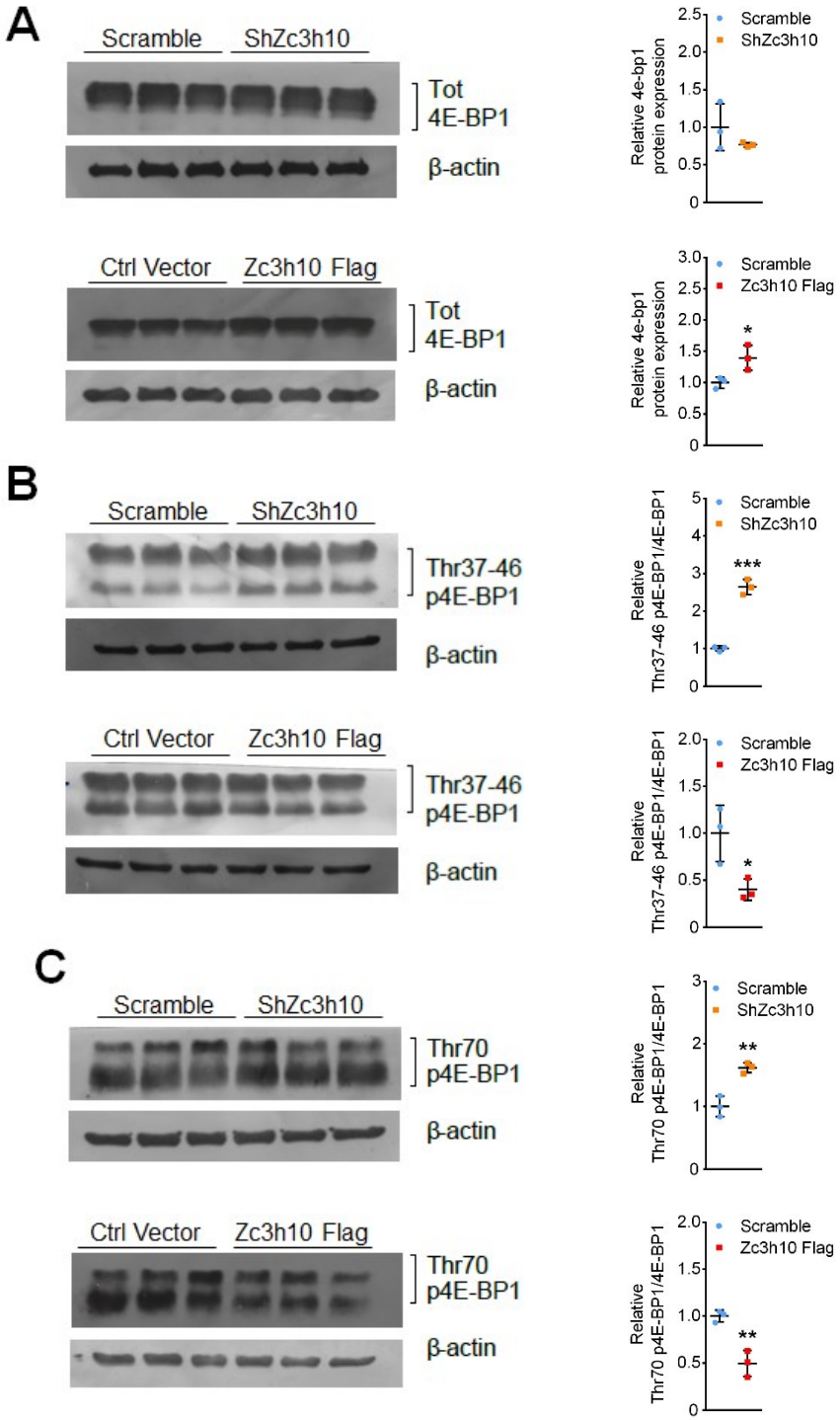

FIGURE 4.11: the effects of Zc3h10 on the phosphorylation state of 4E-BP1. A: Western blot of total 4E-BP1, B: Thr37-46 and C: Thr70 phosphorylated 4EBP-1 with relative quantification in ShZc3h10 and in Zc3h10 Flag 36h differentiated pre-adipocytes; statistical analysis was performed by Student's t-test; *p<0.05, **p<0.01, *** p<0.001 vs Scramble and Control Vector respectively.

4.4 Zc3h10 governs F-actin cytoskeleton organization

Actin filament-based cytoskeleton organization was the other main pathway negatively affected in Zc3h10 depleted pre-adipocytes (80 pre-mRNAs) (Fig. 4.12).

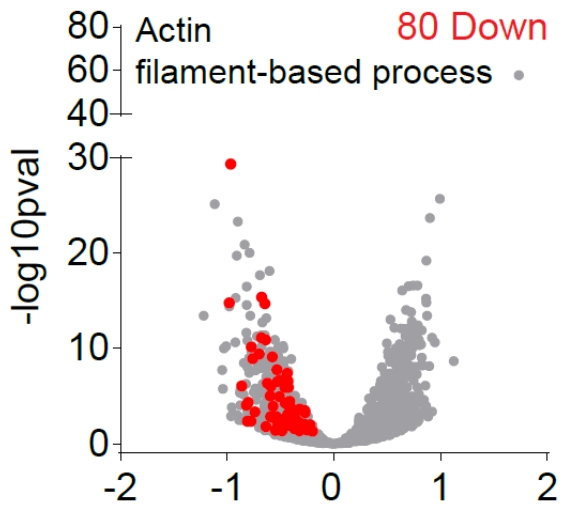

Figure 4.12: Volcano plot of actin filament-based process cluster downregulated in ShZc3h10 compared to Scramble cells, 36h after differentiation induction. Red dots represent DEG in the clusters (FDR< 0.05).

To understand the molecular mechanism of this protein, we quantitatively analyzed F-actin morphology (Valente et al., 2017) using a specific probe that specifically bound F-actin. Initially, we investigate F-actin remodeling during the early stage of adipocyte differentiation in our *in vitro* model (Fig. 4.13). Proliferating MSCs showed several stress fibers that were progressively reorganized. After adipogenic cocktail addition (Day 0), MSCs diminished cell size up to 36 hours. F-actin analysis demonstrated a gradual increase in the number of F-actin networks (Fig. 4.13B) and rod-shaped filaments along with increased rod length (Fig. 4.13C). Moreover, the number of punctate filaments, junctions, and branches were decreased (Fig. 4.13D, E, F) despite a slight increase in branch length (Fig. 4.13F). These findings were not linked to changes in F-actin microfilament area (Fig. 4.13G).

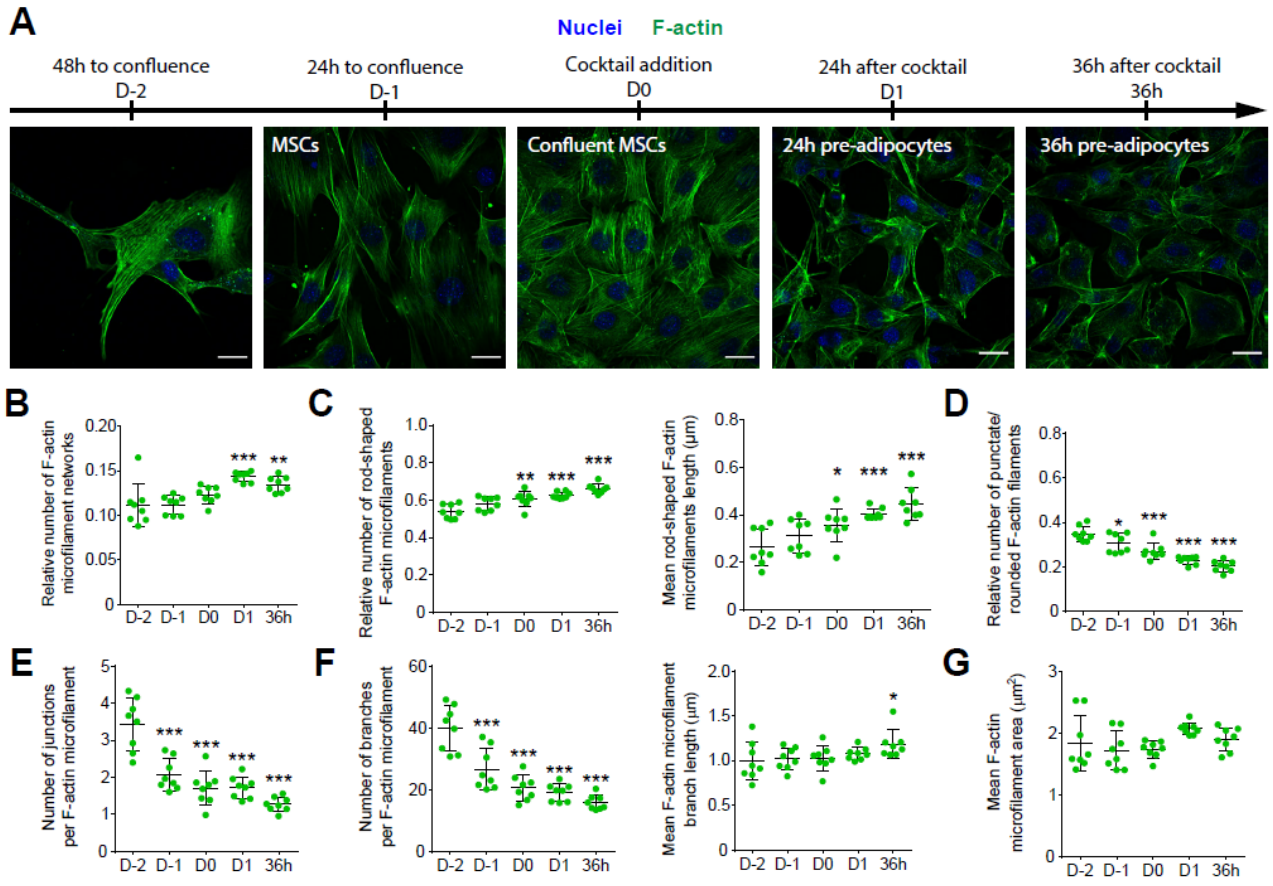

Figure 4.13: Morphological evaluation of F-actin during the early stage of adipocyte differentiation. A: F-actin detected through SiR-actin probe and confocal microscopy and B-G: quantitative analysis of F-actin network during the early phases of C3H10T1/2 differentiation to adipocytes (from proliferating MSCs to 36h differentiated pre-adipocytes). Green: F-actin; blue: nuclei; statistical analysis was performed by One-Way ANOVA followed by Dunnett's post-hoc test; *p<0.05, **p<0.01, ***p<0.01 vs D-2. Scale bar: 25µm.

Next, we evaluated F-actin organization in Zc3h10 silenced pre-adipocytes (Fig 4.14A, B, C). In this condition, F-actin appeared less-organized with a decrease in the number of junctions, branches per F-actin microfilament (Fig. 4.14D). Furthermore, we observed a decrease in F-actin microfilaments area in ShZc3h10 condition compared to Scramble group (Fig. 4.14D).

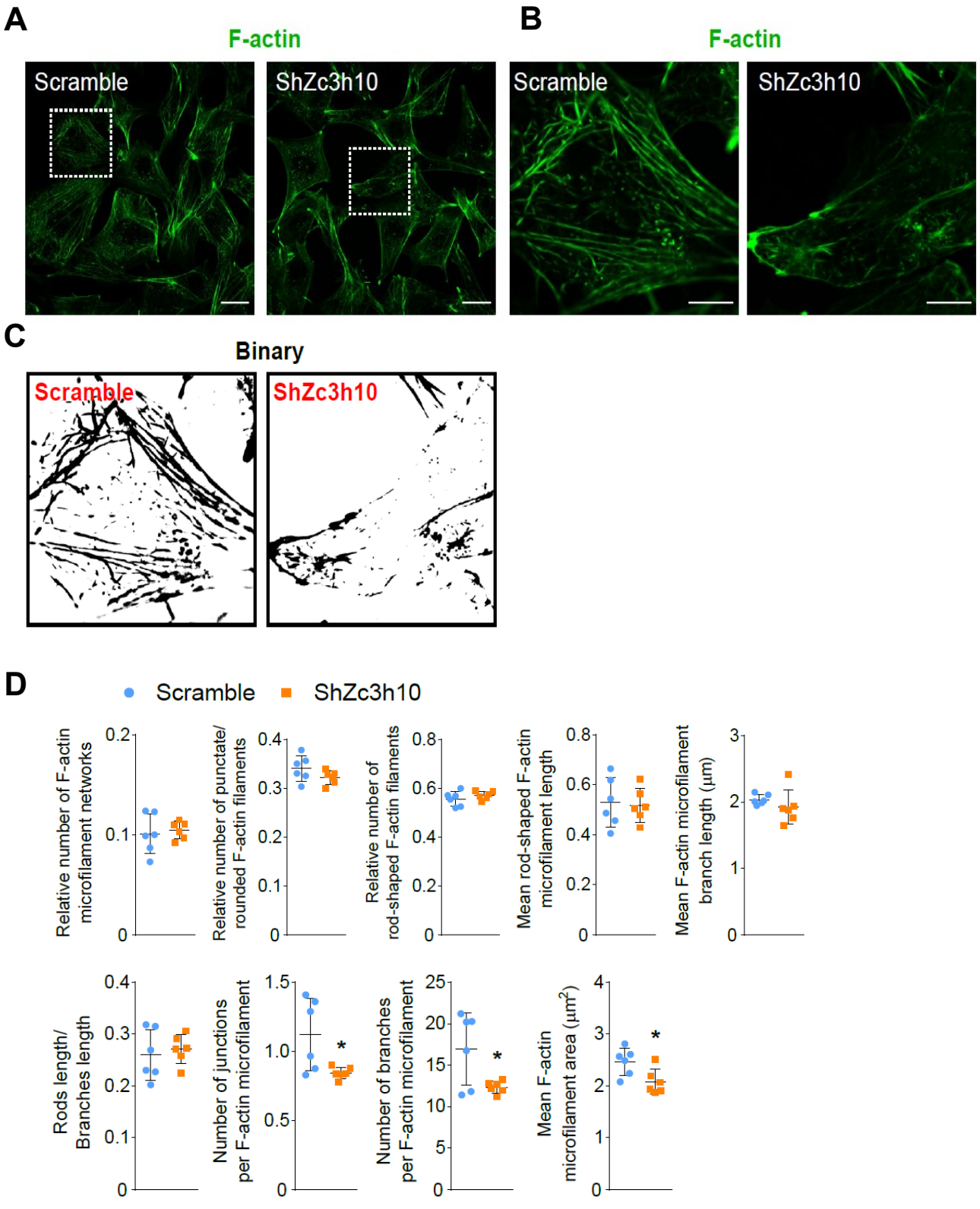

Figure 4.14: Zc3h10 affects F-actin morphology. A: F-actin morphology in Scramble and ShZc3h10 pre-adipocytes, Scale bar: 50µm. B: enlarged images and C: binary of enlarged images, Scale bar 10µm. D: Quantitative analysis of F-actin network in Scramble and ShZc3h10 in 36h differentiated cells; statistical analysis was performed by Student's t-test; *p<0.05 vs Scramble

In contrast, Zc3h10 overexpression enhanced the priming of F-actin reorganization towards the cell periphery (Fig. 4.15A, B, C), as evidenced by a decrease in the number of punctate F-actin microfilaments and in the number of junctions per F-actin filament while increased rod-shaped filaments (Fig. 4.15D).

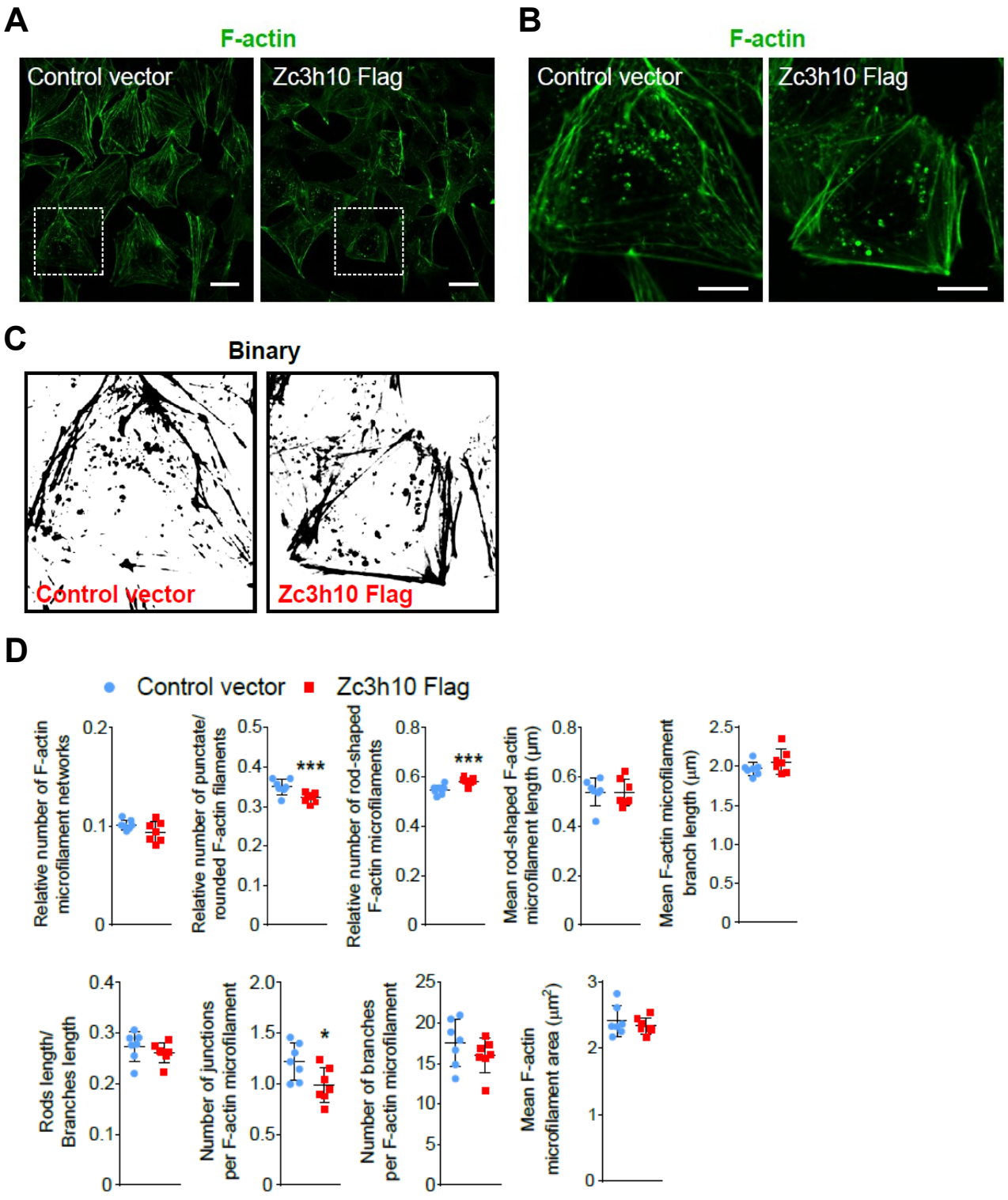

Figure 4.15: Zc3h10 affects F-actin morphology. A: F-actin detected through SiR-actin probe and confocal microscopy in Control Vector and Zc3h10 Flag pre-adipocytes, Scale bar: 50µm. B: enlarged images and C: binary of enlarged images, Scale bar 10µm. D: Quantitative analysis of F-actin network in Control Vector and Zc3h10 Flag in 36h differentiated cells; statistical analysis was performed by Student's t-test; *p<0.05, ***p<0.001 vs Control Vector.

At later stages of the adipogenic program (day 5 after induction of differentiation), Zc3h10 depletion decreased F-actin reorganization: indeed stress fibers were still present within Zc3h10-depleted cells, whereas F-actin organization in control group appeared well organized among the cell periphery (Fig. 4.16A). The lack of cortical F-actin organization was associated with a decrease in lipid accumulation in ShZc3h10 cells (Fig. 4.16A). On the other hand, Zc3h10 overexpressing pre-adipocytes showed peculiar cortical F-actin rings with larger lipid droplets (Fig. 4.16B). Collectively, these results show that Zc3h10 controls, at the transcriptional level, the F-actin network to ensure proper cytoskeleton remodeling in the early phases of adipogenesis.

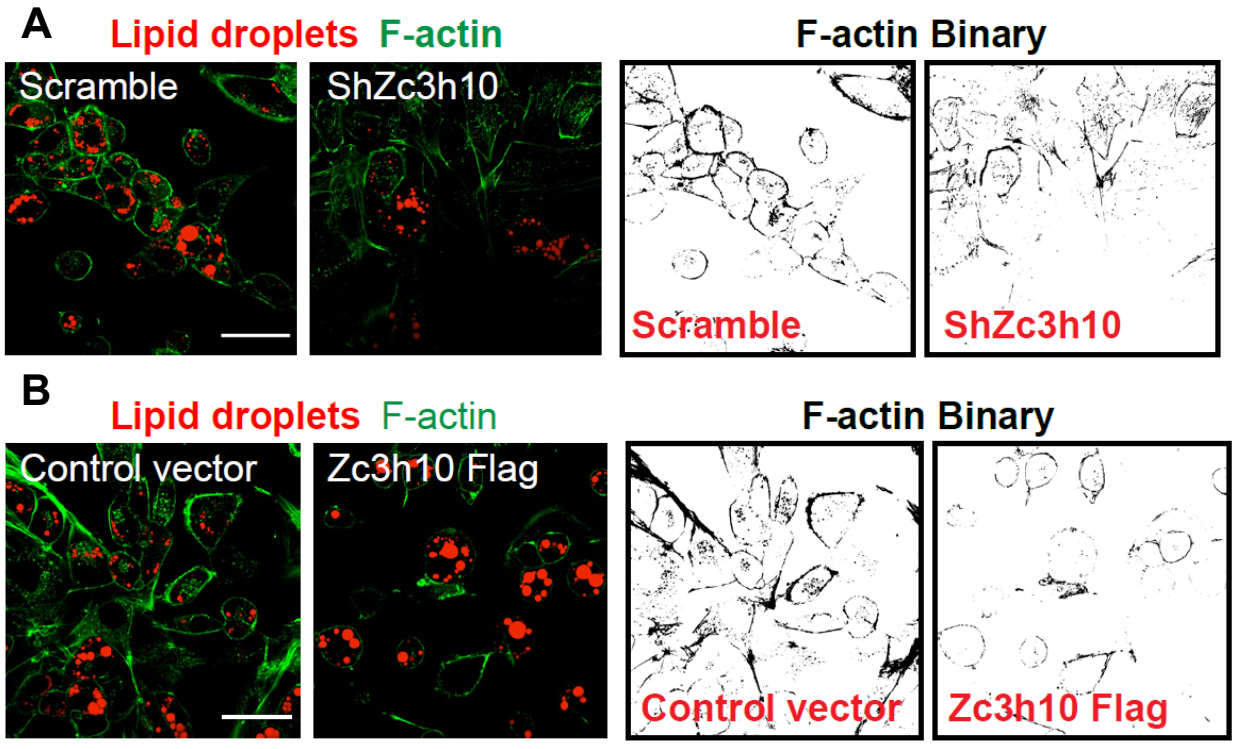

Figure 4.16: Representative images of F-actin cytoskeleton (green), lipid droplet (red) and F-actin binary signal in A: ShZc3h10 and B: Zc3h10 Flag pre-adipocytes (day 5).

4.5 Zc3h10-mediated F-actin remodeling determines mitochondrial network complexity

Given these changes in F-actin's dynamics and because F-actin is a regulator of mitochondrial networks (De Pauw et al., 2009), we also investigated the mitochondrial dynamics during the early phase of differentiation (Fig. 4.17A). Quantitative analysis of mitochondrial morphology revealed a gradual increase in the number of mitochondrial networks (Fig. 4.17B) and decreased rod-shaped mitochondria along with a slight reduction in rod length after 36 hours of differentiation (Fig. 4.17C). Additionally, the number of punctate/rounded mitochondria, junctions, and branches were increased despite unchanged branch length (Fig. 4.17D, E, F). We also observed an increased mitochondrial area after the addition of the differentiation cocktail (day 1) (Fig.4.17G).

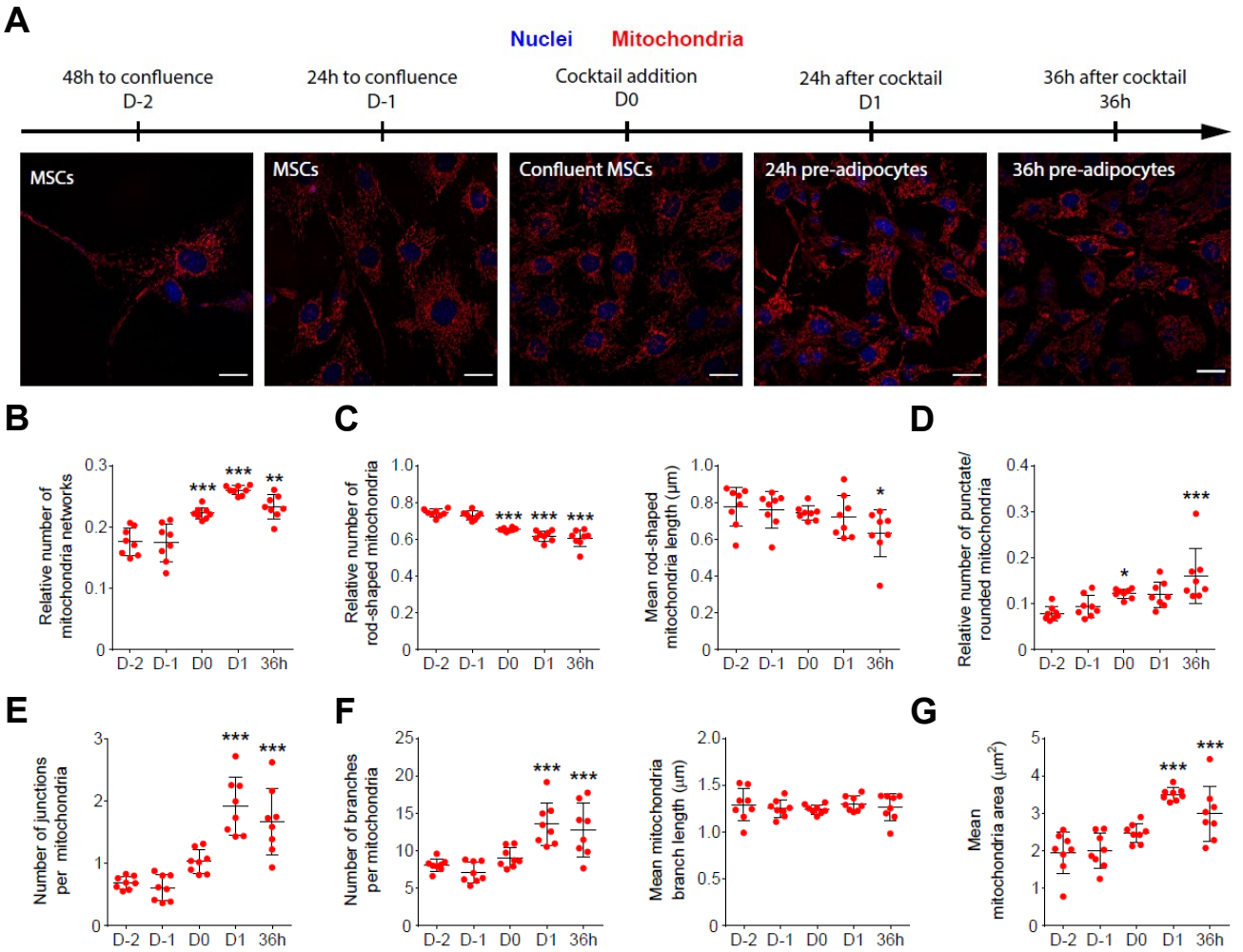

Figure 4.17: Morphological evaluation of mitochondria during the early stage of adipocytes differentiation. A: Representative images and B-G: quantitative analysis of mitochondria network during the early phases of C3H10T1/2 differentiation to adipocytes (from proliferating MSCs to 36h differentiated pre-adipocytes). Red: Mitochondria; blue: nuclei; statistical analysis was performed by One-Way ANOVA followed by Dunnett's post-hoc test; *p<0.05, **p<0.01, ***p<0.01 vs D-2. Scale bar: 25µm.

To better understand whether Zc3h10 plays a role in mitochondrial dynamics, we evaluated mitochondrial morphology under our two different conditions (ShZc3h10 and Zc3h10-Flag) (Fig. 4.18-19). We noted a different mitochondrial pattern between Zc3h10 depleted cells relative to scramble control (Fig. 4.18A, B, C). Quantitative morphological analysis revealed that Zc3h10 silencing increased the rod-shaped mitochondrial length and the ratio of rods length/branches length. Of note, the number of junctions and branches and the mitochondrial area were significantly reduced as well as the mitochondrial area (Fig.4.18D).

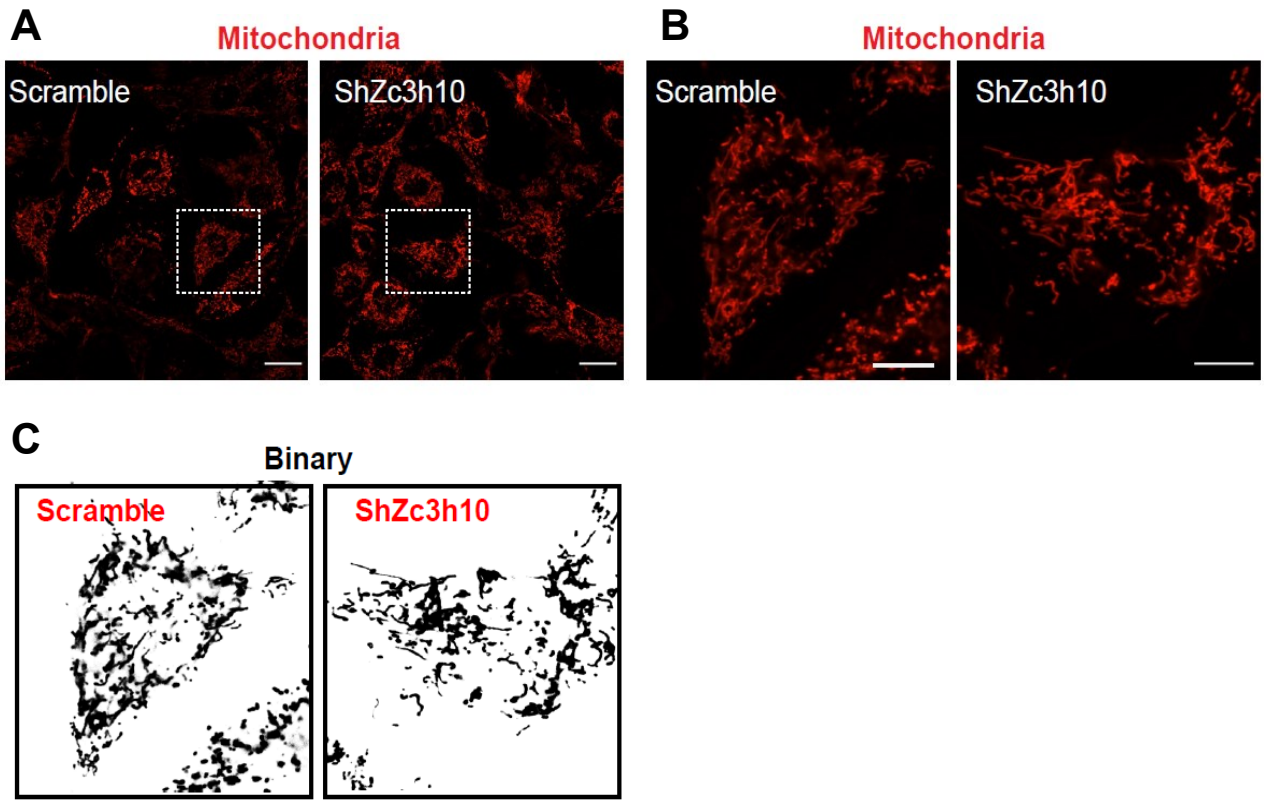

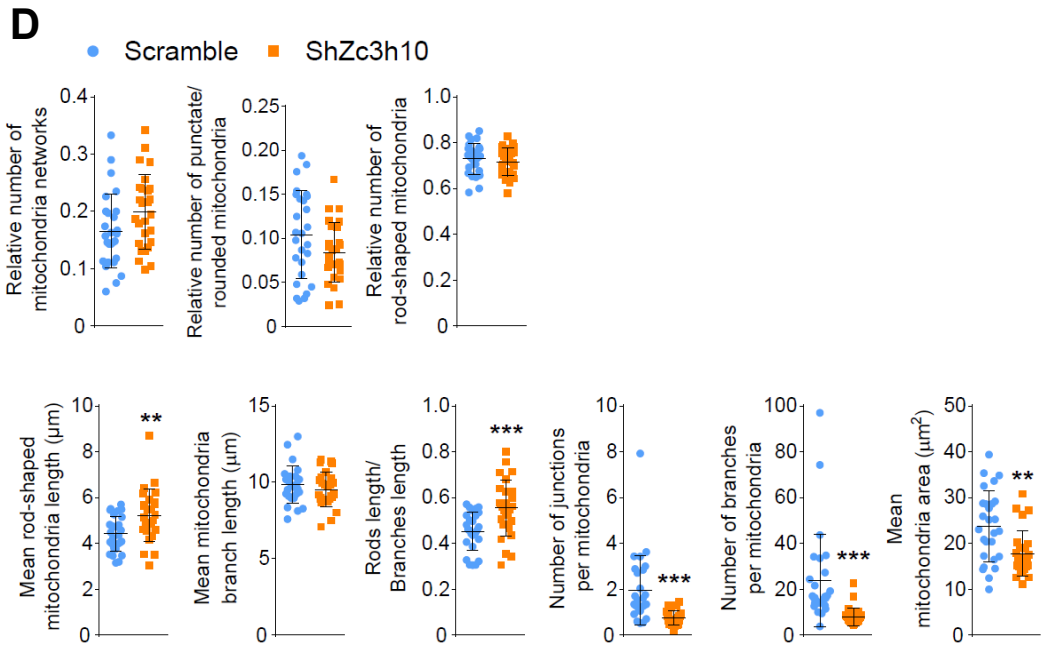

Figure 4.18: Mitochondria network detected by Mitotracker Red CM-H2XROS probe and confocal microscopy. A: mitochondria morphology in Scramble and ShZc3h10 pre-adipocytes (36h), Scale bar: 50µm. B: Enlarged images and C: binary of enlarged images (left images), Scale bar: 10µm. D: quantitative analysis of mitochondria network in Scramble and ShZc3h10 36h differentiated cells; statistical analysis was performed by Student's t-test; **p<0.01, ***p<0.001 vs Scramble.

The priming activity of Zc3h10 on mitochondria structure was also confirmed using the overexpression approach (Fig. 4.19A, B, C). Zc3h10 Flag cells exhibited a significant decrease in the number of punctate/rounded mitochondria and an increase of the number of branches and mitochondrial area (Fig. 4.19D).

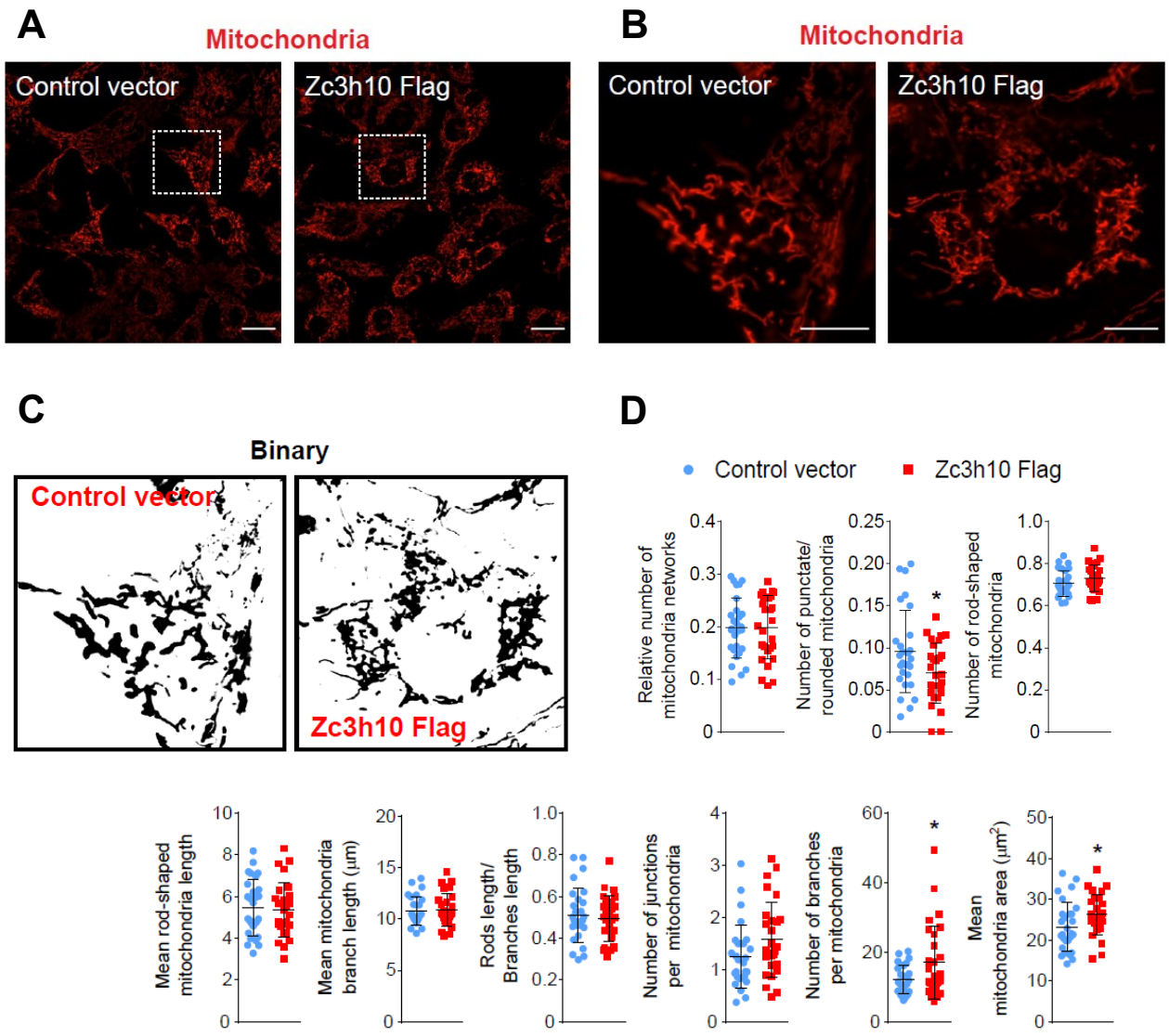

Figure 4.19: A: Representative images of mitochondrial network in Ctrl vector and Zc3h10 Flag pre-adipocytes (36h), scale bar: 50µm. B: Enlarged images and C: binary of enlarged images, Scale bar: 10µm. D: Quantification of mitochondrial network in Ctrl vector and Zc3h10 Flag 36h differentiated cells; statistical analysis was performed by Student's t-test; *p<0.05 vs Ctrl vector.

To further assess the impact of Zc3h10 in mitochondrial dynamic, we measured the expression of proteins involved in mitochondrial dynamics (Fig. 4.20-21). Zc3h10 depleted pre-adipocytes showed decreased levels of the long form of OPA1 (Long-Opa1), which is necessary for mitochondrial fusion while the OPA1 short form (Short-Opa1) was unchanged (Fig. 4.20A). Furthermore, MFN2 levels were unchanged as well as the total DRP1 level (Fig. 4.20B, 4.21A) and DRP1 phosphorylation at Ser637(Fig. 4.21B), whereas DRP1 phosphorylation at Ser616 residue increased (Fig. 4.21C). Of note, the Ser616/Ser637 DRP1 phosphorylation ratio was

significantly increased in Zc3h10 silenced cells, suggesting increased mitochondrial fission (Fig. 4.21D). In contrast, Zc3h10 overexpression led only to a significant increase of MFN2 levels (Fig. 4.20B). Together, these data suggest that Zc3h10 favors mitochondrial network mass and complexity by enhancing mitochondrial fusion, a process that is necessary for the adipocytes' differentiation program.

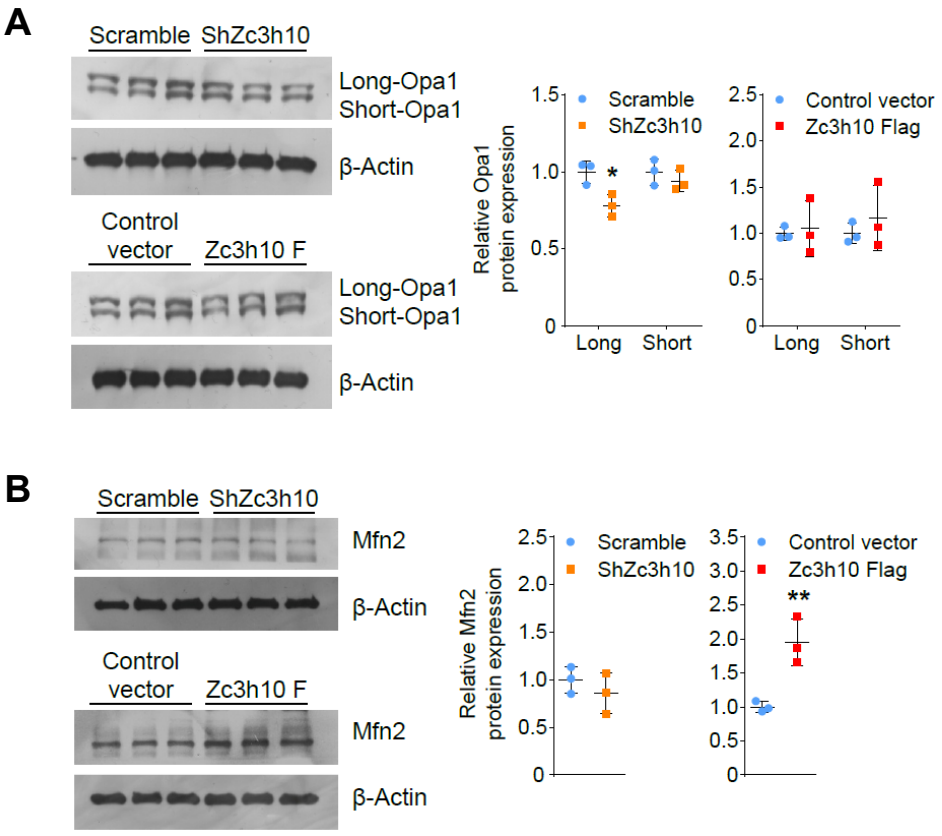

Figure 4.20: Western blot analysis of mitochondrial fusion proteins. A: Opa1 and B: Mfn2 blotting and relative quantification in ShZc3h10 and Zc3h10 Flag pre-adipocytes; statistical analysis was performed by Student's t-test; *p<0.05, **p<0.01 vs Scramble or Ctrl vector, respectively.

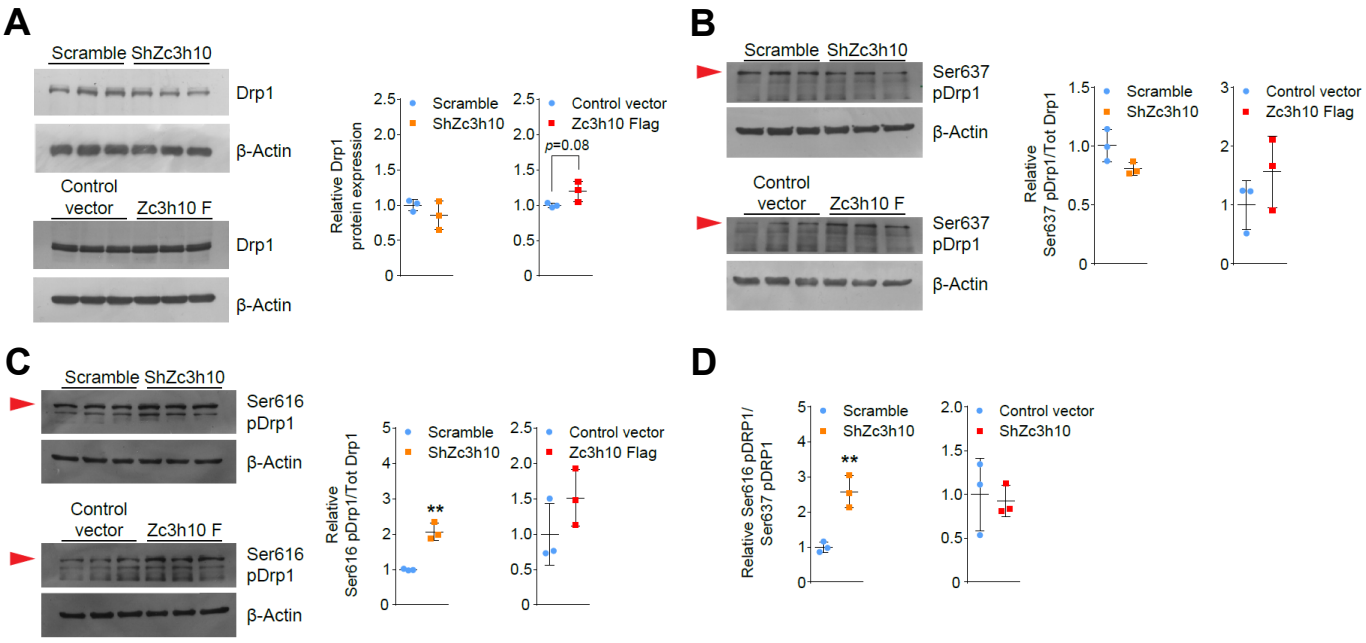

Figure 4.21: Western blot analysis of A: Drp1, mitochondrial fission marker, B: Ser637 phosphorylated Drp1, and C: Ser616 phosphorylated Drp1 with relative quantifications in ShZc3h10 and Zc3h10 Flag pre-adipocytes; statistical analysis was performed by Student's t-test; *p<0.05, **p<0.01 vs Scramble or Ctrl vector, respectively.

We also decided to study the interaction between F-actin and mitochondria during adipogenesis to understand if Zc3h10 is involved in the coordination of mitochondria/F-actin contact. Proliferating MSCs showed high colocalization between F-actin and mitochondria that progressively declined until cellular confluence. Hormonal stimulation favored F-actin reorganization and initially increased the contact F-actin/mitochondria at day 1 and decreased at 36h to promote the adipogenic process (Fig.4.22A, B).

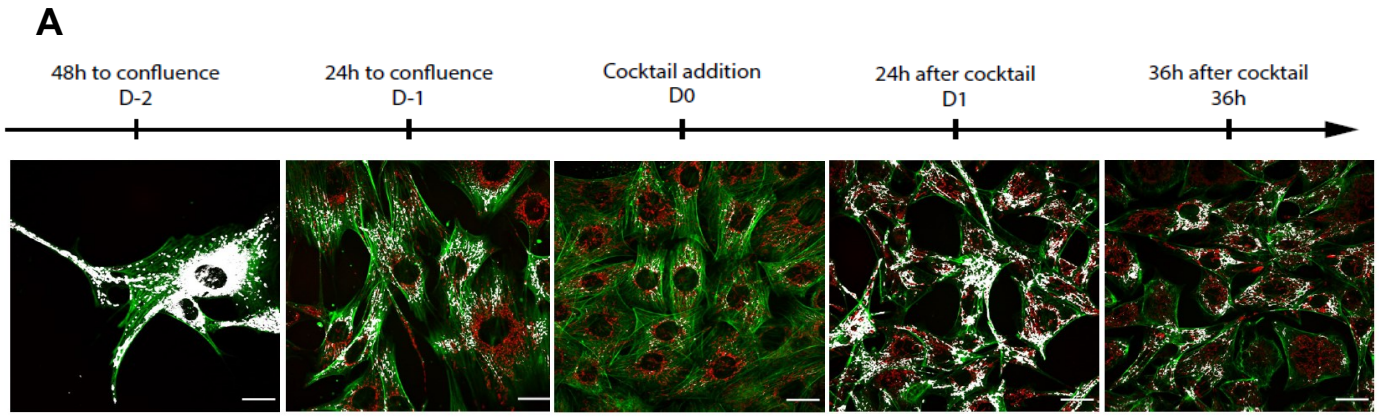

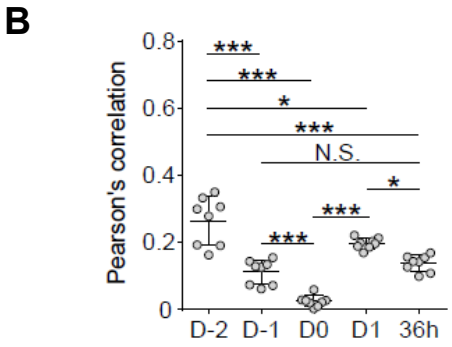

Figure 4.22: A: Representative images and B: quantitative analysis of mitochondria/F-actin colocalization in the early phases of adipogenesis (from proliferating MSCs to 36h differentiated pre-adipocytes). Red: mitochondria; green: F-actin; white: colocalized pixels; statistical analysis was performed by One-Way ANOVA followed by Sidak's post-hoc test; *p<0.05, ***p<0.001. Scale bar: 25µm.

Next, we investigated F-actin/mitochondrial interaction in silenced and overexpressing Zc3h10 pre-adipocytes (Fig. 4.23). We observed a significant increase in F-actin/mitochondria interaction in Zc3h10-depleted adipocytes (Fig.4.23A), while the overexpression of this protein caused the opposite effect, showing less contacts between the organelles (Fig. 4.23B).

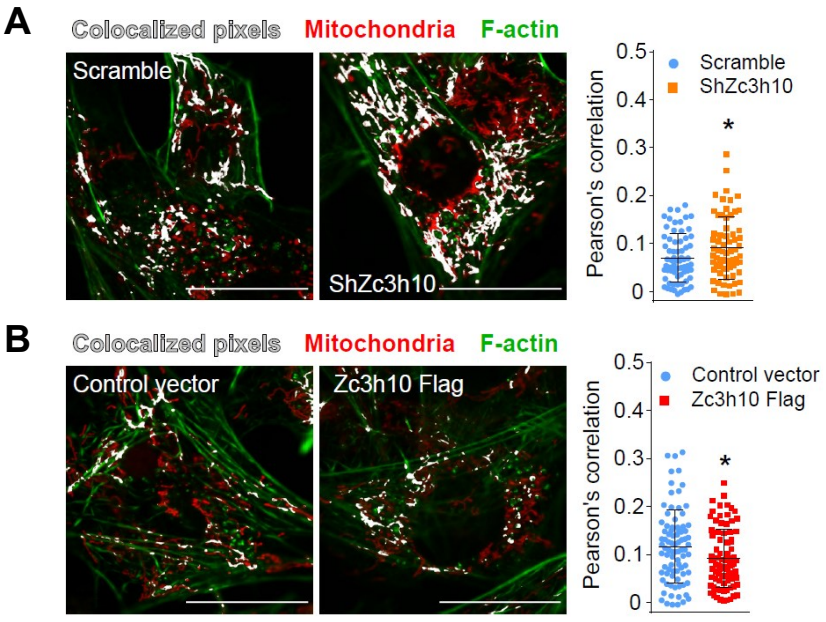

Figure 4.23: A: Colocalization analysis of mitochondria and F-actin in ShZc3h10 and B: Zc3h10 Flag cells; statistical analysis was performed by Student's t-test; *p<0.05 vs Scramble. Scale bar: 25µm.

Finally, we assessed that lipid accumulation is associated with mitochondrial and actin morphology. We found that Zc3h10 depletion altered mitochondrial morphology during all adipogenic program (36 hours, 5, and 9 days after differentiation's induction) (Fig. 4.24). Our results indicated that mitochondrial network complexity and density were decreased in Zc3h10 depleted pre-adipocytes (Fig. 4.24A, B, C). Moreover, we observed that significant interaction between F-actin and mitochondria prevented mitochondrial morphological changes, thus affecting the lipid accumulation and the correct differentiation program in mature adipocytes. Oppositely, Zc3h10-Flag cells showed an increase in mitochondrial density and network, which is reflected by increased lipid accumulation and increased lipid droplets size (Fig. 4.24D, E, F).

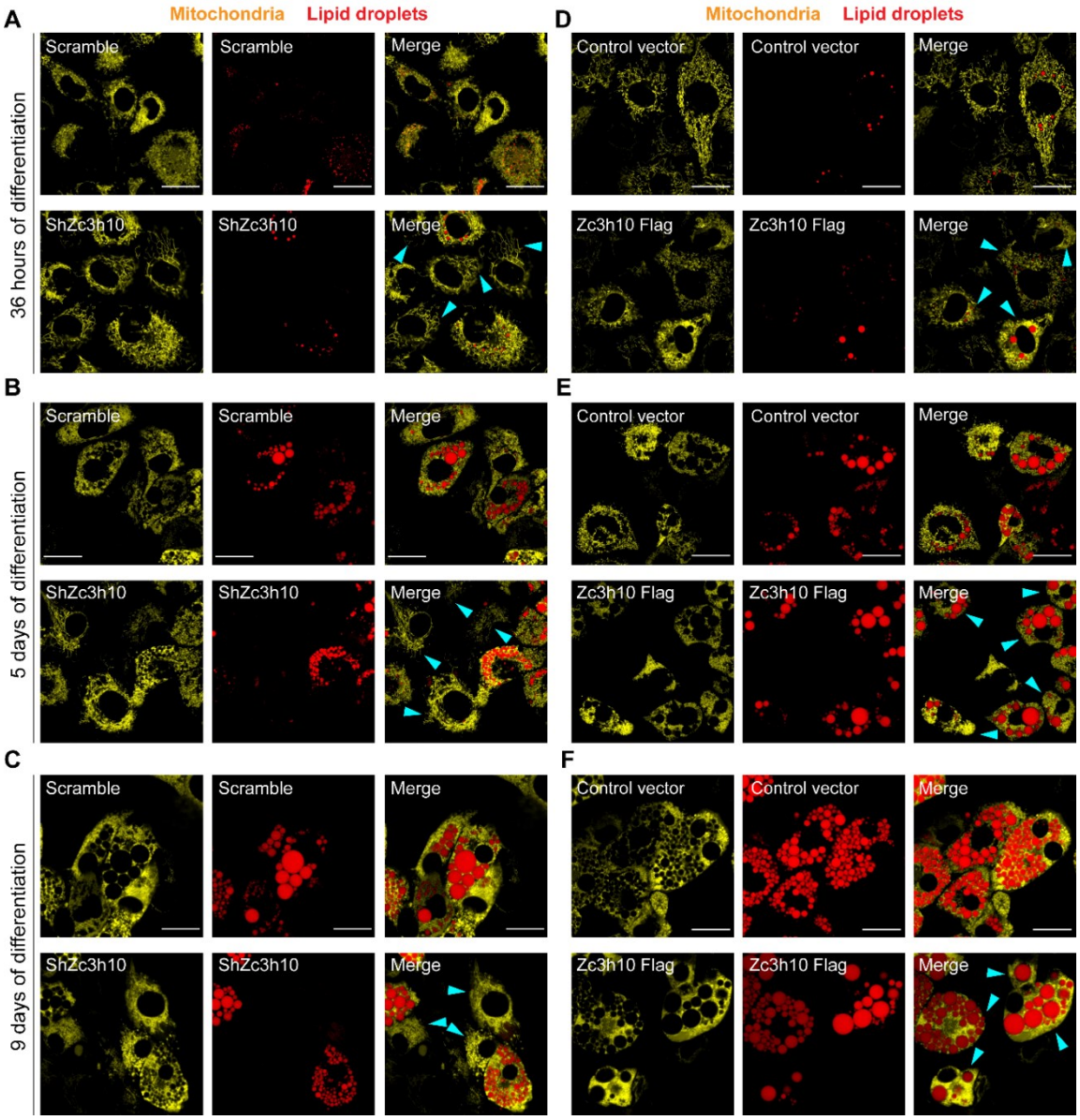

Figure 4.24: Mitochondrial network is regulated by Zc3h10 during adipogenesis and is associated with lipid accumulation. A: Representative images of lipid droplets (red) and mitochondria (yellow) in Scramble and ShZc3h10 differentiated for 36h, B: 5 days and C: 9 days. Cyan arrows indicate major alterations of mitochondrial network. Scale bar: 25µm. D: Representative images of lipid droplets (red) and mitochondria (yellow) in Ctrl vector and Zc3h10 Flag overexpressing cells differentiated for 36h, E: 5 days and F: 9 days. Cyan arrows indicate major differences of mitochondrial network. Scale bar: 25µm.

4.6 Zc3h10 favors Rho-GTPases function to stimulate F-actin remodeling, mitochondrial dynamics, and lipid accumulation

Our previous results showed that Zc3h10 affected the organization of F-actin and mitochondria morphology. Therefore, we assessed if Zc3h10 altered the synthesis of some regulators of cytoskeletal remodeling.

4-sU-seq results demonstrated that Zc3h10 silencing decreased expression of pre-mRNA of the regulatory subunit of PKA (Prkar2b), Platelet Derived Growth Factor Receptor Alpha (Pdgfra), Ephrin B2 (Efnb2), and the Protein Kinase AMP-Activated (AMPK) Non-Catalytic Subunit Gamma 2 (Prkag2). All these proteins are involved in the regulation of Rho-GTPases activities (Feng et al., 2011; Murai and Pasquale, 2003; Herring and Nicoll, 2016; Salt and Hardie, 2017) (Fig. 4.25).

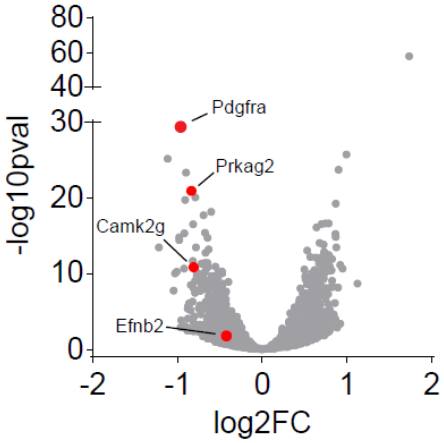

Figure 4.25: Volcano plot of differentially expressed pre-mRNA in ShZc3h10 and Scramble cells. Red dots indicate labelled downregulated genes in ShZc3h10 pre-adipocytes (36 hours after differentiation induction); FDR<0.05.

Cyclic AMP-dependent protein kinase A (PKA) activation is one of the main and early pathways that regulate F-actin remodeling during the adipogenic program by affecting the activity of Rho GTPases (Cristancho and Lazar, 2011; Howe, 2004; Yu et al., 2013); PKA activates Rac1 and Cdc42 and inhibits RhoA pathways (Bachmann et al., 2013; Howe, 2004; O'Connor and Mercurio, 2001; Price et al., 1998). On these premises, by removing from the adipogenic cocktail the PKA activator, 3-isobutyl-1-methylxanthine (IBMX), we tested if Zc3h10 requires PKA activation to favor lipid accumulation.

Scramble control cells, induced with the canonical differentiation cocktail lacking of IBMX, showed an increased number of lipid positive cells, and unchanged lipid droplet size, although the expression of Pparg and Cebpa was significantly reduced and a fibroblast-like cell shape was still present (Fig. 4.26A, B, C, D, E). Zc3h10 overexpression, regardless of IBMX, favored cell shape changes, increased lipid droplet size despite decreased lipid-containing cells (Fig. 4.26A, B, C, D). These data are supported by expression analysis of adipogenic genes, which were significantly downregulated in cells differentiated without IBMX, but were increased in cells overexpressing Zc3h10 differentiated without IBMX even above the levels seen in control cells differentiated with IBMX (Fig. 4.26E).

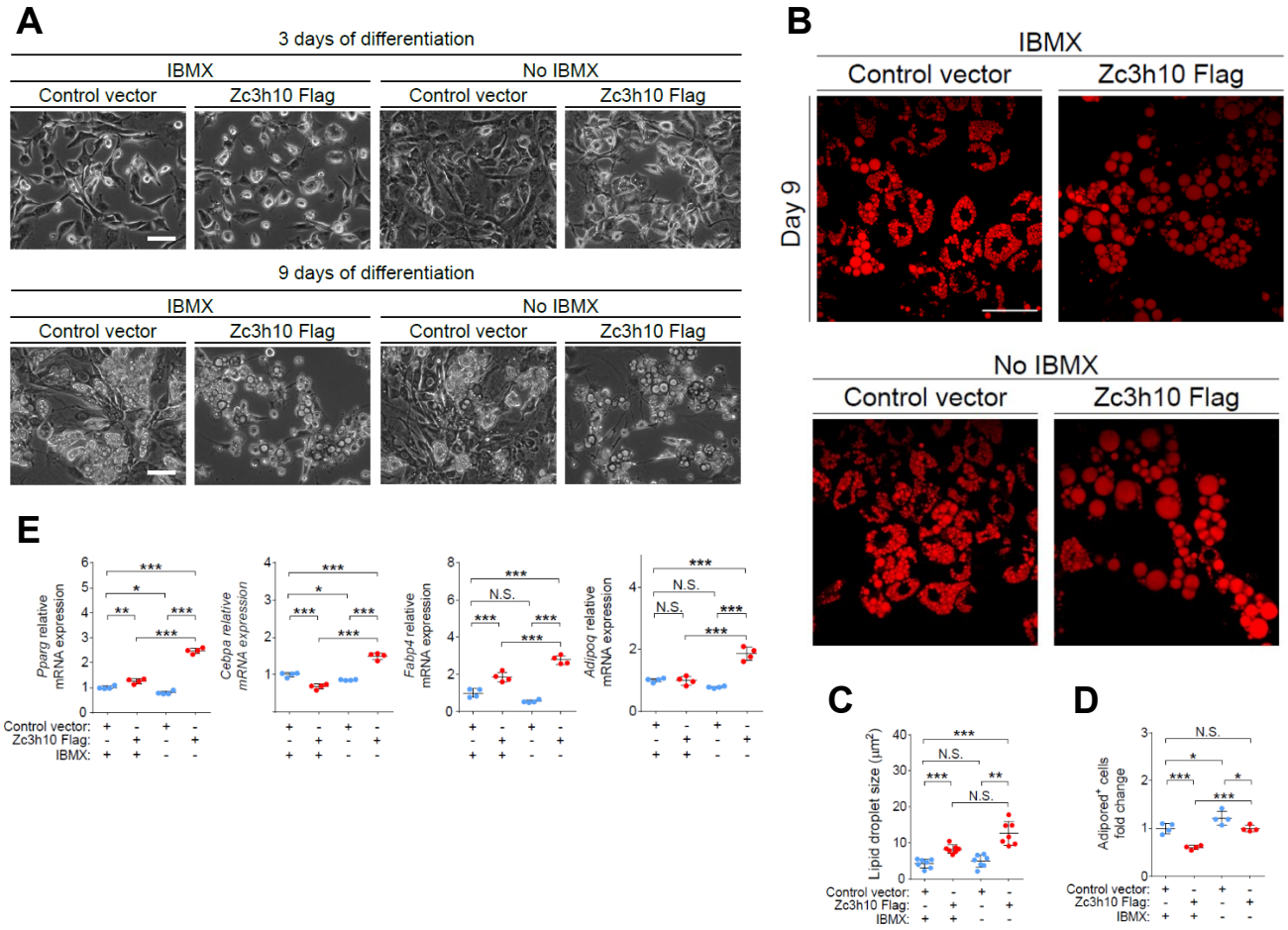

Figure 4.26: A: Brightfield images of Zc3h10 Flag pre-adipocytes and mature adipocytes with or without IBMX in differentiation cocktail. Scale bar: 50µm. B: Lipid droplets images (Scale bar: 50µm), C: size quantification, and D: Adipored positive cells in Ctrl vector and Zc3h10 Flag mature adipocytes with and without IBMX in differentiation cocktail. E: gene expression analysis of adipogenic markers Pparg Cebpa, Fabp4 and Adipoq in Control vector and Zc3h10 Flag mature adipocytes with and without IBMX; statistical analysis was performed by One-Way ANOVA followed by Sidak's post-hoc test;*p<0.05, **p<0.01, ***p<0.001.

Furthermore, we used chemical inhibitors of the three Rho-GTPase pathways to better define the molecular pathways regulated by Zc3h10 that control F-actin remodeling and consequently, mitochondrial function. The treatment of Zc3h10-depleted pre-adipocytes with a ROCK inhibitor (Y27632) rescued the number of junctions per mitochondria, and mitochondrial area (Fig. 4.27A), increase lipid droplets size but did not affect the number of total mature adipocytes (Adipored⁺ cells) (Fig. 4.28A). On the contrary, we treated Zc3h10 overexpressing pre-adipocytes with Cdc42 and Rac1 inhibitors. ML141 (a Cdc42 inhibitor) treatment reduced the

number of mitochondrial junctions, branches and mitochondrial area, but it had no effect on lipid droplet size, lipid positive cells, in Zc3h10 overexpressing cells (Fig. 4.27B and 4.28B). To complete this evaluation, we investigated Rac1 inhibition (NSC23766) and established that this treatment abolished the number of mitochondrial junctions and branches and normalized lipid droplet size (Fig. 4.27C and 4.28C). Regarding mature adipocytes, inhibition of Rac1 caused a decrease in the number of cells positive to lipid accumulation in the Control vector condition and Zc3h10 Flag (Fig. 4.28C).

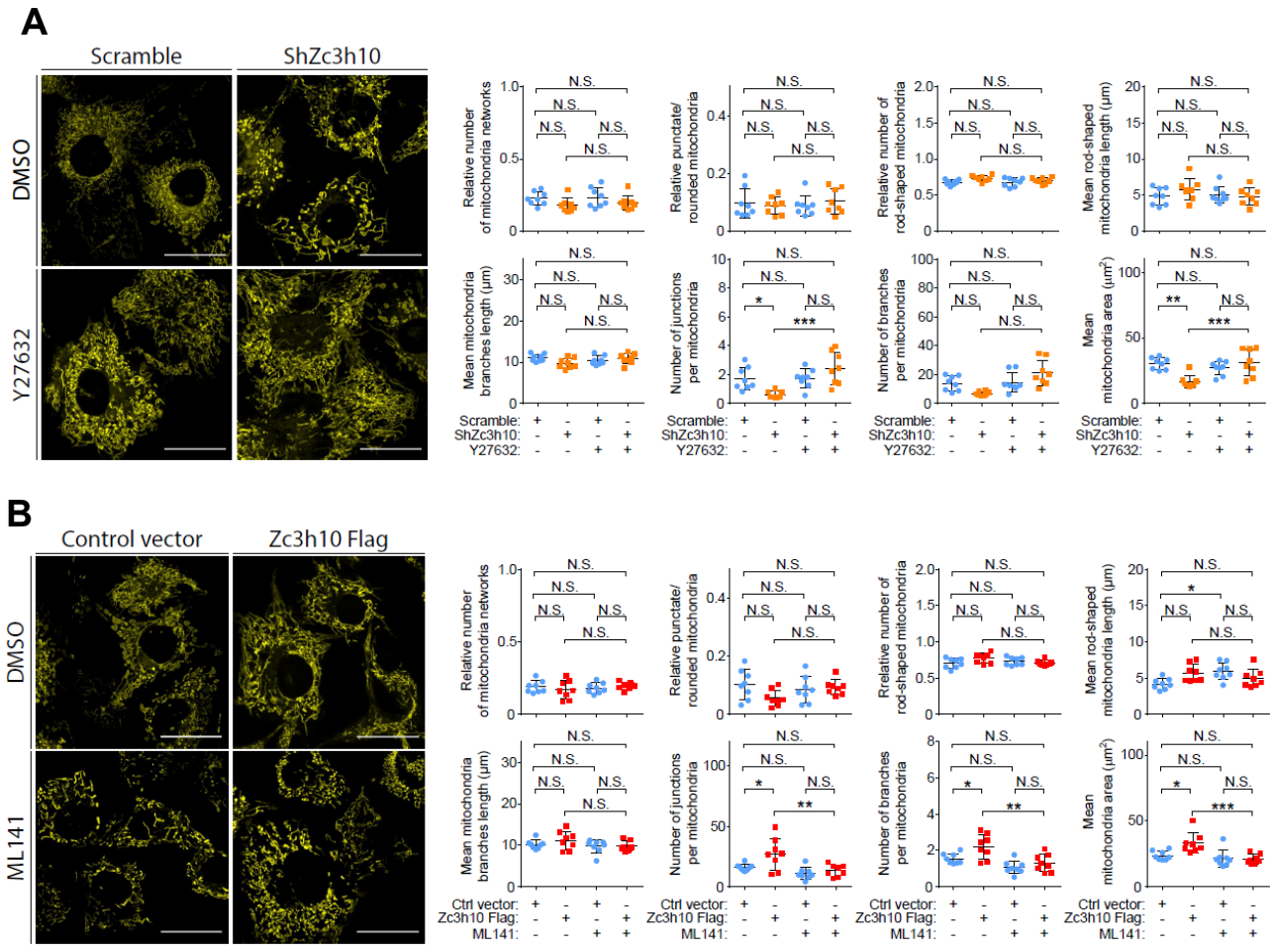

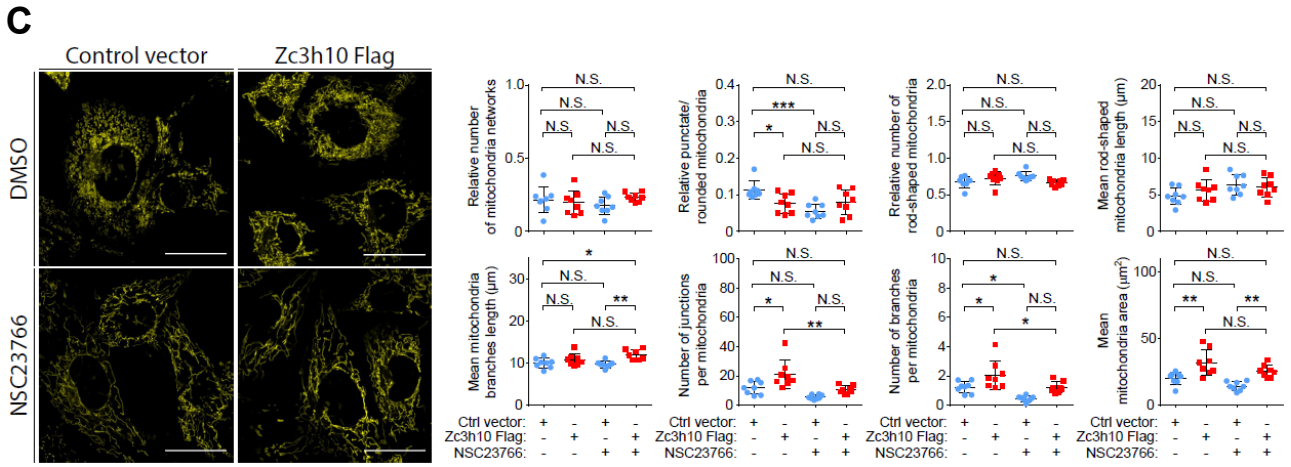

Figure 4.27: ROCK, Cdc42 and Rac1 RhoGTPases mediate Zc3h10 activity on mitochondrial network. A: Confocal images of mitochondria stained with Mitotracker Deep Red FM probe and mitochondrial network analysis in Scramble and ShZc3h10 pre-adipocytes exposed to DMSO or Y27632 10µM and differentiated for 36h. Scale bar: 10µm; statistical analysis was performed by One-Way ANOVA followed by Sidak's post-hoc test; *p<0.05, **p<0.01, ***p<0.001. B: Mitochondrial network and its analysis in Ctrl vector and Zc3h10 Flag pre-adipocytes exposed to DMSO or ML141 10µM and C: NSC23766 50µM and differentiated for 36h. Scale bar: 10µm; statistical analysis was performed by One-Way ANOVA followed by Sidak's post-hoc test; *p<0.05, **p<0.01, ***p<0.001.

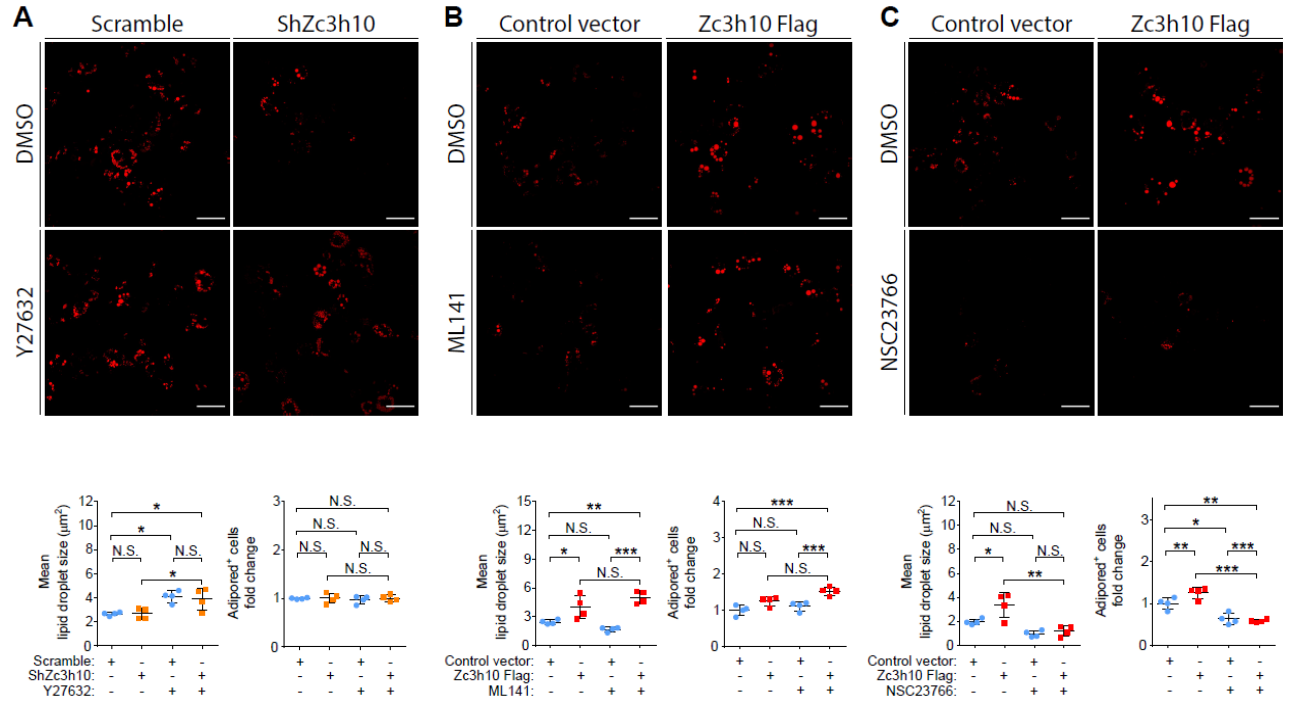

Figure 4.28: RhoGTPases activity is required for adipogenesis. A: Lipid droplets confocal microscopy images (upper panels), size quantification and AdipoRed+ cells (bottom panel) in 5 days differentiated adipocytes exposed to ShZc3h10 with DMSO or Y27632 10µM, B: Zc3h10 Flag with DMSO or ML141 10µM and C: Zc3h10 Flag with DMSO or NSC23766 50µM.

4.7 Zc3h10 controls mitochondrial function and cellular metabolism.

We applied functional and metabolomic analysis to investigate the role of Zc3h10 on mitochondrial function and metabolism during white adipocytes differentiation program. Zc3h10 silenced pre-adipocytes showed reduced maximal respiration, while basal and uncoupled respiration did not change (Fig. 4.29A). Moreover, Zc3h10 depleted pre-adipocytes showed decreased pentose phosphate pathway intermediates, and several tricarboxylic acid (TCA) cycle metabolites, while various amino acids and acylcarnitines were increased compared to scramble control (Fig. 4.29C, D). We evaluated carnitines ratio as an indicator of fatty acid oxidation rate, and we observed that carnitines C2/C0, C2+C3/C0 ratios were increased in ShZc3h10 cells (Fig. 4.29E). Furthermore, carnitine palmitoyl transferase 1a (Cpt1a) activity index (C16:0+C18:0/C0) was raised, indicating an intensification in the transport of fatty acids inside the mitochondria to undergo the beta-oxidation process (Fig. 4.29E). These data were also accompanied by a trend to increase NAD^+/NADH ratio, and reduced energy charge in Zc3h10 silenced pre-adipocytes (Fig. 4.29F and B).

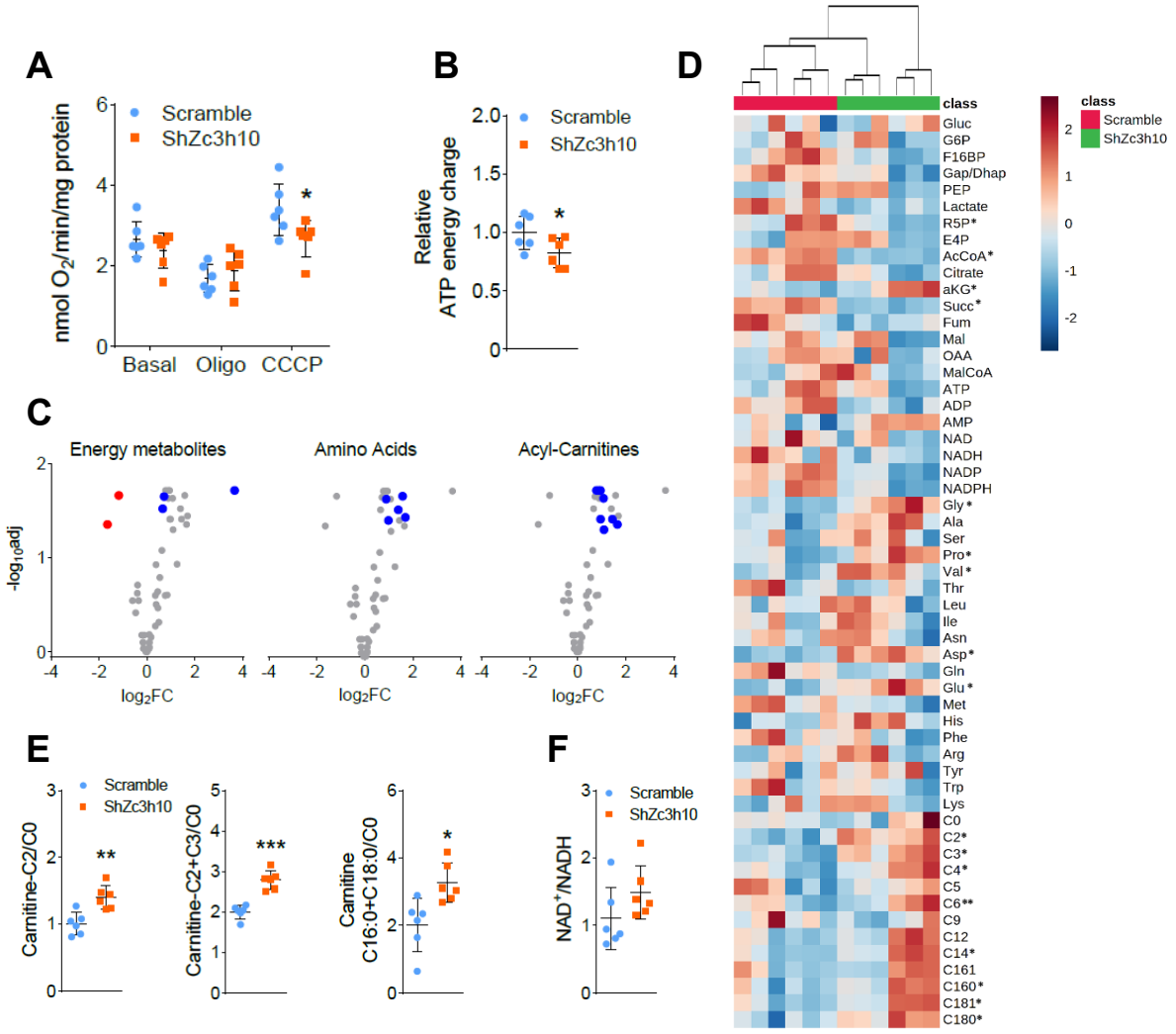

Figure 4.29: Mitochondrial function and metabolism in Zc3h10-depleted pre-adipocytes. A: Basal respiration, uncoupled (Oligo) and maximal uncoupled respiration (CCCP) and B: relative ATP energy charge in ShZc3h10 pre-adipocytes. Statistical analysis was performed by Student's t-test; *p<0.05 vs Scramble. C: Volcano plots representing significantly decreased (red dots), increased (blue dots) and unchanged (gray dots) energy metabolites, amino acids and acyl-carnitines in Scramble and ShZc3h10 pre-adipocytes; statistical analysis was performed by multiple Student's t-test followed by FDR calculation; FDR<0.05 vs Scramble. D: Heatmap of metabolomic analysis in Scramble and ShZc3h10 pre-adipocytes. statistical analysis was performed by multiple Student's t-test followed by FDR calculation; *FDR<0.05 vs Scramble. E: C2 acyl-carnitine/free carnitine (C0), C2+C3 acyl-carnitines/C0 and C16:0+C18:0 acyl-carnitines/C0 ratios and F: NAD^+/NADH ratio in Scramble and ShZc3h10 pre-adipocytes; statistical analysis was performed by Student's t-test; *p<0.05, **p<0.01, ***p<0.001 vs Scramble.

During adipogenesis, the cells are supposed to synthesize lipids (*de novo* lipogenesis) and accumulate them in lipid droplets. In this context, glucose and glutamine represent the main lipogenic substrates (De Pauw et al., 2009b). To better understand how Zc3h10 acts on cell

metabolism, we performed metabolic flux analysis comparing Zc3h10 depleted pre-adipocytes to control (Fig. 4.30). From this analysis, we found a decreased oxidation of glucose-derived ^{13}Carbon in the TCA cycle, such as M2 and M3 citrate, M2, and M3 a-ketoglutarate (a-KG) in ShZc3h10 cells (Fig. 4.30A). These data were consistent with decreased mRNA expression of isocitrate dehydrogenase 3a (Idh3a) and malate dehydrogenase 2 (Mdh2) (Fig. 4.30D). Of note, Zc3h10 silenced cells displayed increased M2 acetyl-CoA (AcCoA), M2 malate, and M4 oxaloacetate (OAA) that were accumulated due to reduced expression of citrate synthase (Cs) (Fig. 4.30A and D). Furthermore, glutamine utilization through oxidative metabolism was impaired, as evidenced by decreased M4 fumarate and M4 OAA as well as reductive glutamine metabolism, as evidenced by M2 AcCoA, M5 citrate, M3 OAA (Fig. 4.30B). These latter data were consistent with decreased mRNA expression of ATP citrate lyase (Acly). Moreover, decreased M2 OAA from glutamine was consistent with reduced levels of pyruvate carboxylase (Pcx) (Fig. 4.30D). Prompted by these results, we tested fatty acid utilization as an alternative energy source in Zc3h10 silenced cells. Zc3h10 depleted cells and relative controls were exposed to [U-$^{13}C_{16}$]palmitate. Palmitate-derived ^{13}Carbon incorporation was increased in M2 AcCoA and in different TCA cycle metabolites such as M2 and M4 citrate, M2, M3, and M4 a-KG, M2 and M3 malate, and M4 OAA (Fig. 4.30C). Thus, partial loss of Zc3h10 in pre-adipocytes led to TCA cycle defects, which blunted metabolic pathways sustained by glucose and glutamine utilization and imposed fatty acid oxidation to maintain energy homeostasis.

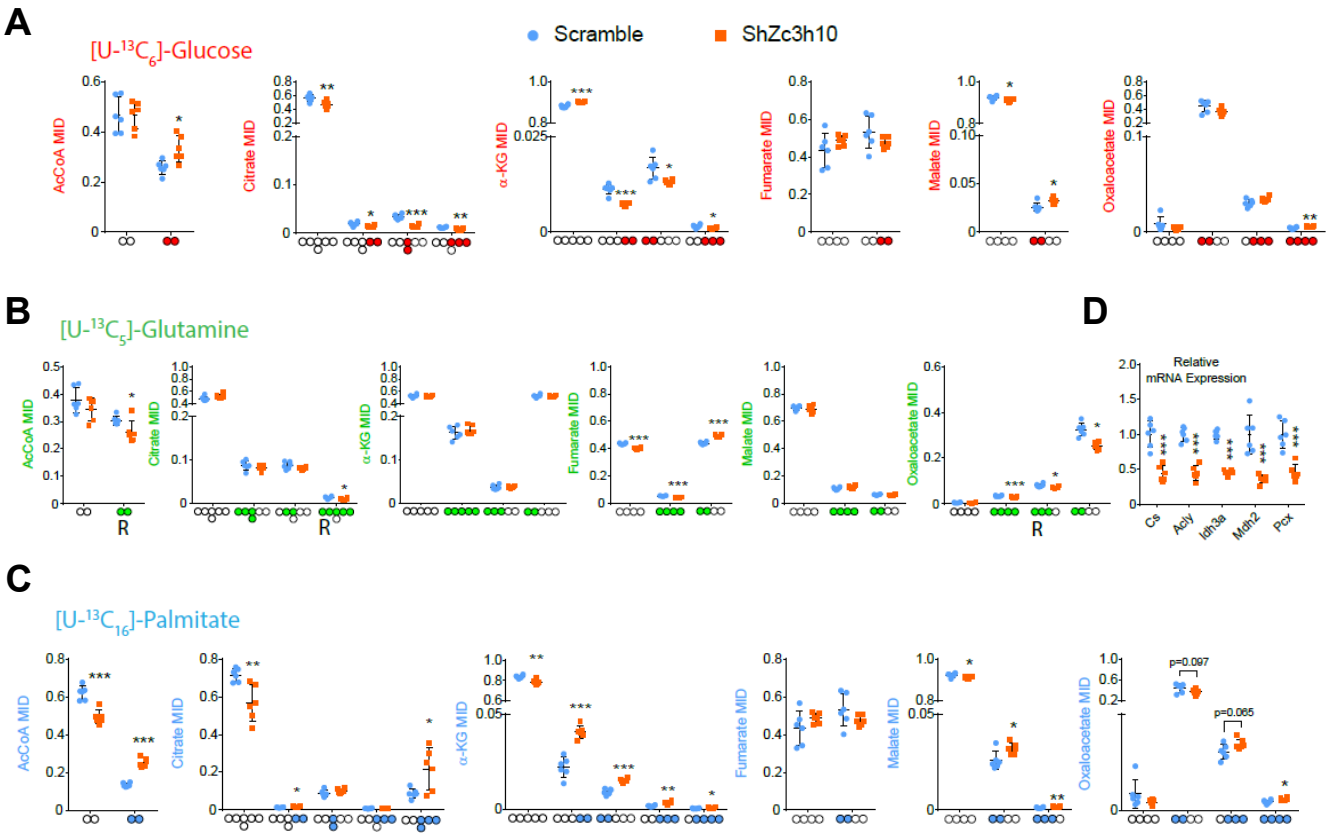

Figure 4.30: TCA cycle flux of glucose, glutamine, and palmitic acid-derived metabolites in Zc3h10-silenced pre-adipocytes. A: Relative abundance of indicated isotopomers belonging to TCA cycle derived from [U-$^{13}C_6$]-Glucose, B: [U-$^{13}C_5$]-Glutamine, and C: [U-$^{13}C_{16}$]-Palmitate in Scramble and ShZc3h10 pre-adipocytes; statistical analysis was performed by Student's t-test; *p<0.05, **p<0.01, ***p<0.001 vs Scramble. D: Relative mRNA expression of metabolic genes citrate synthase (Cs), ATP citrate lyase (Acyl), Isocitrate dehydrogenase α (Idh3α), Malate dehydrogenase 2 (Mdh2) and Pyruvate carboxylase (Pcx) in Scramble and ShZc3h10 pre-adipocytes; statistical analysis was performed by Student's t-test; ***p<0.001 vs Scramble.

Zc3h10 silenced mature adipocytes showed a more severely affected mitochondrial phenotype characterized by decreased coupled, uncoupled, and maximal respiration, as well as blunted expression levels of different Oxphos subunits, Pparγ, and Tfam proteins (Fig. 4.31A, E). Zc3h10 silenced mature adipocytes also showed a more altered metabolic profile than pre-adipocytes (Fig. 4.31C, D), characterized by an unchanged energy charge (Fig. 4.31B), decreased NAD+/NADH ratio (Fig. 4.31G), increased C2/C0, C2+C3/C0 carnitine ratios, and carnitine palmitoyl transferase 1a (Cpt1a) activity index (C16:0+C18:0/C0)(Fig. 4.31F).

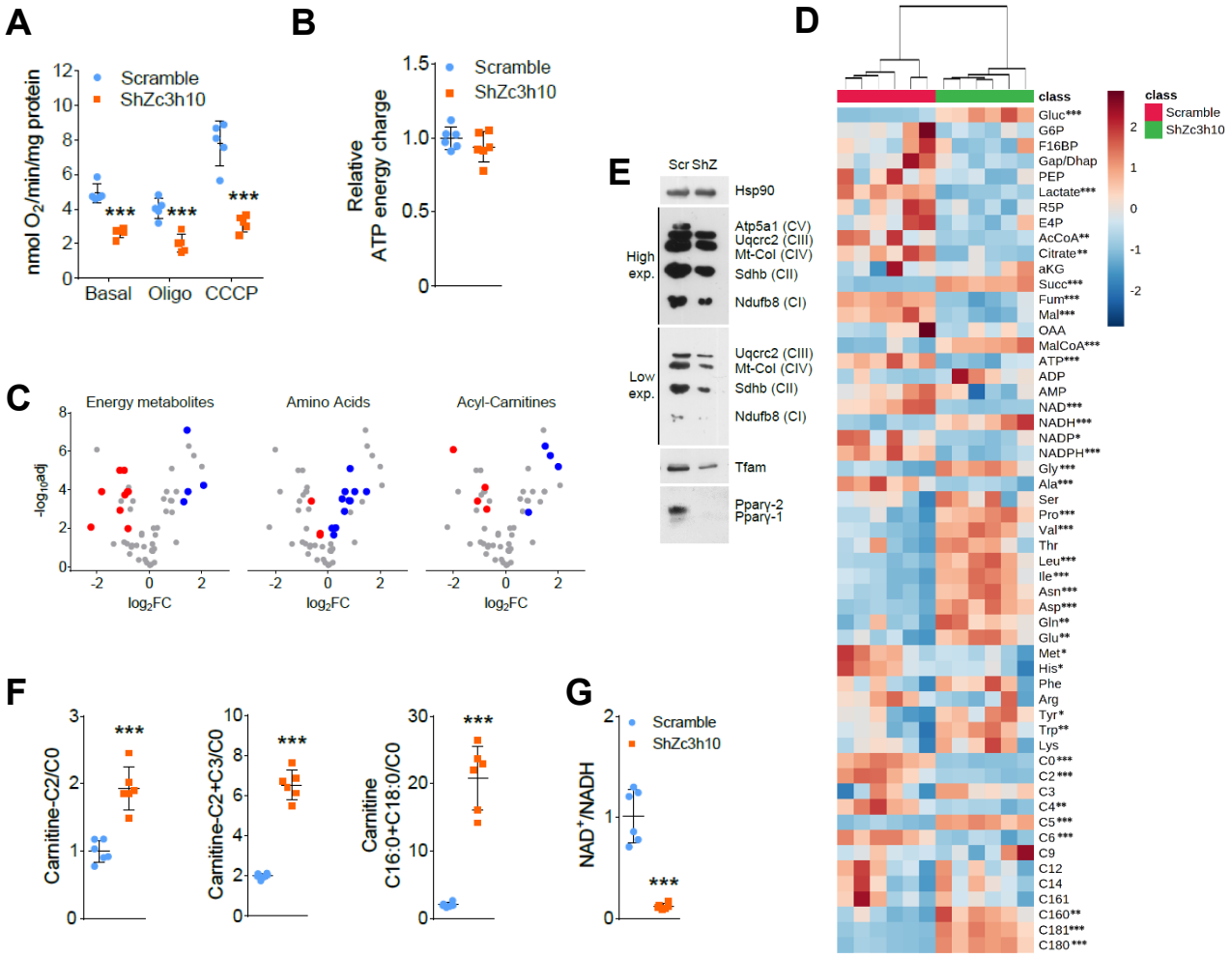

Figure 4.31: Mitochondrial function and metabolism in Zc3h10-depleted mature adipocytes. A: Basal respiration, uncoupled (Oligo) and maximal uncoupled respiration (CCCP) and B: relative ATP energy charge in ShZc3h10 mature adipocytes. Statistical analysis was performed by Student's t-test; ***p<0.001 vs Scramble. C: Volcano plots representing significantly decreased (red dots), increased (blue dots) and unchanged (gray dots) energy metabolites, amino acids and acyl-carnitines in Scramble and ShZc3h10 mature adipocytes; statistical analysis was performed by multiple Student's t-test followed by FDR calculation; FDR<0.05, FDR<0.01, FDR<0.001 vs Scramble. D: Heatmap of metabolomic analysis in Scramble and ShZc3h10 adipocytes. statistical analysis was performed by multiple Student's t-test followed by FDR calculation; *FDR<0.05 vs Scramble. E: Western blot of some oxphos subunits (high exposure and low exposure), Tfam and Pparγ in Scramble and ShZc3h10 mature adipocytes. F: C2 acyl-carnitine/free carnitine (C0), C2+C3 acyl-carnitines/C0 and C16:0+C18:0 acyl-carnitines/C0 ratios and G: NAD^+/NADH ratio in Scramble and ShZc3h10 mature adipocytes; statistical analysis was performed by Student's t-test; ***p<0.001 vs Scramble.

Metabolic flux analysis confirmed that also Zc3h10 depleted adipocytes experience reduced glucose and glutamine oxidative metabolism and increased fatty acid catabolism (Fig. 4.32A, B, C).

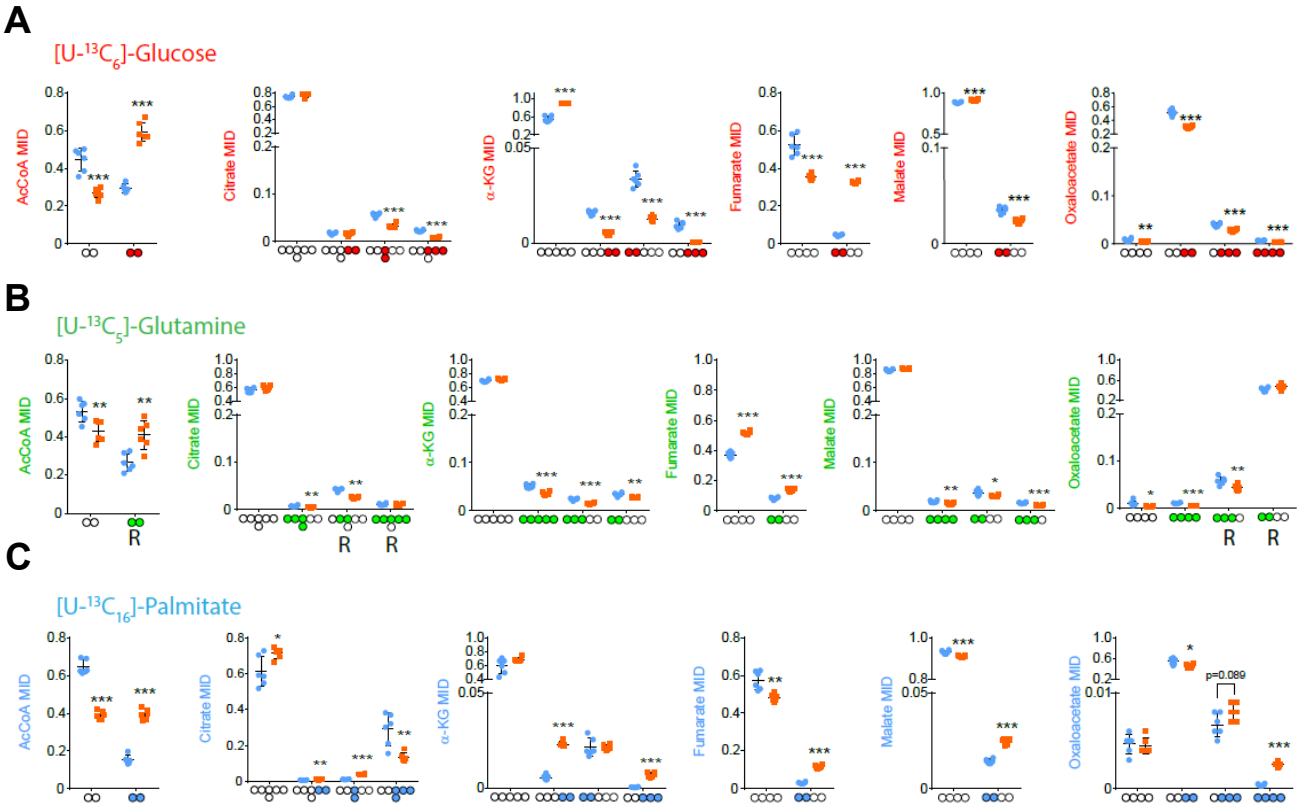

Figure 4.32: TCA cycle flux of glucose, glutamine, and palmitic acid-derived metabolites in Zc3h10-silenced mature adipocytes. A: Relative abundance of indicated isotopomers belonging to TCA cycle derived from [U-$^{13}C_6$]-Glucose, B: [U-$^{13}C_5$]-Glutamine, and C: [U-$^{13}C_{16}$]-Palmitate in Scramble and ShZc3h10 mature adipocytes; statistical analysis was performed by Student's t-test; *p<0.05, **p<0.01, ***p<0.001 vs Scramble.

Moreover, to confirm the increased use of fatty acids (lipolysis) in the absence of Zc3h10, we quantified glycerol into the cell culture's supernatant. A significant increase in glycerol release was observed in the medium of Zc3h10-depleted cells (ShZc3h10) compared to the control group at day 3 (pre-adipocytes) (Fig. 4.33A) and this effect was exacerbated on day 9 (mature adipocytes) after differentiation induction (Fig. 4.33B), indicating an increase in lipid oxidation and fatty acids utilization.

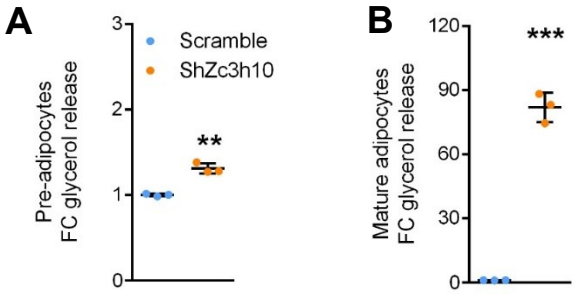

Figure 4.33: Relative quantification of glycerol release in cell media of Zc3h10-depleted pre- (A) and mature (B) adipocytes.

Consistently, transcriptomic profile ultimately revealed that metabolism and mitochondrial function were downregulated pathways in Zc3h10 silenced mature adipocytes. These results substantiate that partial loss of Zc3h10 in pre-adipocytes resulted in dysfunctional mitochondria and metabolism, a condition that lasts until the end of the differentiation process (Fig. 4.34A, B).

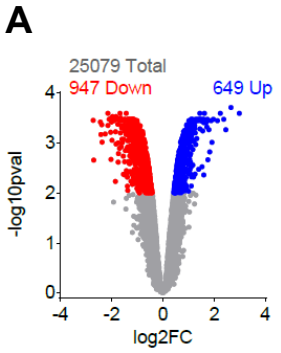

B

Pathway	Direction	NES	DEG (%)	adj pval
Cofactor metabolic process	Down	-9.555	120/338 (35)	2.80E-17
Fatty acid metabolic process	Down	-9.355	112/242 (46)	3.90E-16
Generation of precursor metabolites and energy	Down	-8.230	110/276 (40)	6.80E-13
Nucleoside bisphosphate metabolic process	Down	-7.497	47/77 (61)	9.70E-10
Ribonucleotide metabolic process	Down	-7.412	105/310 (34)	1.10E-10
Small molecule catabolic process	Down	-7.046	80/220 (36)	1.10E-09
Cellular respiration	Down	-6.568	56/124 (45)	2.40E-08
Energy derivation by oxidation of organic compounds	Down	-6.286	73/177 (41)	7.80E-08
Electron transport chain	Down	-6.054	46/100 (46)	4.70E-07
Mitochondrion organization	Down	-5.789	73/356 (20)	6.60E-07
Cell morphogenesis involved in differentiation	Up	6.708	83/454 (18)	4.10E-08
Microtubule-based process	Up	6.706	59/497 (12)	4.10E-08
Plasma membrane bounded cell projection morphogenesis	Up	6.187	75/398 (19)	5.90E-07
Cell projection morphogenesis	Up	6.146	75/400 (19)	5.90E-07
Cell morphogenesis involved in neuron differentiation	Up	5.900	68/359 (19)	1.50E-06
Microtubule cytoskeleton organization	Up	5.806	42/379 (11)	2.20E-06
Actin filament-based process	Up	5.770	81/457 (18)	2.30E-06
Nuclear division	Up	5.753	22/266 (8)	3.00E-06
Cell projection assembly	Up	5.706	37/314 (12)	3.30E-06
Cell division	Up	5.642	42/421 (10)	3.90E-06

Figure 4.34: Transcriptomic analysis in Zc3h10-deplited mature adipocytes compared to Scramble group. A. Volcano plot of significantly (FDR<0.01) downregulated (red), upregulated (blue) and unchanged (gray) mRNAs in ShZc3h10 compared to Scramble mature adipocytes (Day 9). Kruskal-Wallis test of Rank with Dunn's post-hoc test; ***p<0.001 vs Scramble. B: GAGE pathway analysis of significant down and upregulated mRNAs clusters from Scramble and ShZc3h10 mature adipocytes. Table indicates pathway name, trend, normalized enrichment score (NES), number of differentially

expressed genes with percentage compared to total genes in the cluster (DEG (%)) and adjusted p-value (adj pval).

4.8 Zc3h10 levels modulate cell cycle progression during adipogenesis.

Transcriptomic analysis (Fig. 4.34) also showed that several gene clusters related to mitosis were upregulated in Zc3h10 depleted adipocytes. Based on these upregulated clusters, we characterized the effect of Zc3h10 on MCE by analyzing the distribution of cells in the different phases of the cell cycle and the proliferation rate during adipogenesis (Fig. 4.35-36).

In C3H10T1/2 cells, the MCE is detected at day 4 after induction of differentiation. At pre-MCE stage, Zc3h10 depleted cells were higher in S (day 3) and G2/M (day 1 and 2) phases compared to scramble control. At the MCE (day 4), Zc3h10 silencing led to retention in G2/M, decreasing the number of cells in G0/G1, suggesting a failure to exit from G2/M. In post-MCE stage, Zc3h10 knock-down cells exhibited a similar accumulation in S and G2/M phases observed before MCE, with a concomitant decrease of cells in G0/G1. These effects on cell cycle were associated with defects in cell division; Zc3h10 depleted adipocytes showed a significant decrease in the number of dividing cells starting from day 3, and this difference was amplified post-MCE (Fig. 4.35A, B).

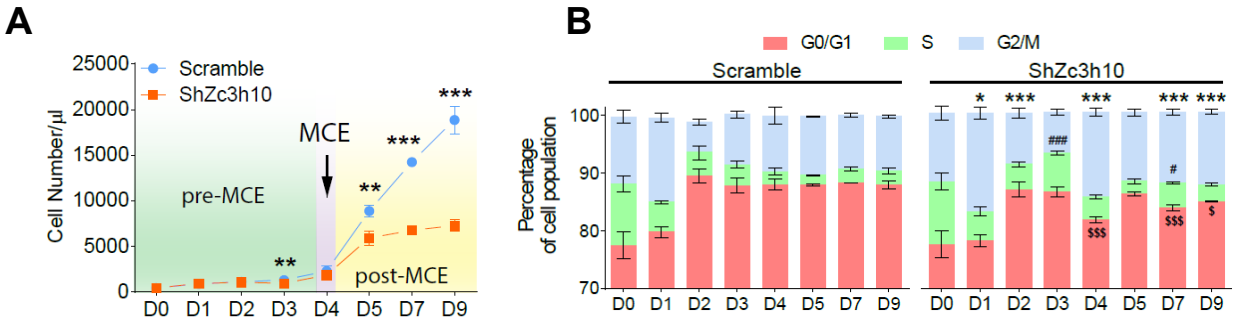

Figure 4.35: Zc3h10 silencing compromises MCE by blocking cells in G2/M phases. A: total cell number count by cytofluorimetry analysis of ShZc3h10 cells. Green, purple, and yellow boxes indicate pre-MCE,

MCE and post-MCE phases, respectively; statistical analysis was performed by multiple Student's t-test; **p<0.01, ***p<0.001 vs Scramble. B: Cell cycle distribution (light red: G0/G1, green: S, light blue: G2/M phases) and schematic results (significantly downregulated: red; upregulated: blue) of ShZc3h10 cells during adipogenesis.

Conversely, in Zc3h10 overexpressed cells we observed a decrease in the number of cells in S (day 1 and 3) and G2/M (day 1) and a concomitant increase of G0/G1 (days 1 and 3) phases, resulting in a precocious MCE. Also, in this context, cell cycle alteration was associated with cell number changes that increased already at day 3 after differentiation induction. At the physiological MCE (day 4), Zc3h10 overexpressing cells showed a higher distribution in G0/G1 and decreased levels in S and G2/M phases, resulting in a reduced number of cells at the end of the differentiation program (Fig. 4.36A, B). These results show that the inability to proceed correctly through the different phases of the cell cycle causes an incorrect MCE and, consequently, support the findings discussed above that either Zc3h10 silencing or overexpression led to improper adipogenic process with fewer lipid-containing cells in C3H10T1/2 and primary mouse adipocytes.

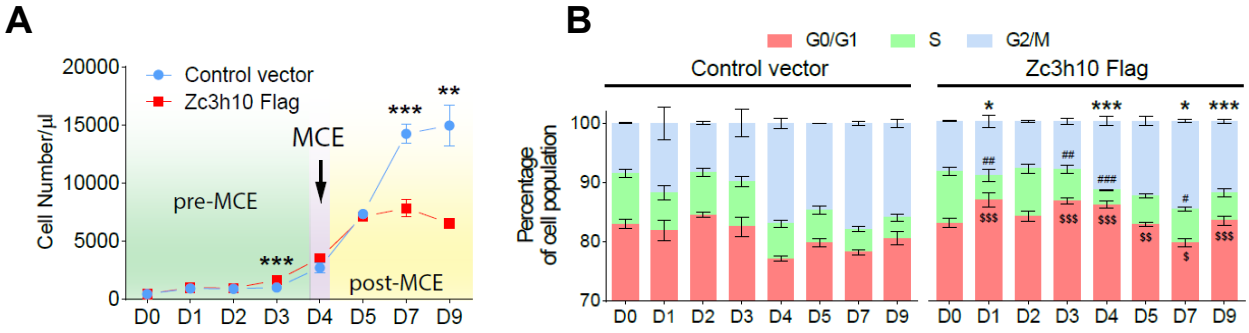

Figure 4.36: Zc3h10 overexpressing cells are blocking cells in G0/G1 phases. A: total cell number count by cytofluorimetry analysis of Zc3h10 Flag cells. Green, purple and yellow boxes indicate pre-MCE, MCE and post-MCE phases, respectively; statistical analysis was performed by multiple Student's t-test; **p<0.01, ***p<0.001 vs Control vector. B: Cell cycle distribution (light red: G0/G1, green: S, light blue: G2/M phases) and schematic results (significantly downregulated: red; upregulated: blue) of Zc3h10 Flag cells during adipogenesis.

5. DISCUSSION

Zc3h10 is a poorly characterized protein belonging to the CCCH (Cys-Cys-Cys-His) zinc finger family. Zinc finger proteins are involved in an extraordinary variety of cellular functions, including nucleic acid interactions, protein folding, and lipid binding (Liang et al., 2008). As reported by Castello and Colleagues, Zc3h10 is a RNA-binding protein that can bind mRNA in Hela cells (Castello et al., 2012).

In literature, Zc3h10 is described as a tumor suppressor in MCF-7 cells (Guardiola-Serrano et al., 2008), and as a mitochondrial regulator in murine cell lines and in human peripheral blood mononuclear cells (PBMCs) (Audano et al. 2018). Recently, a basic leucine-zipper domain, positioned between the last zinc finger and the proline-rich domain, has been identified in Zc3h10 protein and shown to be required for Zc3h10 DNA binding activity. Furthermore, mutational studies demonstrated that Zc3h10 RNA binding activity is not required to activate a thermogenic transcriptional program in brown adipose tissue indicating that Zc3h10 acts as a transcription factor (Yi et al., 2019). Nonetheless, the role of Zc3h10 during white adipogenic program has not been investigated yet.

Adipogenesis is a complex process by which undifferentiated mesenchymal stem cells became pre-adipocytes. It is a multi-step process that involved different transcription factors. A hormonal regimen is widely used to commit MSCs to pre-adipocytes, that eventually differentiate into lipid-filled mature white adipocytes (Tang and Lane, 2012). When MSCs reach confluency, they enter in a temporary quiescence state, arresting at the G0/G1 phase. The addition of hormone cocktail stimulates confluent cells to reenter the cell cycle and undergo multiple mitosis rounds, a process known as mitotic clonal expansion (MCE). Differentiating pre-adipocytes then exit the cell cycle, change their morphology, and start to accumulate triglycerides. The early phases of this multistep process require the reduction of translation to

arrest cell proliferation (Marcon et al., 2017, 2019; Tsukiyama-Kohara et al., 2001), the cytoskeleton remodeling involving F-actin reorganization (Hansson et al., 2019; Spiegelman and Farmer, 1982), and the increase of mitochondria network complexity (De Pauw et al., 2009b; Tharp et al., 2018; Wilson-Fritch et al., 2003).

However, knowledge of the molecular mechanisms that control these events in a coordinated fashion remains still incomplete. In this study, we used gain and loss of function approaches to unravel the biochemical and molecular function of Zc3h10 during the white adipogenic program.

We demonstrate that Zc3h10 protein level increased 36 hours after differentiation induction. Furthermore, we find that Zc3h10 resides in the chromatin fraction and is required in the early stages of differentiation. The depletion of Zc3h10 in pre-adipocytes results in reduced lipid accumulation and impaired adipocytes differentiation, while its silencing at the late stage does not affect terminal differentiation. On the other hand, Zc3h10 overexpression, before its physiological expression, leads to increased lipid droplet size, although it reduces the number of mature adipocyte cells. These results highlight the importance of the fine-tuned and time-controlled expression of Zc3h10 during the white adipogenic program.

Genome-wide transcriptomic analyses performed in the early phase of adipogenesis reveal that Zc3h10 controls expression of genes belonging to translation and actin cytoskeleton organization pathways. Functional validation experiments demonstrate that Zc3h10 depletion in pre-adipocytes is associated with the inhibition of protein translation. The protein translation machinery is finely tuned by 4E-BP1 activity. Hypophosphorylated 4E-BP1 status is linked with an active translational process, whereas hyperphosphorylated status occurs within an inhibited translational activity. The phosphorylation sites of 4E-BP1 are threonine (Thr)37, Thr46, Thr70, and serine (Ser)65. Importantly, the substitution of Thr37, Thr46, Thr70 to alanines prevents 4E-BP1 release of eIF4E, while mutation of Ser65 to alanine does not affect

dissociation of the eIF4E/4E-BP1 complex (Gingras et al., 2001; Proud, 2007). Therefore, the hierarchical phosphorylation of 4E-BP1 starts with the priming sites of Thr37 and Thr46 residues followed by phosphorylation of Thr70 and, ultimately, of Ser65 (Gingras et al., 2001, 1999; Proud, 2007). Our results show that Thr37-46 and Thr70 are significantly hyperphosphorylated in Zc3h10-depleted pre-adipocytes while Zc3h10 overexpressing cells present a hypophosphorylation of the same amino acid residues, suggesting that the lack of Zc3h10 enhances protein translational activity and negative impact the beginning of adipogenesis.

In the early phases of adipogenesis, further validations indicate the key role of Zc3h10 in orchestrating F-actin remodeling. During adipogenesis, cells must reorganize their cytoskeleton and change their shape from elongated and irregular appearance (fibroblast-like) to a round shape that allows them to maximize lipid accumulation (Spiegelman and Farmer 1982). This latter process is strongly influenced by actin polymerization/depolymerization state. Current knowledge shows that adipocytes differentiation is associated with a shift in F-actin structures: from prolonged stress fibers organized across the cell body, typically observed in precursor cells and pre-adipocytes, to cortical fibers presented in fully differentiated adipocytes. F-actin in Zc3h10 silenced pre-adipocytes appeared less-organized while, Zc3h10 overexpression enhanced the priming of F-actin reorganization towards the cell periphery. F-actin acts as a regulator of mitochondrial network, which is different between our experimental conditions. Zc3h10 silencing increased the rod-shaped mitochondrial length and the ratio of rods length/branches length. Of note, the number of junctions and branches and the mitochondrial area were significantly blunted, and for this reason mitochondrial network is dramatically reduced. Usually, the mitochondrial network is associated with an increase in mitochondrial function and activity that are fundamental steps required for the increased ATP demand during adipogenic process. On the contrary, Zc3h10 overexpressing cells present an

increase in the number of branches and mitochondrial area. These results indicate that Zc3h10 favors the breakdown of F-actin stress fibers and peripheral reorganization, increasing the remodeling of the mitochondrial network. During adipogenesis, mitochondrial dynamics are dependent on interactions with F-actin, and Zc3h10 plays a role in coordinating mitochondria/F-actin contacts. Zc3h10 depletion in pre-adipocytes led to a significant increase in F-actin/mitochondria interaction, preventing mitochondrial dynamics and increasing mitochondrial fission. This data is confirmed by the rise of expression of phosphorylated DRP1 (Ser616) in ShZc3h10 pre-adipocytes. DRP1 activity is essential for mitochondrial fission and is regulated by post-translational modifications that control its translocation to mitochondria (Alaimo et al., 2014). DRP1 phosphorylation on Ser616 by cyclin-dependent kinase (CDK) 1/Cyclin B or CDK5 favors mitochondrial fission during mitosis (Giacomello et al., 2020; Liesa et al., 2009; Taguchi et al., 2007). Conversely, DRP1 phosphorylation at Ser637 by protein kinase A (PKA) promotes the release of DRP1 from mitochondria resulting in inhibition of mitochondrial fission (Giacomello et al., 2020; Kashatus et al., 2011; Wang et al., 2012). Hence, the DRP1 Ser616/Ser637 phosphorylation ratio represents an index for the capacity of DRP1-mediated mitochondrial dynamics, and this ratio is significantly increased in Zc3h10 silenced cells, suggesting increased mitochondrial fission. In contrast, overexpression of Zc3h10 reduced F-actin/mitochondria interactions and increased MFN2 levels, enhancing mitochondrial fusion. Based on this data, Zc3h10 plays a crucial role in orchestrating F-actin remodeling to determine, on the one hand, a discrete subpopulation of functional mitochondria to provide energy and anabolic substrates for the build-up of lipids and, on the other hand, the proper cell shape to allow lipid accumulation.

Rho GTPases are the main controllers of cytoskeleton remodeling, cell shape, and organelle development (Hall, 2012; Heasman and Ridley, 2008; Jaffe and Hall, 2005). The three most common members of this family are Cell division control protein 42 homolog (Cdc42), Ras-

related C3 botulinum toxin substrate 1(Rac1), and Ras homolog family member A (RhoA) (Hall, 2012; Heasman and Ridley, 2008; Jaffe and Hall, 2005). Activation of Rho pathway leads to F-actin formation, stress fiber contractility, and force generation leading to inhibition of adipogenesis (Halder et al., 2012). Conversely, Rho/Rho Associated Protein Kinase (ROCK) inhibition favors adipogenesis (Nobusue et al., 2014; Noguchi et al., 2007; Romani et al., 2019). Rac1 and Cdc42 activation in the early phases of the adipogenic program regulates cell cycle progression (Lamarche et al., 1996), dorsal F-actin organization to promote cell shape rearrangements and terminal adipogenesis (Cristancho and Lazar, 2011; Liu et al., 2005). PKA activates Rac1 and Cdc42 and inhibits RhoA pathways (Bachmann et al., 2013; Howe, 2004; O'Connor and Mercurio, 2001; Price et al., 1998). We used the chemical inhibition of Rho-GTPases to investigate the effect of Zc3h10 knockdown or overexpression. Our results support the hypothesis that Zc3h10 triggers a transcriptional program to enable Rho-GTPases activities such as F-actin remodeling to define cell morphology, mitochondrial network complexity, and functions.

To further analyze the effect of Zc3h10 in the late stage of the adipogenic process, we perform transcriptomic analysis, and we discover that Zc3h10 modulates the expression of genes involved in mitochondrial function and cell cycle. All these early events controlled by Zc3h10 allow proper MCE, providing the correct cell distribution into different cell cycle phases and consequently, forming mature adipocytes. This concept is sustained by the analyses conducted at the late phase of adipogenesis, showing that Zc3h10 depleted mature adipocytes experience mitochondrial dysfunction leading to fatty acid utilization instead of accumulation, ultimately resulting in the impaired adipogenic program.

In closing, we define a physiological role of Zc3h10 as a transcription factor that, by the coordinated control of translation, cytoskeletal structure, cell shape, mitochondrial

dynamic/function, and metabolism in the early phases of adipogenesis, sets the basis for the white adipogenic program.

6. BIBLIOGRAPHY

Abarca-GÃ, L., Abdeen, Z.A., Abdul Hamid, Z., Abu-Rmeileh, N.M., Acosta-Cazares, B., Acuin, C., Adams, R.J., Aekplakorn, W., Afsana, K., Aguilar-Salinas, C.A., et al. (2017). Worldwide trends in body-mass index, underweight, overweight, and obesity from 1975 to 2016: a pooled analysis of 2416 population-based measurement studies in 128·9 million children, adolescents, and adults NCD Risk Factor Collaboration (NCD-RisC). Lancet *390*, 2627–2642.

Alaimo, A., Gorojod, R.M., Beauquis, J., Muñoz, M.J., Saravia, F., and Kotler, M.L. (2014). Deregulation of Mitochondria-Shaping Proteins Opa-1 and Drp-1 in Manganese-Induced Apoptosis. PLoS One *9*, e91848.

Ali, A.T., Hochfeld, W.E., Myburgh, R., and Pepper, M.S. (2013). Adipocyte and adipogenesis. Eur. J. Cell Biol. *92*, 229–236.

Anesti, V., and Scorrano, L. (2006). The relationship between mitochondrial shape and function and the cytoskeleton. Biochim. Biophys. Acta - Bioenerg. *1757*, 692–699.

Armani, A., Mammi, C., Marzolla, V., Calanchini, M., Antelmi, A., Rosano, G.M.C., Fabbri, A., and Caprio, M. (2010). Cellular models for understanding adipogenesis, adipose dysfunction, and obesity. J. Cell. Biochem. *110*, 564–572.

Audano, M., Pedretti, S., Cermenati, G., Brioschi, E., Diaferia, G.R., Ghisletti, S., Cuomo, A., Bonaldi, T., Salerno, F., Mora, M., et al. (2018). Zc3h10 is a novel mitochondrial regulator. EMBO Rep. *19*, pii: e45531.

Austenaa, L.M.I., Barozzi, I., Simonatto, M., Masella, S., Della Chiara, G., Ghisletti, S., Curina, A., de Wit, E., Bouwman, B.A.M., de Pretis, S., et al. (2015). Transcription of Mammalian cis-Regulatory Elements Is Restrained by Actively Enforced Early Termination. Mol. Cell.

Bach, D., Pich, S., Soriano, F.X., Vega, N., Baumgartner, B., Oriola, J., Daugaard, J.R., Lloberas, J., Camps, M., Zierath, J.R., et al. (2003). Mitofusin-2 determines mitochondrial network architecture and mitochondrial metabolism. A novel regulatory mechanism altered in obesity.

Bachmann, V.A., Riml, A., Huber, R.G., Baillie, G.S., Liedl, K.R., Valovka, T., and Stefan, E. (2013). Reciprocal regulation of PKA and Rac signaling. Proc. Natl. Acad. Sci. U. S. A. *110*, 8531–8536.

Baisamy, L., Jurisch, N., and Diviani, D. (2005). Leucine zipper-mediated homo-oligomerization regulates the Rho-GEF activity of AKAP-Lbc. J. Biol. Chem. *280*, 15405–15412.

Bartness, T.J., Vaughan, C.H., and Song, C.K. (2010). Sympathetic and sensory innervation of brown adipose tissue. Int. J. Obes. *34*, 36–42.

Birsoy, K., Chen, Z., and Friedman, J. (2008). Transcriptional Regulation of Adipogenesis by KLF4. Cell Metab. *7*, 339–347.

Blüher, M. (2019). Obesity: global epidemiology and pathogenesis. Nat. Rev. Endocrinol. *15*, 288–298.

Castello, A., Fischer, B., Eichelbaum, K., Horos, R., Beckmann, B.M., Strein, C., Davey, N.E., Humphreys, D.T., Preiss, T., Steinmetz, L.M., et al. (2012). Insights into RNA Biology from an Atlas of Mammalian mRNA-Binding Proteins. Cell *149*, 1393–1406.

Cawthorn, W.P., Scheller, E.L., and Macdougald, O.A. (2012). Adipose tissue stem cells meet

preadipocyte commitment: going back to the future. J. Lipid Res. *53*, 227–246.

Chan, D.C. (2006). Mitochondria: Dynamic Organelles in Disease, Aging, and Development. Cell *125*, 1241–1252.

Chawta, A., Repa, J.J., Evans, R.M., and Mangelsdorf, D.J. (2001). Nuclear receptors and lipid physiology: Opening the x-files. Science (80-.). *294*, 1866–1870.

Chen, H., Chomyn, A., and Chan, D.C. (2005a). Disruption of Fusion Results in Mitochondrial Heterogeneity and Dysfunction.

Chen, Q., Shou, P., Zheng, C., Jiang, M., Cao, G., Yang, Q., Cao, J., Xie, N., Velletri, T., Zhang, X., et al. (2016). Fate decision of mesenchymal stem cells: adipocytes or osteoblasts? Cell Death Differ. *23*, 1128–1139.

Chen, Z., Torrens, J.I., Anand, A., Spiegelman, B.M., and Friedman, J.M. (2005b). Krox20 stimulates adipogenesis via C/EBPβ-dependent and -independent mechanisms. Cell Metab. *1*, 93–106.

Choe, S.S., Huh, J.Y., Hwang, I.J., Kim, J.I., and Kim, J.B. (2016). Adipose Tissue Remodeling: its Role in energy Metabolism and Metabolic Disorders. Front. Endocrinol. (Lausanne). *7*, 1.

Cristancho, A.G., and Lazar, M.A. (2011). Forming functional fat: A growing understanding of adipocyte differentiation. Nat. Rev. Mol. Cell Biol. *12*, 722–734.

Diviani, D., Abuin, L., Cotecchia, S., and Pansier, L. (2004). Anchoring of both PKA and 14-3-3 inhibits the Rho-GEF activity of the AKAP-Lbc signaling complex. EMBO J. *23*, 2811–2820.

Dong, J.M., Leung, T., Manser, E., and Lim, L. (1998). cAMP-induced morphological changes are counteracted by the activated RhoA small GTPase and the Rho kinase ROKα. J. Biol. Chem. *273*, 22554–22562.

Edwards, D.C., Sanders, L.C., Bokoch, G.M., and Gill, G.N. (1999). Activation of LIM-kinase by Pak1 couples Rac/Cdc42 GTPase signalling to actin cytoskeletal dynamics. Nat. Cell Biol. *1*, 253–259.

Feng, T., Szabo, E., Dziak, E., and Opas, M. (2010). Cytoskeletal disassembly and cell rounding promotes adipogenesis from ES cells. Stem Cell Rev. Reports *6*, 74–85.

Fletcher, D.A., and Mullins, R.D. (2010). Cell mechanics and the cytoskeleton. Nature *463*, 485–492.

Forni, M.F., Peloggia, J., Trudeau, K., Shirihai, O., and Kowaltowski, A.J. (2016). Murine Mesenchymal Stem Cell Commitment to Differentiation is Regulated by Mitochondrial Dynamics HHS Public Access. Stem Cells *34*, 743–755.

Frayn, K. (2002). Adipose tissue as a buffer for daily lipid flux. Diabetologia *45*, 1201–1210.

Friedman, J., and Halaas, D. (1998). Leptin and the regulation of body composition. Nature *395*, 763–770.

Gao, J., Schatton, D., Martinelli, P., Hansen, H., Pla-Martin, D., Barth, E., Becker, C., Altmueller, J., Frommolt, P., Sardiello, M., et al. (2014). CLUH regulates mitochondrial biogenesis by binding mRNAs of nuclear-encoded mitochondrial proteins. J. Cell Biol. *207*, 213–223.

Giacomello, M., Pyakurel, A., Glytsou, C., and Scorrano, L. (2020). The cell biology of mitochondrial membrane dynamics. Nat. Rev. Mol. Cell Biol. 1–21.

Gingras, A.-C.C., Raught, B., Gygi, S.P., Niedzwiecka, A., Miron, M., Burley, S.K., Polakiewicz, R.D., Wyslouch-Cieszynska, A., Aebersold, R., and Sonenberg, N. (2001). Hierarchical phosphorylation of the translation inhibitor 4E-BP1. Genes Dev. *15*, 2852–2864.

Gingras, A.C., Gygi, S.P., Raught, B., Polakiewicz, R.D., Abraham, R.T., Hoekstra, M.F., Aebersold, R., and Sonenberg, N. (1999). Regulation of 4E-BP1 phosphorylation: A novel two step mechanism. Genes Dev. *13*, 1422–1437.

Goto, T., Kim, M., Takahashi, H., Takahashi, N., and Kawada, T. (2016). Food Intake and Thermogenesis in Adipose Tissue. Korean J. Obes. *25*, 109–114.

Green, H., and Meuth, M. (1974). An established pre-adipose cell line and its differentiation in culture. Cell *3*, 127–133.

Gregoire, F.M., Smas, C.M., Sul, S., and Sul, H.S. (1998). Understanding adipocyte differentiation. Physiol. Rev. *78*, 783–809.

Guardiola-Serrano, F., Haendeler, J., Lukosz, M., Sturm, K., Melchner, H., and Altschmied, J. (2008). Gene trapping identifies a putative tumor suppressor and a new inducer of cell migration. Biochem Biophys Res Commun *376*, 748–752.

Halder, G., Dupont, S., and Piccolo, S. (2012). Transduction of mechanical and cytoskeletal cues by YAP and TAZ. Nat. Rev. Mol. Cell Biol. *13*, 591–600.

Hall, A. (1998). Rho GTpases and the actin cytoskeleton. Science (80-.). *279*, 509–514.

Hall, A. (2012). Rho family GTPases. In Biochemical Society Transactions, pp. 1378–1382.

Hansson, B., Morén, B., Fryklund, C., Vliex, L., Wasserstrom, S., Albinsson, S., Berger, K., and Stenkula, K.G. (2019). Adipose cell size changes are associated with a drastic actin remodeling. Sci. Rep. *9*.

Heasman, S.J., and Ridley, A.J. (2008). Mammalian Rho GTPases: New insights into their functions from in vivo studies. Nat. Rev. Mol. Cell Biol. *9*, 690–701.

Howe, A.K. (2004). Regulation of actin-based cell migration by cAMP/PKA. Biochim. Biophys. Acta - Mol. Cell Res. *1692*, 159–174.

Huang, H.-Y., Zhang, W.-T., Jiang, W.-Y., Chen, S.-Z., Liu, Y., Ge, X., Li, X., Dang, Y.-J., Wen, B., Liu, X.-H., et al. (2015). RhoGDI Inhibits Bone Morphogenetic Protein 4 (BMP4)-induced Adipocyte Lineage Commitment and Favors Smooth Muscle-like Cell Differentiation *. J. Biol. Chem. *290*, 11119–111129.

Jaffe, A.B., and Hall, A. (2005). RHO GTPASES: Biochemistry and Biology. Annu. Rev. Cell Dev. Biol. *21*, 247–269.

Jheng, H.-F., Tsai, P.-J., Guo, S.-M., Kuo, L.-H., Chang, C.-S., Su, I.-J., Chang, C.-R., and Tsai, Y.-S. (2012). Mitochondrial Fission Contributes to Mitochondrial Dysfunction and Insulin Resistance in Skeletal Muscle.

Ji, Y., Cao, M., Liu, J., Chen, Y., Li, X., Zhao, J., and Qu, C. (2017). Rock signaling control PPARγ expression and actin polymerization during adipogenesis. Saudi J. Biol. Sci. *24*, 1866–1870.

Jung, J.S., Shin, K.K., Kim, Y.S., Kim, J.Y., and Chan Bae, Y. (2014). miR-137 Controls Proliferation and Differentiation of Human Adipose Tissue Stromal Cells. Cell Physiol Biochem *33*, 758–768.

Kanzaki, M., and Pessin, J.E. (2001). Insulin-stimulated GLUT4 Translocation in Adipocytes Is

Dependent upon Cortical Actin Remodeling. JBC *276*, 42436–42444.

Kashatus, D.F., Lim, K.H., Brady, D.C., Pershing, N.L., Cox, A.D., and Counter, C.M. (2011). RALA and RALBP1 regulate mitochondrial fission at mitosis. Nat Cell Biol *13*, 1108–1115.

Kim, J.B., Wright, H.M., Wright, M., and Spiegelman, B.M. (1998). ADD1/SREBP1 activates PPAR through the production of endogenous ligand (fatty acid metabolismnuclear hormone receptoradipocyte differentiation).

Kim, J.I., Park, J., Ji, Y., Jo, K., Han, S.M., Sohn, J.H., Shin, K.C., Han, J.S., Jeon, Y.G., Nahmgoong, H., et al. (2019). During Adipocyte Remodeling, Lipid Droplet Configurations Regulate Insulin Sensitivity through F-Actin and G-Actin Reorganization.

Klemm, D.J., Wayne Leitner, J., Watson, P., Nesterova, A., E-B Reusch, J., Goalstone, M.L., and Draznin, B. (2001). Insulin-induced Adipocyte Differentiation. ACTIVATION OF CREB RESCUES ADIPOGENESIS FROM THE ARREST CAUSED BY INHIBITION OF PRENYLATION. J. Biol. Chem. *276*, 28430–28435.

Kligys, K., Claiborne, J.N., DeBiase, P.J., Hopkinson, S.B., Wu, Y., Mizuno, K., and Jones, J.C.R. (2007). The slingshot family of phosphatases mediates Rac1 regulation of cofilin phosphorylation, laminin-332 organization, and motility behavior of keratinocytes. J. Biol. Chem. *282*, 32520–32528.

Koefoed Petersen, R., Madsen, L., Møller Pedersen, L., Hallenborg, P., Hagland, H., Viste, K., Ove Døskeland, S., and Kristiansen, K. (2008). Cyclic AMP (cAMP)-Mediated Stimulation of Adipocyte Differentiation Requires the Synergistic Action of Epac-and cAMP-Dependent Protein Kinase-Dependent Processes. Mol. Cell. Biol. *28*, 3804–3816.

Kopelman, P.G. (2000). Obesity as a medical problem.

Kras, K.M., Hausman, D.B., Hausman, G.J., and Martin, R.J. (1999). Adipocyte Development is Dependent Upon Stem Cell Recruitment and Proliferation of Preadipocytes. Obes. Res. *7*, 491–497.

Kubota, N., Terauchi, Y., Yamauchi, T., Kubota, T., Moroi, M., Matsui, J., Eto, K., Yamashita, T., Kamon, J., Satoh, H., et al. (2002). Disruption of adiponectin causes insulin resistance and neointimal formation. J. Biol. Chem. *277*, 25863–25866.

Kusuyama, J., Bandow, K., Shamoto, M., Kakimoto, K., Ohnishi, T., and Matsuguchi, T. (2014). Low intensity pulsed ultrasound (LIPUS) influences the multilineage differentiation of mesenchymal stem and progenitor cell lines through ROCK-Cot/Tpl2-MEK-ERK signaling pathway. J. Biol. Chem. *289*, 10330–10344.

Lamarche, N., Tapon, N., Stowers, L., Burbelo, P.D., Aspenström, P., Bridges, T., Chant, J., and Hall, A. (1996). Rac and Cdc42 induce actin polymerization and G1 cell cycle progression independently of p65(PAK) and the JNK/SAPK MAP kinase cascade. Cell *87*, 519–529.

Lang, P., Gesbert, F., Delespine-Carmagnat, M., Stancou, R., Pouchelet, M., and Bertoglio, J. (1996). Protein kinase A phosphorylation of RhoA mediates the morphological and functional effects of cyclic AMP in cytotoxic lymphocytes. EMBO J. *15*, 510–519.

Lee, S.H., and Dominguez, R. (2010). Regulation of actin cytoskeleton dynamics in cells. Mol. Cells *29*, 311–325.

Lefterova, M.I., and Lazar, M.A. (2009). New developments in adipogenesis. Trends Endocrinol. Metab. *20*, 107–114.

Leigh-Brown, S., Antonio Enriquez, J., and Odom, D.T. (2010). Nuclear transcription factors in mammalian mitochondria.

Leterrier, J.F., Rusakov, D.A., Nelson, B.D., and Linden, M. (1994). Interactions between brain mitochondria and cytoskeleton: Evidence for specialized outer membrane domains involved in the association of cytoskeleton-associated proteins to mitochondria in situ and in vitro. Microsc. Res. Tech. *27*, 233–261.

Li, D., Yea, S., Li, S., Chen, Z., Narla, G., Banck, M., Laborda, J., Tan, S., Friedman, J.M., Friedman, S.L., et al. (2005). Krüppel-like factor-6 promotes preadipocyte differentiation through histone deacetylase 3-dependent repression of DLK1. J. Biol. Chem. *280*, 26941–26952.

Liang, J., Song, W., Tromp, G., Kolattukudy, P.E., and Fu, M. (2008). Genome-Wide Survey and Expression Profiling of CCCH-Zinc Finger Family Reveals a Functional Module in Macrophage Activation. PLoS One *3*, 2880.

Liesa, M., Palacín, M., and Zorzano, A. (2009). Mitochondrial dynamics in mammalian health and disease. Physiol. Rev. *89*, 799–845.

Liu, J., DeYoung, S.M., Zhang, M., Zhang, M., Cheng, A., and Saltiel, A.R. (2005). Changes in integrin expression during adipocyte differentiation. Cell Metab. *2*, 165–177.

Londos, C., Brasaemle, D.L., Schultz, C.J., Segrest, J.P., and Kimmel, A.R. (1999). Perilipins, ADRP, and other proteins that associate with intracellular neutral lipid droplets in animal cells. Semin. Cell Dev. Biol. *10*, 51–58.

Luo, L., and Liu, M. (2016). Adipose tissue in control of metabolism. J. Endocrinol. *231*, R77–R99.

Marcon, B.H., Holetz, F.B., Eastman, G., Origa-Alves, A.C., Amorós, M.A., de Aguiar, A.M., Rebelatto, C.K., Brofman, P.R.S., Sotelo-Silveira, J., and Dallagiovanna, B. (2017). Downregulation of the protein synthesis machinery is a major regulatory event during early adipogenic differentiation of human adipose-derived stromal cells. Stem Cell Res. *25*, 191–201.

Marcon, B.H., Shigunov, P., Spangenberg, L., Pereira, I.T., de Aguiar, A.M., Amorín, R., Rebelatto, C.K., Correa, A., and Dallagiovanna, B. (2019). Cell cycle genes are downregulated after adipogenic triggering in human adipose tissue-derived stem cells by regulation of mRNA abundance. Sci. Rep. *9*, 1–10.

Marx, N., Bourcier, T., Sukhova, G.K., Libby, P., and Plutzky, J. (1999). PPARγ activation in human endothelial cells increases plasminogen activator inhibitor type-1 expression: PPARγ as a potential mediator in vascular disease. Arterioscler. Thromb. Vasc. Biol. *19*, 546–551.

McBride, H.M., Neuspiel, M., and Wasiak, S. (2006). Mitochondria: More Than Just a Powerhouse. Curr. Biol. *16*.

Minokoshi, Y., Kim, Y.B., Peroni, O.D., Fryer, L.G.D., Müller, C., Carling, D., and Kahn, B.B. (2002). Leptin stimulates fatty-acid oxidation by activating AMP-activated protein kinase. Nature *415*, 339–343.

Møller, L.L.V., Klip, A., and Sylow, L. (2019). Rho GTPases—Emerging Regulators of Glucose Homeostasis and Metabolic Health. Cells *8*, 434.

Moore, A.S., Wong, Y.C., Simpson, C.L., and Holzbaur, E.L.F.F. (2016). Dynamic actin cycling through mitochondrial subpopulations locally regulates the fission-fusion balance within mitochondrial networks. *7*, 1–13.

Narumiya, S., Tanji, M., and Ishizaki, T. (2009). Rho signaling, ROCK and mDia1, in transformation, metastasis and invasion. Cancer Metastasis Rev *28*, 65–76.

Nobusue, H., Onishi, N., Shimizu, T., Sugihara, E., Oki, Y., Sumikawa, Y., Chiyoda, T., Akashi, K., Saya, H., and Kano, K. (2014). Regulation of MKL1 via actin cytoskeleton dynamics drives adipocyte differentiation. Nat. Commun. *5*, 3368.

Nogales, E. (2000). Structural Insights into Microtubule Function. Annu. Rev. Biochem. *69*, 277–302.

Noguchi, M., Hosoda, K., Fujikura, J., Fujimoto, M., Iwakura, H., Tomita, T., Ishii, T., Arai, N., Hirata, M., Ebihara, K., et al. (2007). Genetic and Pharmacological Inhibition of Rho-associated Kinase II Enhances Adipogenesis.

O'Connor, K.L., and Mercurio, A.M. (2001). Protein Kinase A Regulates Rac and Is Required for the Growth Factor-stimulated Migration of Carcinoma Cells. J. Biol. Chem. *276*, 47895–47900.

Oishi, Y., Manabe, I., Tobe, K., Tsushima, K., Shindo, T., Fujiu, K., Nishimura, G., Maemura, K., Yamauchi, T., Kubota, N., et al. (2005). Krüppel-like transcription factor KLF5 is a key regulator of adipocyte differentiation. Cell Metab. *1*, 27–39.

Olson, M.F., Ashworth, A., and Hall, A. (1995). An essential role for Rho, Rac, and Cdc42 GTPases in cell cycle progression through G1 . Science (80-.). *269*, 1270–1272.

Patel, Y.M., and Lane, M.D. (2000). Mitotic clonal expansion during preadipocyte differentiation: Calpain- mediated turnover of p27. J. Biol. Chem. *275*, 17653–17660.

De Pauw, A., Tejerina, S., Raes, M., Keijer, J., and Arnould, T. (2009a). Mitochondrial (dys)function in adipocyte (de)differentiation and systemic metabolic alterations (American Society for Investigative Pathology Inc.).

De Pauw, A., Tejerina, S., Raes, M., Keijer, J., and Arnould, T. (2009b). Mitochondrial (dys)function in adipocyte (de)differentiation and systemic metabolic alterations. Am J Pathol *175*, 927–939.

Peirce, V., Carobbio, S., and Vidal-Puig, A. (2014). The different shades of fat. Nature *510*, 76–83.

Pich, S., Bach, D., Briones, P., Liesa, M., Camps, M., Testar, X., Palacín, M., and Zorzano, A. (2005). The Charcot-Marie-Tooth type 2A gene product, Mfn2, up-regulates fuel oxidation through expression of OXPHOS system. Hum. Mol. Genet. *14*, 1405–1415.

Price, L.S., Leng, J., Schwartz, M.A., and Bokoch, G.M. (1998). Activation of Rac and Cdc42 by integrins mediates cell spreading. Mol. Biol. Cell *9*, 1863–1871.

Proud, C.G. (2007). Signalling to translation: How signal transduction pathways control the protein synthetic machinery. Biochem. J. *403*, 217–234.

Rabani, M., Levin, J.Z., Fan, L., Adiconis, X., Raychowdhury, R., Garber, M., Gnirke, A., Nusbaum, C., Hacohen, N., Friedman, N., et al. (2011). Metabolic labeling of RNA uncovers principles of RNA production and degradation dynamics in mammalian cells. *29*, 436–442.

Ramalingam, L., Oh, E., and Thurmond, D.C. (2013). Novel roles for insulin receptor (IR) in adipocytes and skeletal muscle cells via new and unexpected substrates. Cell. Mol. Life Sci. *70*, 2815–2834.

Ravanidis, S., and Doxakis, E. (2020). RNA-Binding Proteins Implicated in Mitochondrial Damage and Mitophagy. Front. Cell Dev. Biol. *8*, 372.

Ricote, M., Li, A.C., Willson, T.M., Kelly, C.J., and Glass, C.K. (1998). The peroxisome proliferator-activated receptor-γ is a negative regulator of macrophage activation. Nature *391*, 79–82.

Romani, P., Brian, I., Santinon, G., Pocaterra, A., Audano, M., Pedretti, S., Mathieu, S., Forcato, M., Bicciato, S., Manneville, J.-B.B., et al. (2019). Extracellular matrix mechanical cues regulate lipid metabolism through Lipin-1 and SREBP. Nat. Cell Biol. *21*, 338–347.

Rosen, E.D., and Spiegelman, B.M. (2014). What we talk about when we talk about fat. Cell *156*, 20–44.

Rosen, E.D., Sarraf, P., Troy, A.E., Bradwin, G., Moore, K., Milstone, D.S., Spiegelman, B.M., and Mortensen, R.M. (1999). PPARγ is required for the differentiation of adipose tissue in vivo and in vitro. Mol. Cell *4*, 611–617.

Rosen, E.D., Hsu, C.-H., Wang, X., Sakai, S., Freeman, M.W., Gonzalez, F.J., and Spiegelman, B.M. (2002). C/EBP induces adipogenesis through PPAR: a unified pathway.

Sanchez-Gurmaches, J., Hung, C.M., Sparks, C.A., Tang, Y., Li, H., and Guertin, D.A. (2012). PTEN loss in the Myf5 lineage redistributes body fat and reveals subsets of white adipocytes that arise from Myf5 precursors. Cell Metab. *16*, 348–362.

Sarraf, P., Mueller, E., Jones, D., King, F.J., DeAngelo, D.J., Partridge, J.B., Holden, S.A., Chen, L.B., Singer, S., Fletcher, C., et al. (1998). Differentiation and reversal of malignant changes in colon cancer through PPARγ. Nat. Med. *4*, 1046–1052.

Schatton, D., and Rugarli, E.I. (2018). A concert of RNA-binding proteins coordinates mitochondrial function. Crit. Rev. Biochem. Mol. Biol. *53*, 652–666.

Spiegelman, B.M., and Farmer, S.R. (1982). Decreases in tubulin and actin gene expression prior to morphological differentiation of 3T3 Adipocytes. Cell *29*, 53–60.

Spiering, D., and Hodgson, L. (2011). Dynamics of the Rho-family small GTPases in actin regulation and motility. Cell Adh. Migr. *5*, 170–180.

Taanman, J.W. (1999). The mitochondrial genome: Structure, transcription, translation and replication. Biochim. Biophys. Acta - Bioenerg. *1410*, 103–123.

Taguchi, N., Ishihara, N., Jofuku, A., Oka, T., and Mihara, K. (2007). Mitotic phosphorylation of dynamin-related GTPase Drp1 participates in mitochondrial fission. J Biol Chem *282*, 11521–11529.

Tang, Q.-Q., and Daniel Lane, M. (1999). Activation and centromeric localization of CCAAT/enhancer-binding proteins during the mitotic clonal expansion of adipocyte differentiation.

Tang, Q.Q., and Daniel Lane, M. (2012). Adipogenesis: From Stem Cell to Adipocyte Keywords.

Tang, Q.Q., and Lane, M.D. (2012). Adipogenesis: from stem cell to adipocyte. Annu Rev Biochem *81*, 715–736.

Tang, Q.-Q., Grønborg, M., Huang, H., Kim, J.-W., Otto, T.C., Pandey, A., and Daniel Lane, M. (2005). Sequential phosphorylation of CCAAT enhancer-binding protein by MAPK and glycogen synthase kinase 3 is required for adipogenesis Materials and Methods Cell Culture, Induction of Differentiation, and Transfection of 3T3-L1.

Tang, Q.-Q.Q., Otto, T.C., and Lane, M.D. (2003a). CCAAT/enhancer-binding protein β is required for mitotic clonal expansion during adipogenesis. Proc. Natl. Acad. Sci. U. S. A. *100*, 850–855.

Tang, Q.Q., Otto, T.C., and Daniel Lane, M. (2003b). Mitotic clonal expansion: A synchronous process required for adipogenesis. Proc. Natl. Acad. Sci. U. S. A. *100*, 44–49.

Tang, Q.Q., Otto, T.C., and Lane, M.D. (2004). Commitment of C3H10T1/2 pluripotent stem cells to the adipocyte lineage. Proc. Natl. Acad. Sci. U. S. A. *101*, 9607–9611.

Tharp, K.M., Kang, M.S., Timblin, G.A., Dempersmier, J., Dempsey, G.E., Zushin, P.J.H., Benavides, J., Choi, C., Li, C.X., Jha, A.K., et al. (2018). Actomyosin-Mediated Tension Orchestrates Uncoupled Respiration in Adipose Tissues. Cell Metab. *27*, 602-615.e4.

Tilokani, L., Nagashima, S., Paupe, V., and Prudent, J. (2018). Mitochondrial dynamics: overview of molecular mechanisms. Essays Biochem. *62*, 341–360.

Tontonoz, P., and Spiegelman, B.M. (2008). Fat and Beyond: The Diverse Biology of PPARγ.

Tontonoz, P., Hu, E., and Spiegelman, B.M. (1994). Stimulation of adipogenesis in fibroblasts by PPARγ2, a lipid-activated transcription factor. Cell *79*, 1147–1156.

Treiber, T., Treiber, N., Plessmann, U., Harlander, S., Daiß, J.L., Eichner, N., Lehmann, G., Schall, K., Urlaub, H., and Meister, G. (2017). A Compendium of RNA-Binding Proteins that Regulate MicroRNA Biogenesis. Mol. Cell *66*, 270-284.e13.

Tsukiyama-Kohara, K., Poulin, F., Kohara, M., DeMaria, C.T., Cheng, A., Wu, Z., Gingras, A.C., Katsume, A., Elchebly, M., Spiegelman, B.M., et al. (2001). Adipose tissue reduction in mice lacking the translational inhibitor 4E-BP1. Nat. Med. *7*, 1128–1132.

Valente, A.J., Maddalena, L.A., Robb, E.L., Moradi, F., and Stuart, J.A. (2017). A simple ImageJ macro tool for analyzing mitochondrial network morphology in mammalian cell culture. Acta Histochem. *119*, 315–326.

Wai, T., and Langer, T. (2016). Mitochondrial Dynamics and Metabolic Regulation. Trends Endocrinol. Metab. *27*, 105–117.

Wakil, S.J., and Abu-Elheiga, L.A. (2009). Fatty acid metabolism: Target for metabolic syndrome. J. Lipid Res. *50*.

Wang, N.-D.;, Finegold, M.J.;, and Bradley, A. Impaired energy homeostasis in C/EBPalpha knockout mice.

Wang, Z., Jiang, H., Chen, S., Du, F., and Wang, X. (2012). The mitochondrial phosphatase PGAM5 functions at the convergence point of multiple necrotic death pathways. Cell *148*, 228–243.

Williams, E.P., Mesidor, M., Winters, K., Dubbert, P.M., and Wyatt, S.B. (2015). Overweight and Obesity: Prevalence, Consequences, and Causes of a Growing Public Health Problem. Curr. Obes. Rep. *4*, 363–370.

Wilson-Fritch, L., Burkart, A., Bell, G., Mendelson, K., Leszyk, J., Nicoloro, S., Czech, M., and Corvera, S. (2003). Mitochondrial biogenesis and remodeling during adipogenesis and in response to the insulin sensitizer rosiglitazone. Mol Cell Biol *23*, 1085–1094.

Wu, Z., Rosen, E.D., Brun, R., Hauser, S., Adelmant, G., Troy, A.E., McKeon, C., Darlington, G.J., and Spiegelman, B.M. (1999). Cross-regulation of C/EBPα and PPARγ controls the transcriptional pathway of adipogenesis and insulin sensitivity. Mol. Cell *3*, 151–158.

Xu, T., Wu, M., Feng, J., Lin, X., and Gu, Z. (2012). RhoA/Rho kinase signaling regulates transforming growth factor-β1-induced chondrogenesis and actin organization of synovium-derived mesenchymal stem cells through interaction with the Smad pathway. Int. J. Mol. Med.

30, 1119–1125.

Yang, J., Croniger, C.M., Lekstrom-Himes, J., Zhang, P., Fenyus, M., Tenen, D.G., Darlington, G.J., and Hanson, R.W. (2005). Metabolic Response of Mice to a Postnatal Ablation of CCAAT/Enhancer-binding Protein alpha. J Biol Chem *280*, 38689–38699.

Yang, W., Thein, S., Wang, X., Bi, X., Ericksen, R.E., Xu, F., and Han, W. (2014a). BSCL2/seipin regulates adipogenesis through actin cytoskeleton remodelling. Hum. Mol. Genet. *23*, 502–513.

Yang, W., Thein, S., Lim, C.Y., Ericksen, R.E., Sugii, S., Xu, F., Robinson, R.C., Kim, J.B., and Han, W. (2014b). Arp2/3 complex regulates adipogenesis by controlling cortical actin remodelling. Biochem. J. *464*, 179–192.

Yanovski, J.A. (2018). Obesity: Trends in underweight and obesity - scale of the problem. Nat. Rev. Endocrinol. *14*, 5–6.

Yi, D., Dempersmier, J.M., Nguyen, H.P., Viscarra, J.A., Dinh, J., Tabuchi, C., Wang, Y., and Sul, H.S. (2019). Zc3h10 Acts as a Transcription Factor and Is Phosphorylated to Activate the Thermogenic Program. Cell Rep. *29*, 2621-2633.e4.

Yu, F.X., Zhang, Y., Park, H.W., Jewell, J.L., Chen, Q., Deng, Y., Pan, D., Taylor, S.S., Lai, Z.C., and Guan, K.L. (2013). Protein kinase A activates the Hippo pathway to modulate cell proliferation and differentiation. Genes Dev. *27*, 1223–1232.

Zhang, J., Fu, M., Cui, T., Xiong, C., Xu, K., Zhong, W., Xiao, Y., Floyd, D., Liang, J., Li, E., et al. (2004). Selective disruption of PPAR2 impairs the development of adipose tissue and insulin sensitivity.

Zhang, Y., Proenca, R., Maffei, M., Barone, M., Leopold, L., and Friedman, J.M. (1994). Positional cloning of the mouse obese gene and its human homologue. Nature *372*, 425–432.

Zhang, Y., Marsboom, G., Toth, P.T., and Rehman, J. (2013). Mitochondrial Respiration Regulates Adipogenic Differentiation of Human Mesenchymal Stem Cells. PLoS One *8*, 77077.